Wide bandgap detectors: present status and future perspectives

Mara Bruzzi

University of Florence

I.N.F.N Sezione di Firenze

Istituto Nazionale di Fisica Nucleare

UNIVERSITÀ DEGLI STUDI FIRENZE

Outline

- **Introduction : electronic properties of WBG Semiconductors**
- Growth processes
- Beyond wafers: the perovskite family
- Lattice disorder, defects and energy levels; how to detect
- Research on WBG Radiation Detectors
  - Explorative studies (blue sky research) in the HEP community
  - Applications in medical field: proton and Flash therapy

Istituto Nazionale di Fisica Nucleare

UNIVERSITÀ DEGLI STUDI FIRENZE

Applications of Wide Band Gap Semiconductors

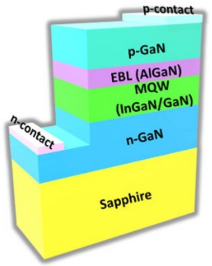

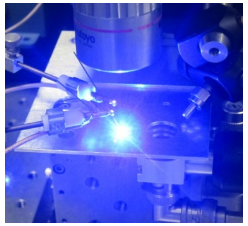

Sketch of a GaN-based LED

ECS Jour Sol St Sci Tech,2020 9066002

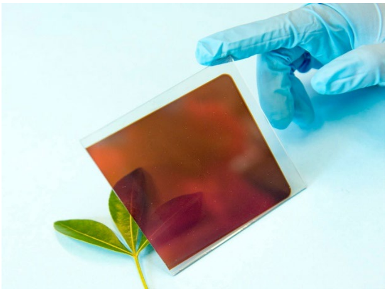

Perovskite solar cell

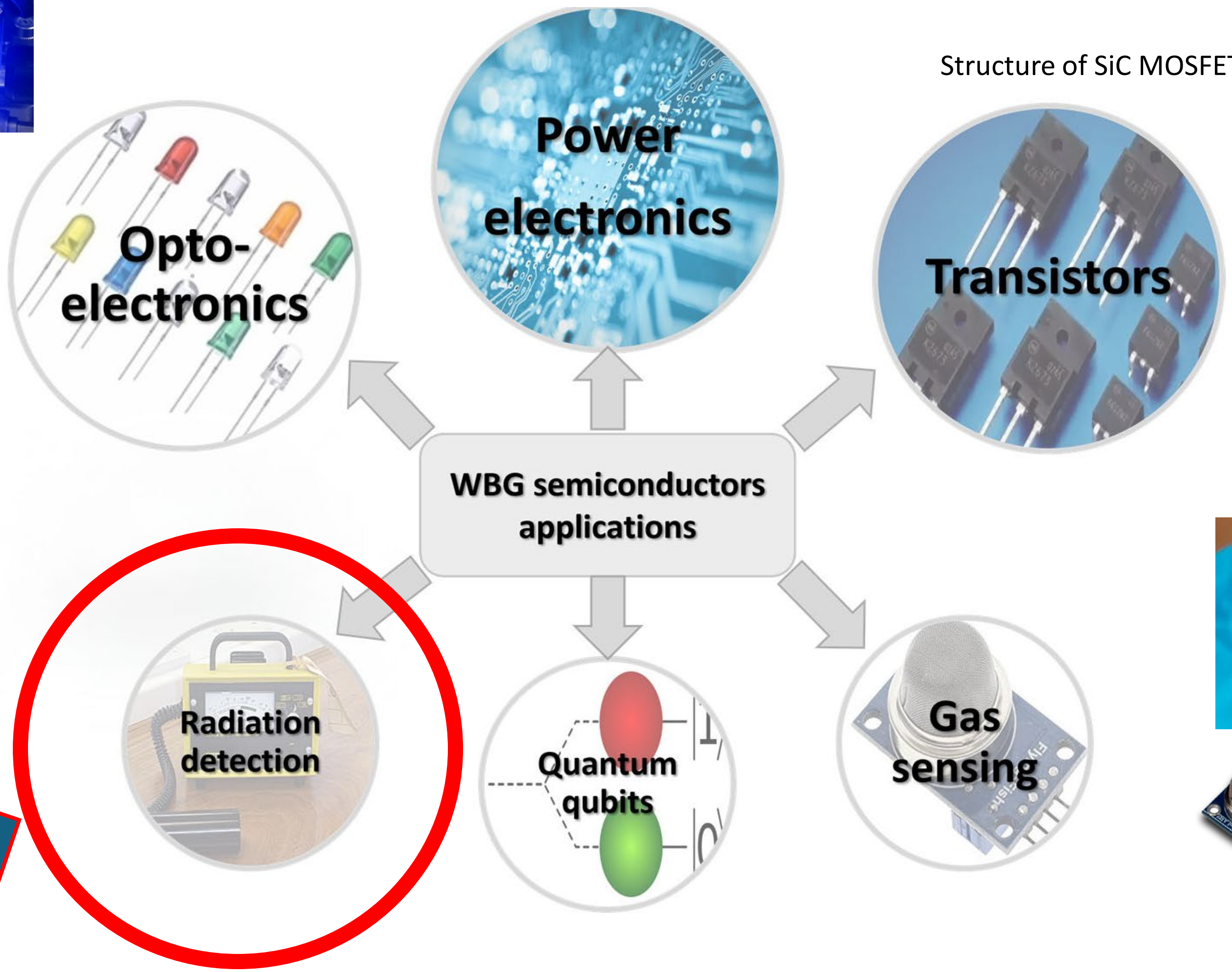

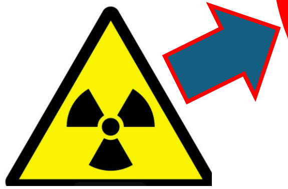

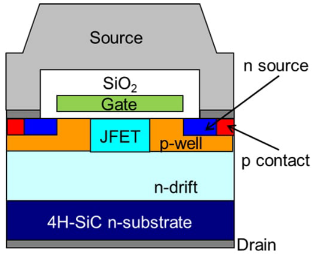

Structure of SiC MOSFET Chip

semiconductor
gas sensors

Istituto Nazionale di Fisica Nucleare

UNIVERSITÀ DEGLI STUDI FIRENZE

Particle Detector: General Design and working principle

- Semiconductor material with electrodes (pn junction)
- e-h pairs collected at electrodes
- read-out collected charge by bump-bonded electronic
- Single pixels 150x150μm^2 or less to read-out position
-

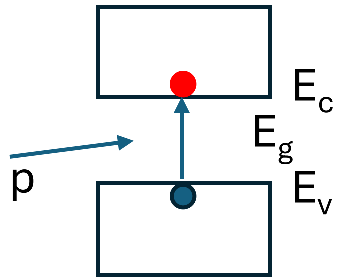

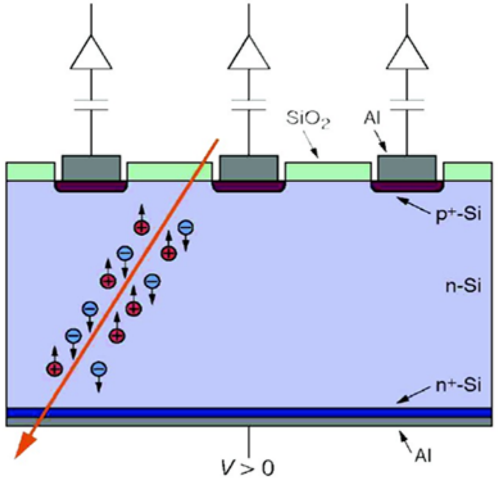

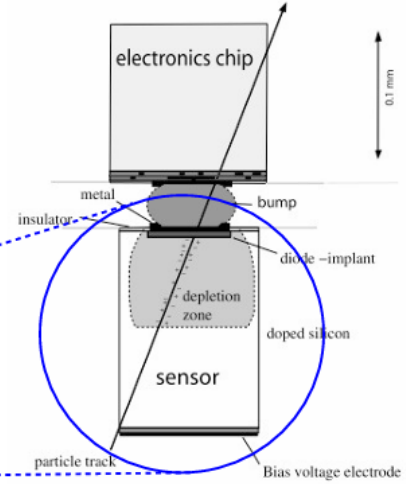

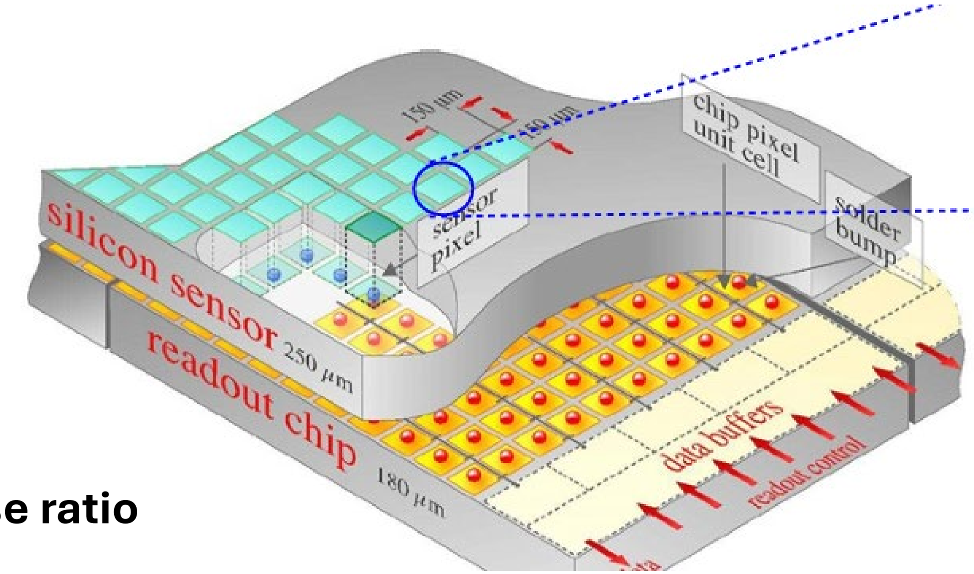

IDEAL DETECTOR : **highest Signal to noise ratio**

SIGNAL : Number of e-h pairs generated by the particle, highest for smaller E_g
NOISE: Thermally generated e-h pairs, lower for higher E_g

Best compromize in between →→ **search for optimal wide bandgap material**

Beyond Si: Why?

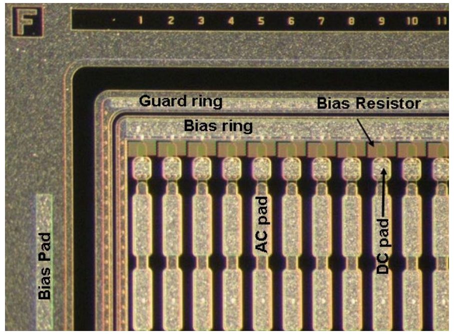

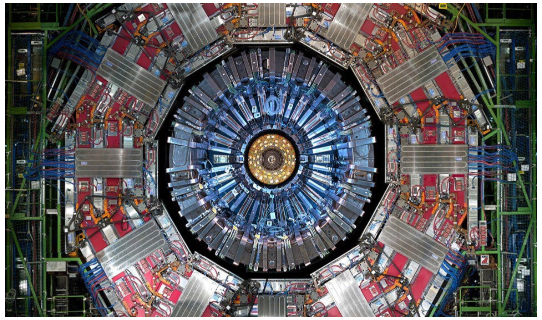

Limitations of traditional semiconductors

- **Radiation Damage** → Limited lifetime
- **High current, high voltage** → power consumption
- **Low Temperature operation** → cooling required
- Bulky, high-purity monocrystalline → high production costs
- Free-standing → electronic read-out match
- Rigid, fragile → limited conformation

Wide-bandgap semiconductors (WBG)

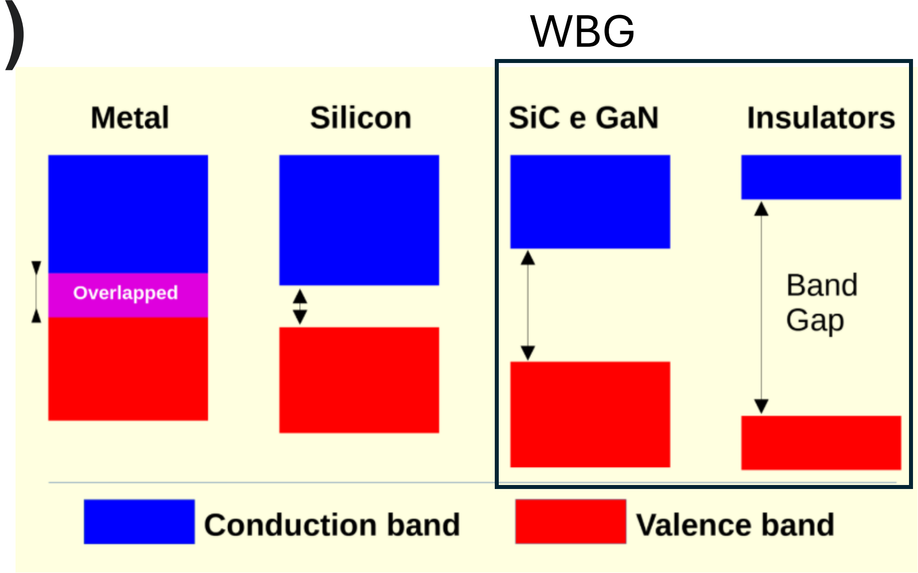

Larger bandgap **than conventional semiconductors**

- **Ge, Si, GaAs** : E_g = 0.7 – 1.4 eV,
- **WBG** E_g > 2 eV

- WBG permit devices to operate **at much higher voltages and temperatures** than conventional semiconductor materials.

- Low leakage currents even after heavy irradiation fluences

- Higher critical electrical field density, and saturation velocities, which allows them to **work at higher speeds.**

Origin of Bandgap

Lattice structure of a crystalline solid (diamond, Si, Ge, GaAs...)
$\rightarrow$ FCC (face centered cubic) symmetry with a basis of two atoms.

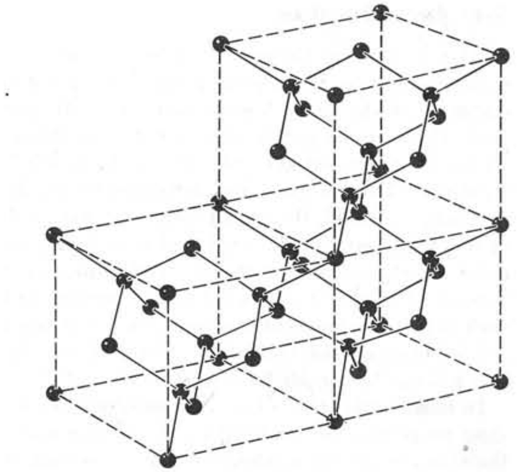

In a lattice of N atoms, every atomic energy level gives rise to bands of N closely spaced levels, with spacing and position depending on interionic separation *a*.

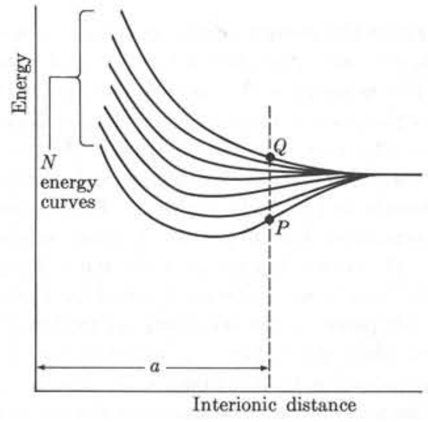

Bands in the inner complete shells are complete.

T = 0 K

Valence band = uppermost band complete
Conduction band = empty band above it

Bandgap = forbidden energy between
Valence and conduction band

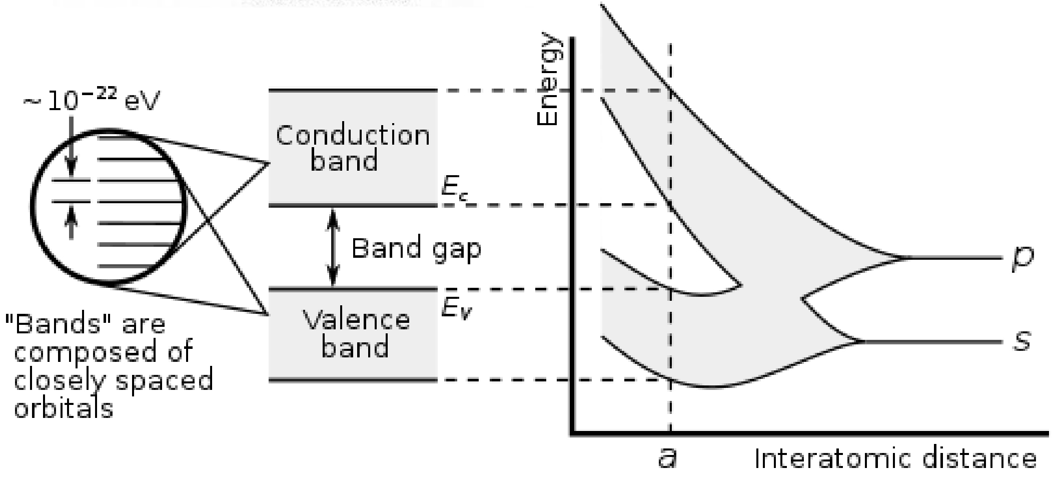

Group IV Semiconductors

Same structure but different lattice constant → different bandgap

	a [Å]	Eg (300K*)	Structure
C (diamond)	3.567	5.5	Diamond (FCC)
Si	5.431	1.12	Diamond (FCC)
Ge	5.658	0.67	Diamond (FCC)
Sn (gray α)	6.4	metal	Diamond (FCC)

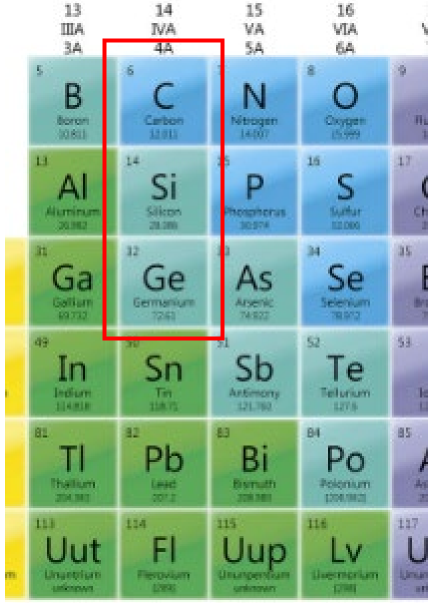

* Gap depend on T $E_g(T) = E_g(0) - \dfrac{\alpha T^2}{T+\beta}$, where $E_g(0)$, α and β are material constants

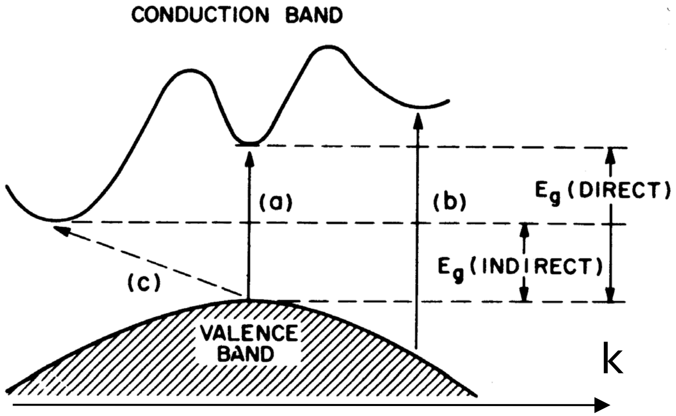

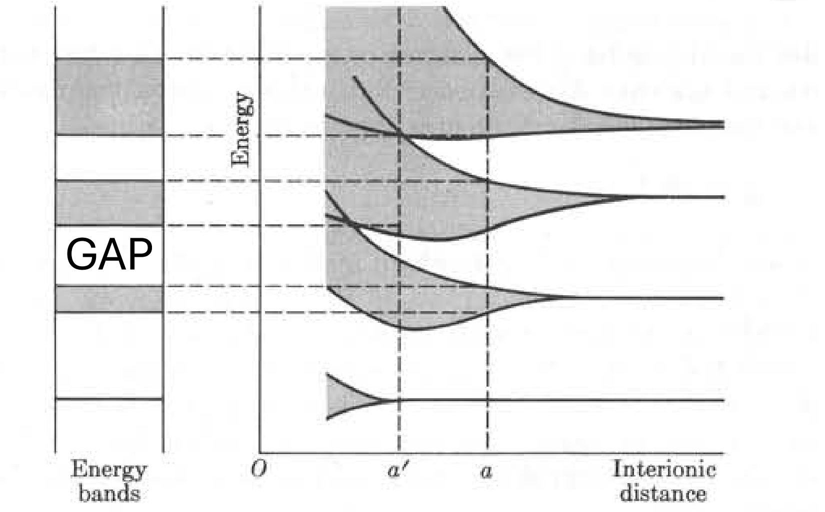

DIRECT GAP GaAs - INDIRECT GAP Si, Ge: phonons involved.

SiC – Family

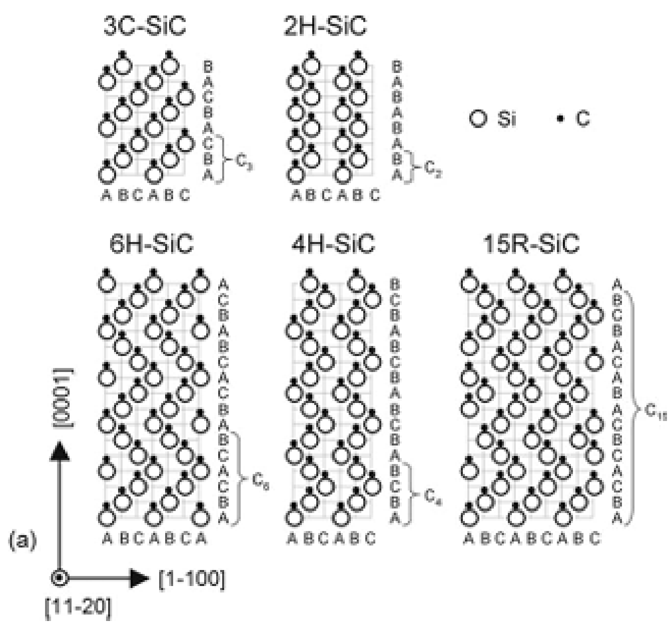

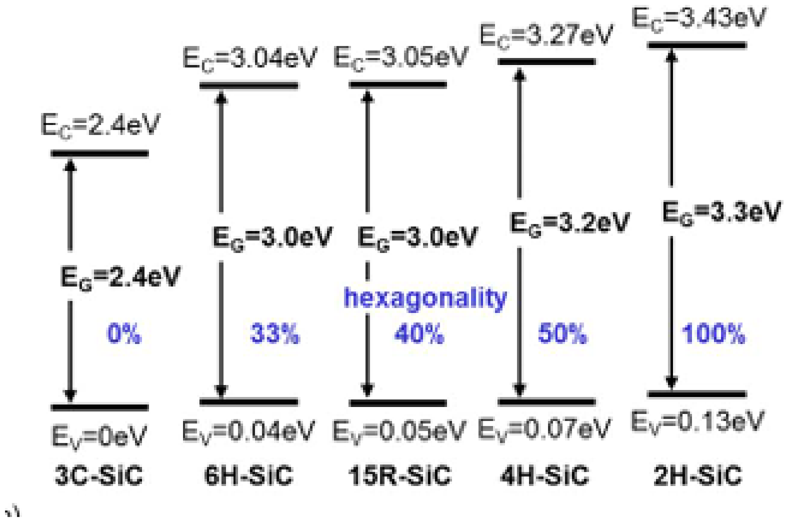

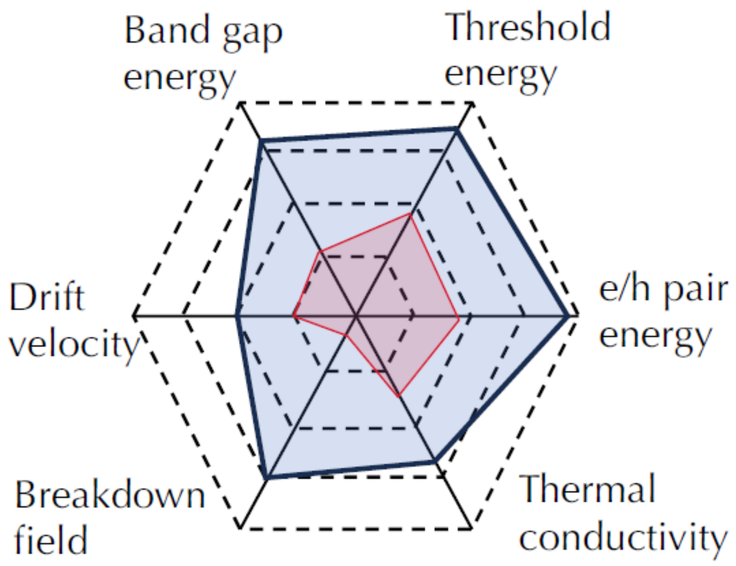

Semicond.Sci.Technol.33(2018)103001

Physical Parameter	Si	4H-SiC
Band gap energy [eV]	1.12	3.26
Thermal conductivity [W/K·cm]	1.5	4.9
Breakdown field [MV/cm]	0.3	3.0
Electron saturation drift velocity (cm/s)	1×10^7	2×10^7
Hole saturation drift velocity (cm/s)	0.6×10^7	1.8×10^7
Mean ionization energy for e/h pair (eV)	3.6	7.8
Atomic shift threshold energy(eV)	13	22

Main application

- Power electronics devices

INFN Istituto Nazionale di Fisica Nucleare

Università degli Studi Firenze

Group III-V binary Semiconductors

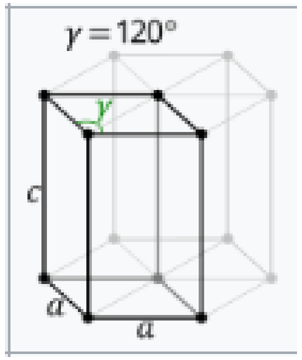

	a,c [Å]	Eg (300K)	Structure
GaAs	3.567	1.42	Zinc-blende (FCC)
GaN	*a* = 3.189 *c* = 5.185	3.4	HCP- Wurtzite

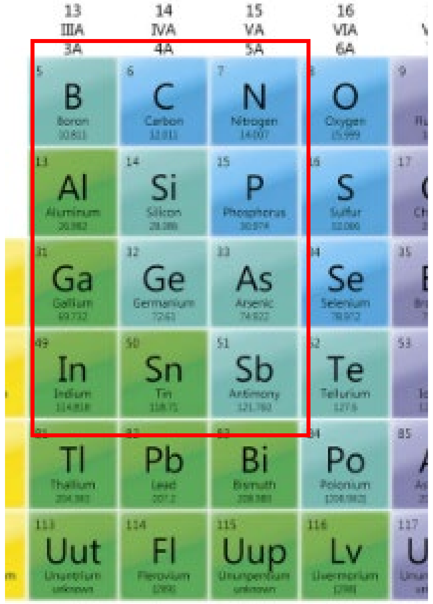

Each of the two individual atom types forms a sublattice which is hexagonal close-packed (HCP-type).

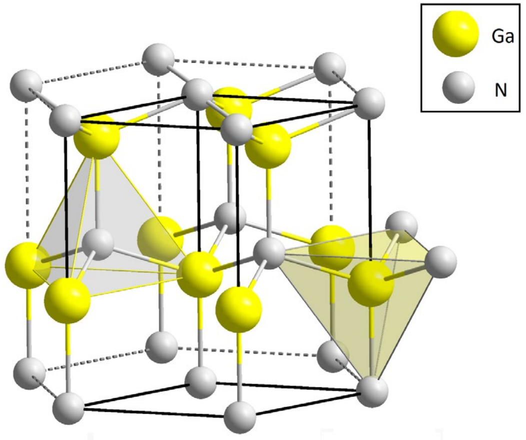

Main application :

- GaN LEDs
- GaAs solar cells, LED, lasers, microwave

https://commons.wikimedia.org/w/index.php?curid=48456361

VI group based Widegap Semiconductors

	a [Å]	Eg (300K) [eV]	
CdTe	6.48	1.5	Zinc-blende (FCC)
CdZnTe (CZT)		1.5-2.3	Zinc-blende (FCC)

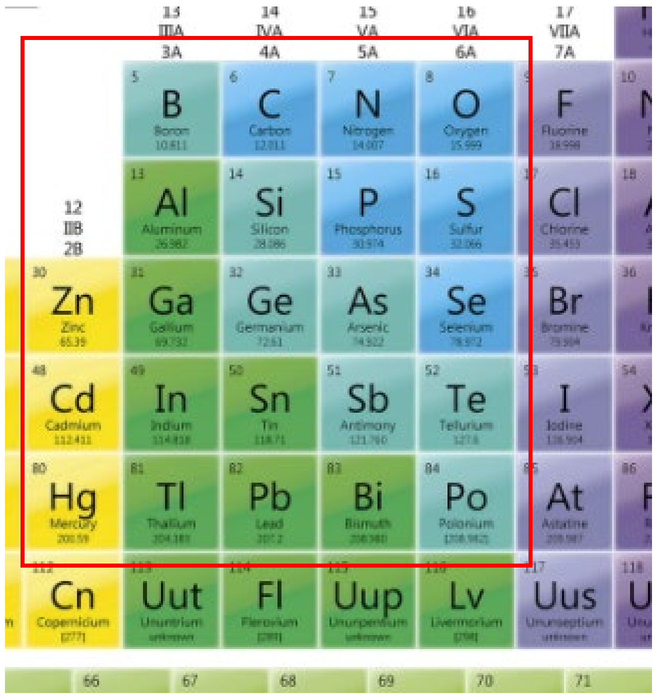

CZT crystal: CdTe and ZnTe crystals in (1-x):x ratio with a cubic zinc-blende structure. Varying x different compounds are obtained with different chemico-physical properties and gap in the range 1.49-2.26eV.

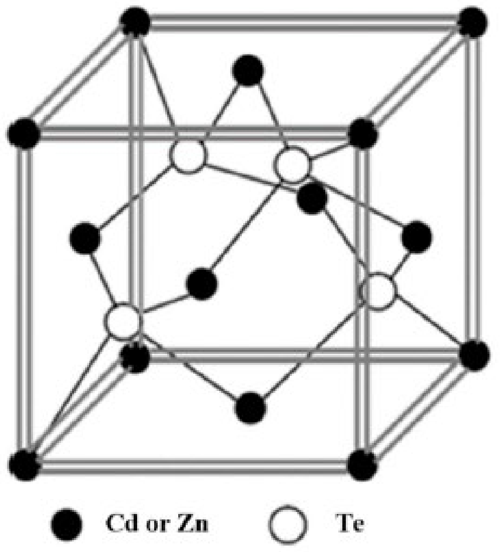

Main application :

- CdTe thin film solar cells
- CZT Scintillating crystals

insulator	a [Å]	Eg (300K) [eV]	Structure
Al_2O_3 (sapphire)	*a* = 4.78 *c* = 13	9.9	trigonal

nearly HCP structure with Al ions filling two-thirds of the octahedral interstices

Main application :

- LED substrates

INTRINSIC CARRIER CONCENTRATION IN SEMICONDUCTOR

Free carrier concentration n_i

$$n_i = \sqrt{N_C \; N_V} e^{-\frac{\varepsilon_g}{2K_B T}} \rightarrow\rightarrow n_i \;\alpha\; T^{\frac{3}{2}} e^{-\frac{\varepsilon_g}{2K_B T}}$$

N_c, N_v effective density of states of valence and conduction bands

	n_i 300K (cm^{-3})	ε_g (eV)
Ge	2.4×10^{13}	0.66
Si	1.45×10^{10}	1.12
GaAs	1.79×10^{6}	1.42
4H-SiC	5×10^{-9}	3.0
Diamond	$\approx 10^{-16}$	5.5

$$\rho_i = \frac{1}{n_i e(\mu_n + \mu_p)}$$

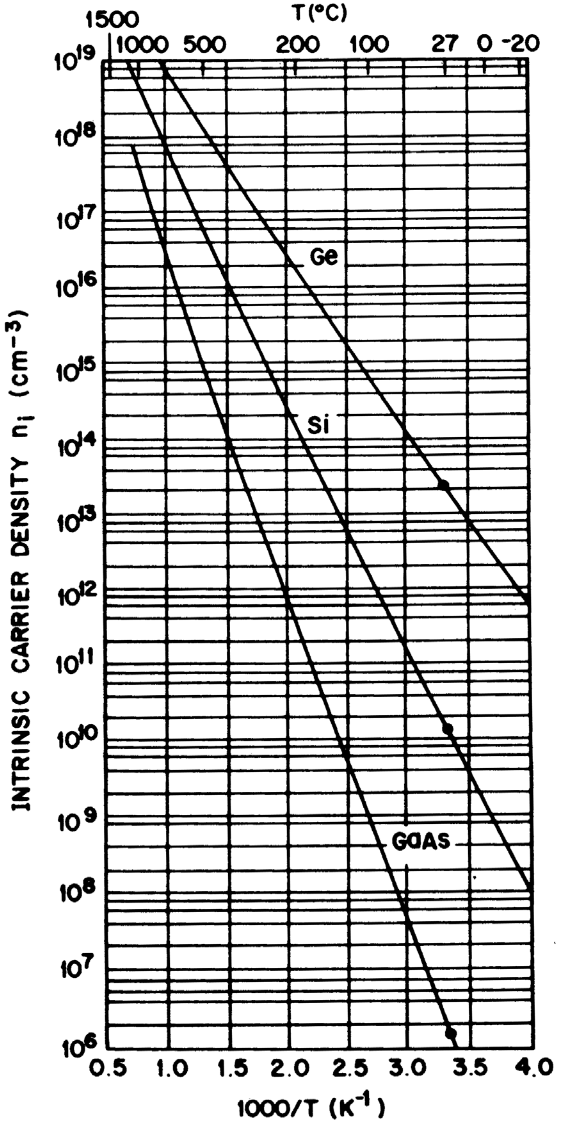

WBG are characterized by very low n_i and high resistivity at RT

Effective mass and mobility

Effective mass

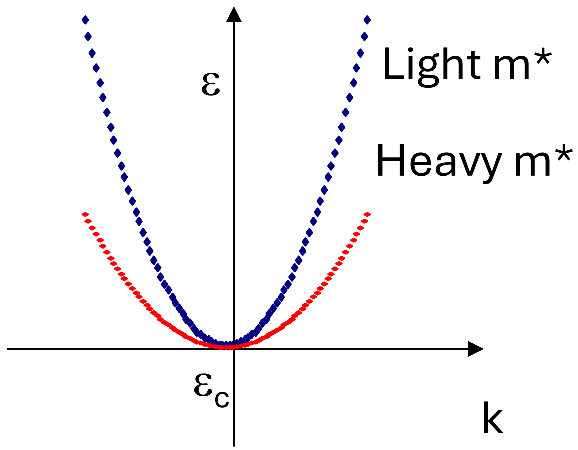

mobility $\mu_n = \dfrac{e\tau_n}{m_e^*}$ $\quad \mu_p = \dfrac{e\tau_p}{m_h^*}$

$$\tau = \tau_0 \left(\frac{\varepsilon}{K_B T}\right)^r$$

Scattering due to impurities neutral / charged (r = -½ ; +3/2) / lattice vibration (r = -3/2)

Drift velocity

$$v_{d,n} = \mu_n E$$

$$v_{d,p} = \mu_p E$$

Low electric field, E

Holes mobility lower than for electrons

Mobilities depend on T and doping

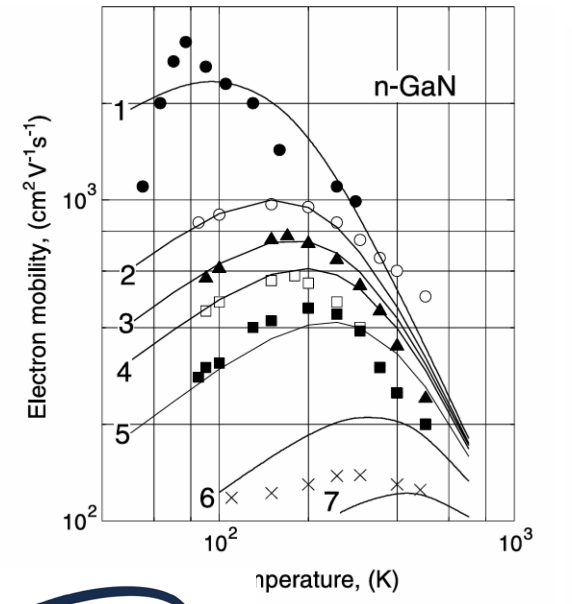

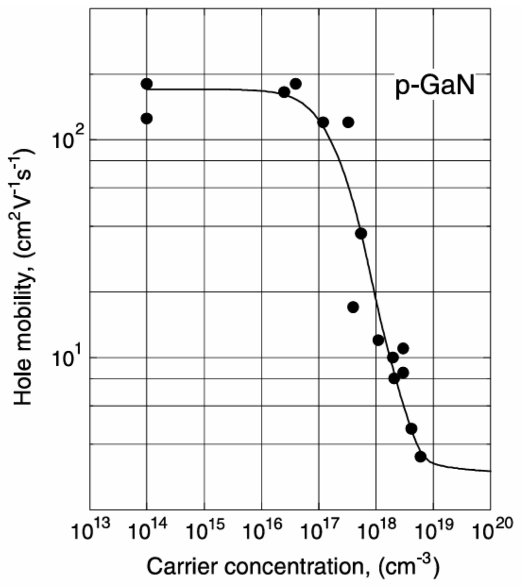

$$\frac{\mu_n}{\mu_p} \cong 3 \; in \; Si$$

Material	Gap [eV]	μ_e [cm²/(Vs)]	μ_h [cm²/(Vs)]
Si	1.12	1450	450
4H-SiC	3.26	950	115
Diamond	5.5	4500	3800
GaN	3.4	2000	100

WBG are characterized by high electron mobility

K.A.Stewart et al. Journal of Non-Crystalline Solids 432 (2016) 199

al. / Solid-State Electronics 47 (2003) 111–115

saturation velocity

Drift velocity

Low electric field, E

$$v_{d,n} = \mu_n E$$
$$v_{d,p} = \mu_p E$$

Intermediate electric field

$$v = \frac{v_s}{\left(1 + \frac{E_s}{E}\right)^{1/\gamma}}$$

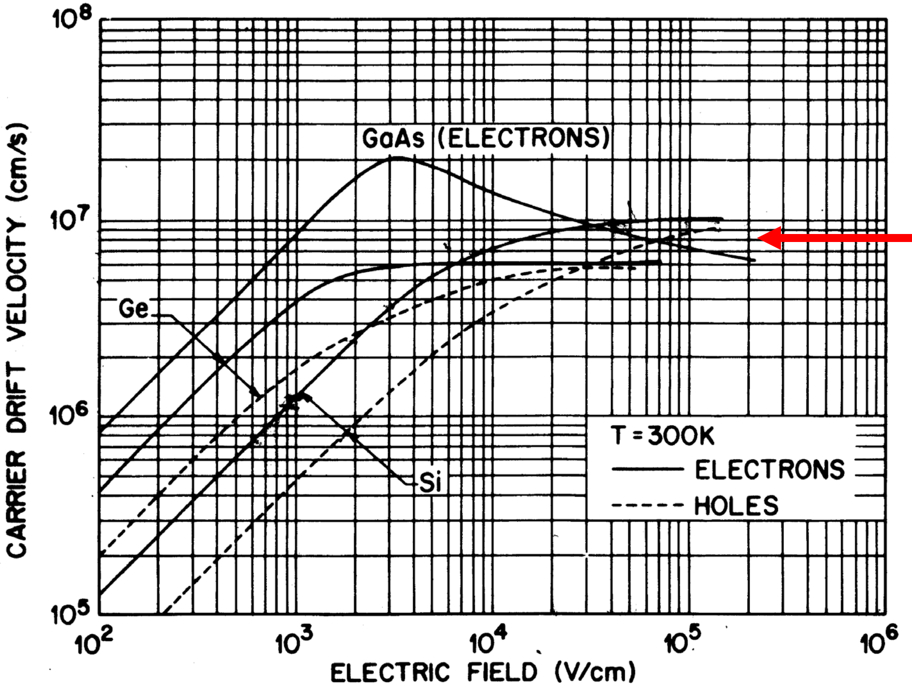

High electric field

v_{sat} **saturation velocity**

$$v_s = \left(\frac{8\hbar\omega_0}{3\pi\ m^*}\right)^{1/2}$$

Carriers emit optical phonon

$\hbar\omega_0$ **Shockley/Ryder (1954)**

GaAs $v_{sa<<<<<}$eak due to multy-valley conduction

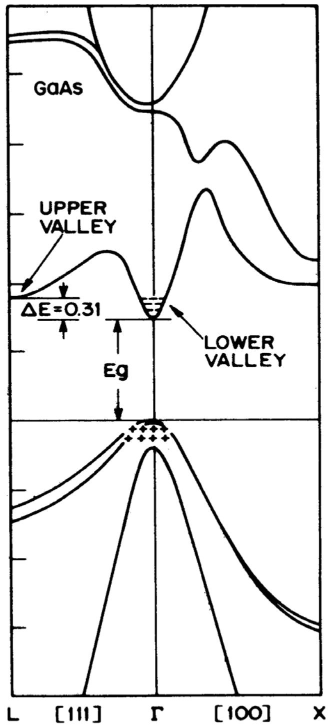

Material	Gap [eV]	E_{crit} [MV/cm]	V_{sat} 10^7 [cm/s]
Si	1.12	0.3	1
4H-SiC	3.26	2.5	2
Diamond	5.5	10	2.3
GaN	3.4	3.3	2.4

Diamond SiC GaN: high saturation velocity and critical field

Mean Ionization Energy

The Klein law: Phenomenological model to estimate average amount of radiation energy consumed per e-h pair by high-energy radiation.

Three contributions:

- Intrinsic bandgap *(E_G)*
- Optical phonon losses *$r(h\omega_R)$*
- Residual kinetic energy (9/5) E_G, related to a threshold for impact ionization

Material	Ei [eV]
Si	3.6
SiC	7.8
Diamond	13-16

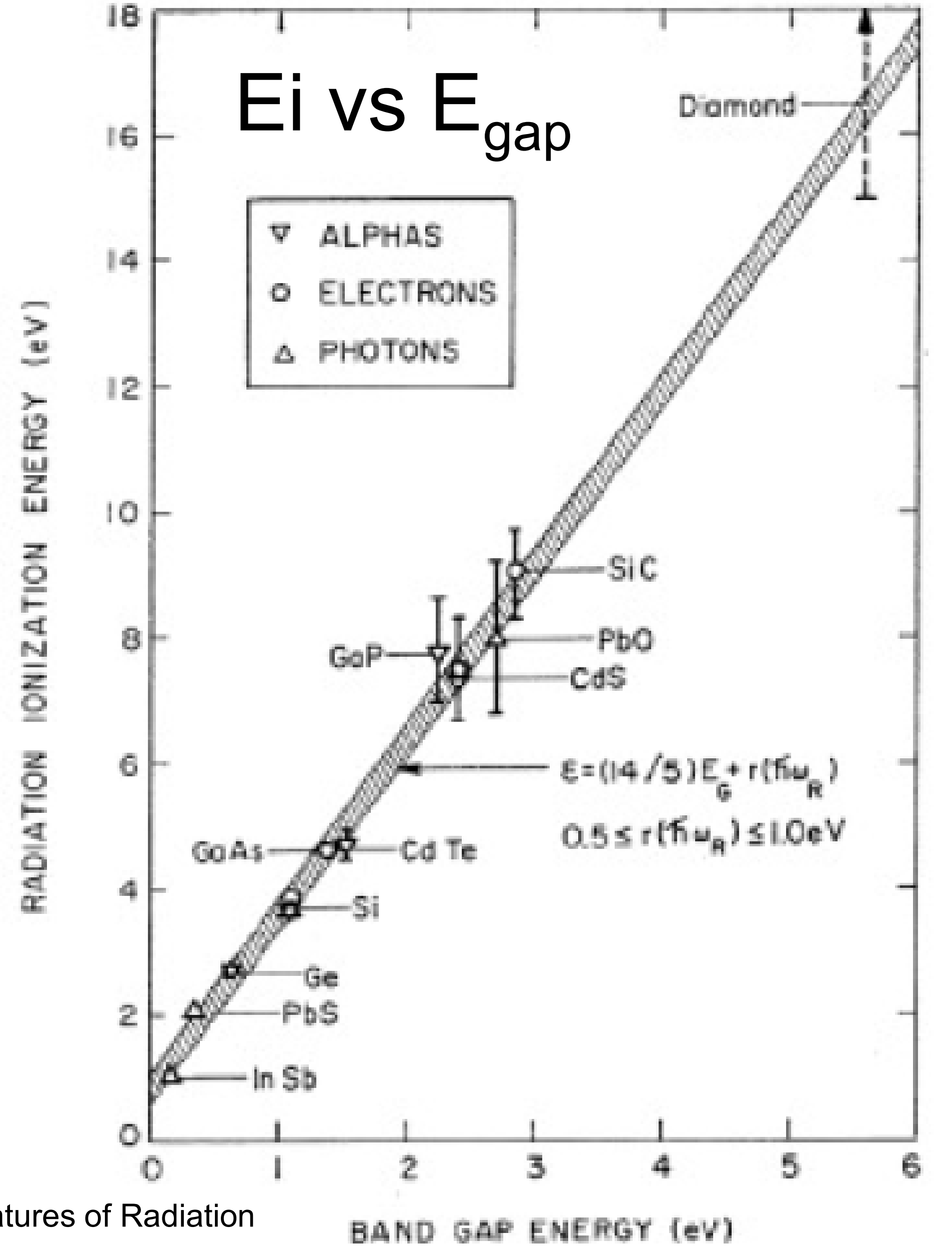

Bandgap Dependence and Related Features of Radiation Ionization Energies in Semiconductors
C.A. Klein J. Appl. Phys. 39, 2029 (1968); 10.1063/1.1656484

outline

- Introduction : electronic properties of WBG Semiconductors
- **Growth processes**
  - Beyond wafers: the perovskite family
- Lattice disorder, defects and energy levels; how to detect
- Research on WBG Radiation Detectors
  - Explorative studies (blue sky research) in the HEP community
  - Applications in medical field: proton and Flash therapy

Istituto Nazionale di Fisica Nucleare

UNIVERSITÀ DEGLI STUDI FIRENZE

Growth process

Monocrystalline Si

Czochralski process

- Pull Si-crystal from a Si-melt contained in a silica crucible while rotating.
- Silica crucible is dissolving oxygen into the melt ⇨ high concentration of O in CZ
- Material used by IC industry (cheap)

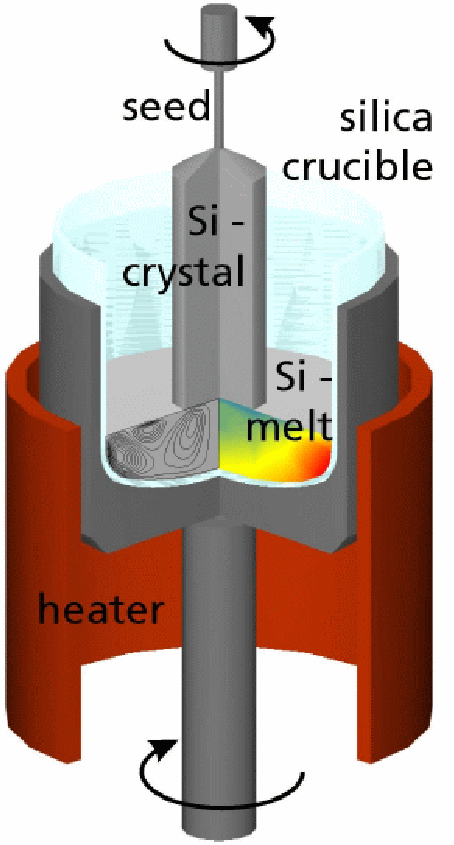

Float Zone process

Using a single Si crystal seed, melt the vertically oriented rod onto the seed using RF power and "pull" the monocrystalline ingot

- Highly pure crystal : Low concentration of [O] and [C] $10^{15}cm^{-3}$

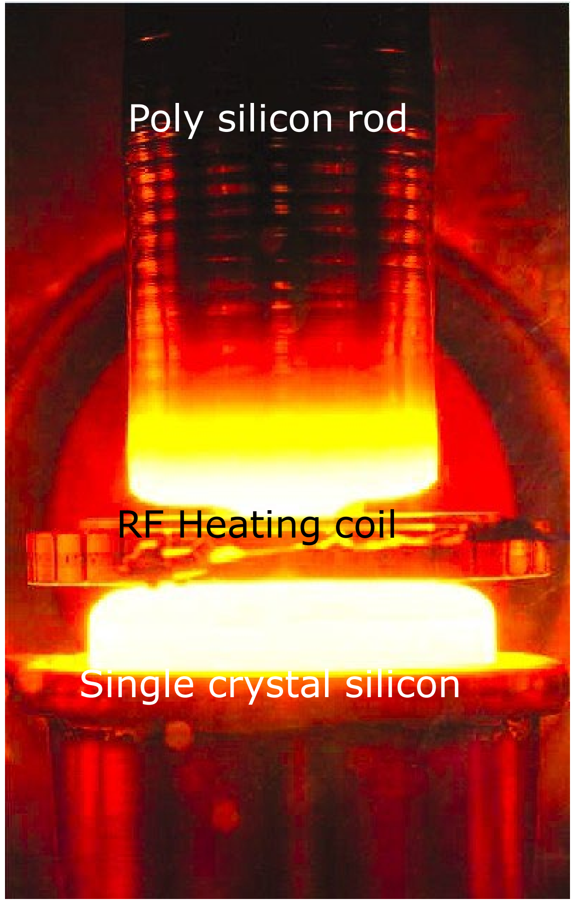

Mono-crystalline Ingot

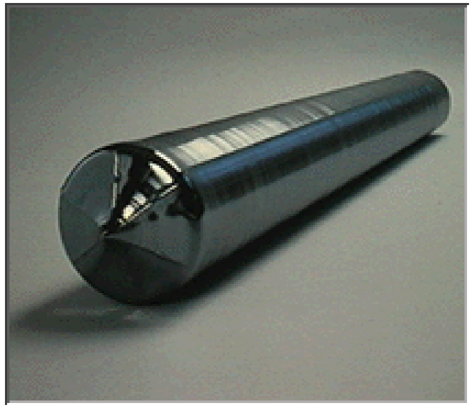

Wafer production

- Slicing, lapping, etching, polishing

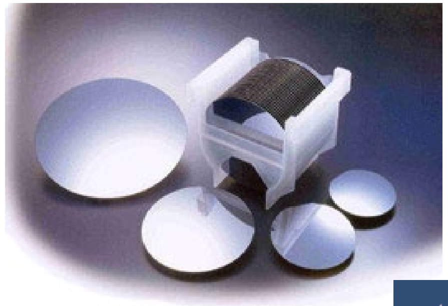

Chemical Vapor Deposition (CVD)

Synthetic diamond:

- HPHT very high temperature and pressures to convert graphite to diamond; grains are very small.

→ Plasma Enhanced CVD: uses plasma to enhance chemical reactions from gas precursors, enabling uniform coatings at lower temperatures. Ideal for semiconductors, optics, and protective coatings, PECVD improves adhesion and film quality.

→ Single crystals with diamond HPHT seed

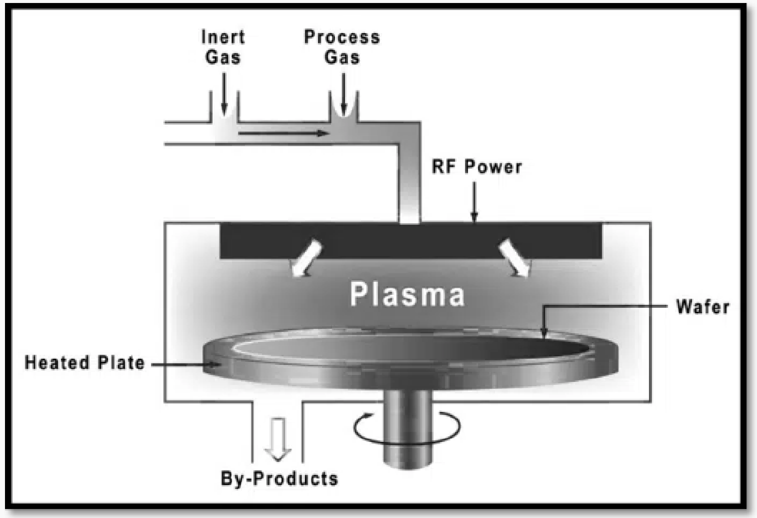

Figure: *Schematic of plasma-enhanced CVD*

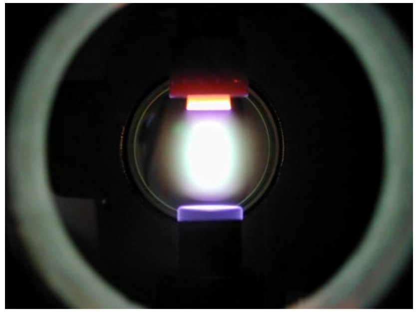

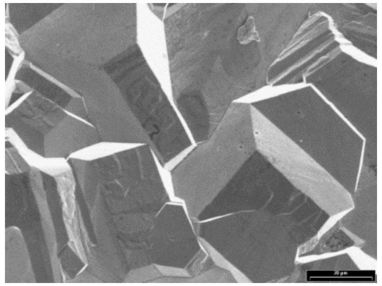

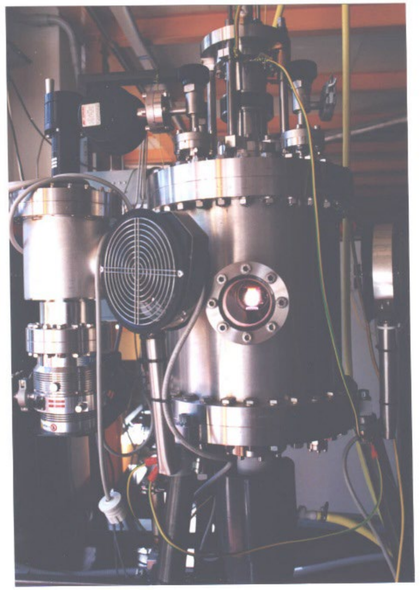

→ DC Plasma Enhanced CVD

System at UNIFI / INFN Florence (1998)

INFN
Istituto Nazionale di Fisica Nucleare

UNIVERSITÀ DEGLI STUDI FIRENZE

Growth methods : epitaxy

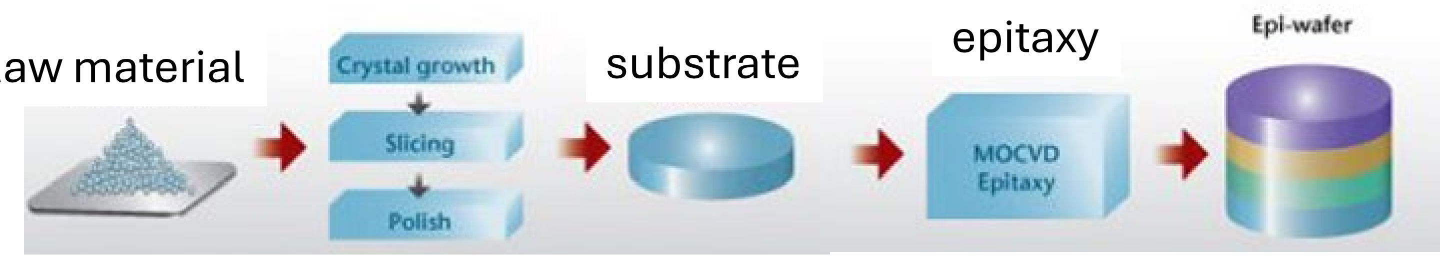

Metalorganic CVD

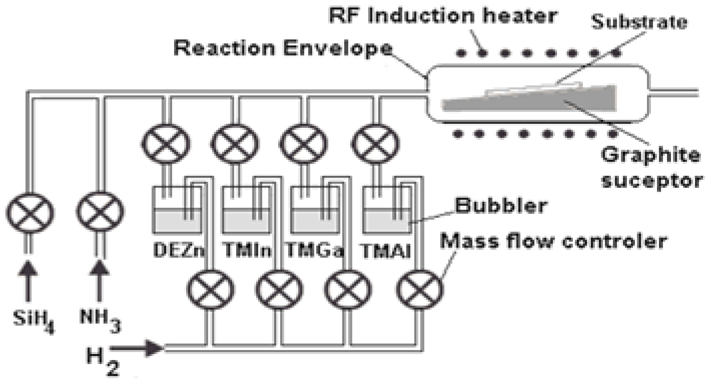

Figure 2. Schematic diagram of MOCVD technique [33].

- Ultrapure precursor gases injected into the reactor,
- metal-organic containing metals and organic ligands

Molecular Beam Epitaxy (MBE):
- sublimation of main elements and dopants
- carried out under UHV pressures 10^{-8} to 10^{-10} Torr.

Method/ type of substrate	Growth temperature/ pressure
MOCVD/Si (111) and etched (001)	AlN: 1050–1200°C; GaN: 1000–1150°C/ atmospheric pressure (101.32 kPa)
MBE/HVPE-grown GaN substrate	660–76°C
MBE/4H-SiC	700–800°C

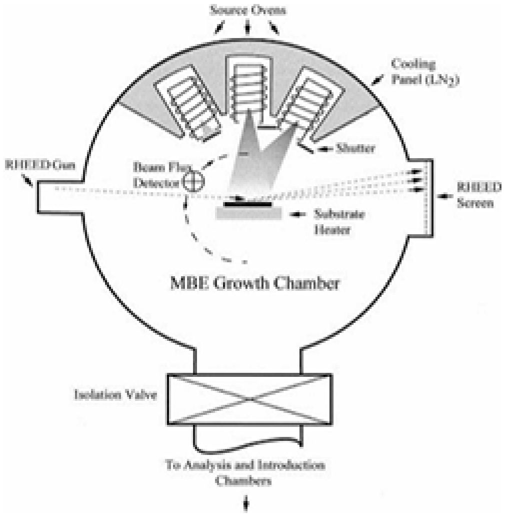

Figure 3. Schematic diagram of the top view of a simple MBE chamber [51].

International Journal of Nanoelectronics and Materials Volume 13, No. 1, 2020 [199-220]

ABX$_3$ crystal structure

Beyond wafers: Emerging WBG semiconductors
The perovskite family

ABX$_3$ structure ($CaTiO_3$) A = inorganic/organic cation, B metal cation (Pb_2^+), X halide ($I^-$and/or Br^-).

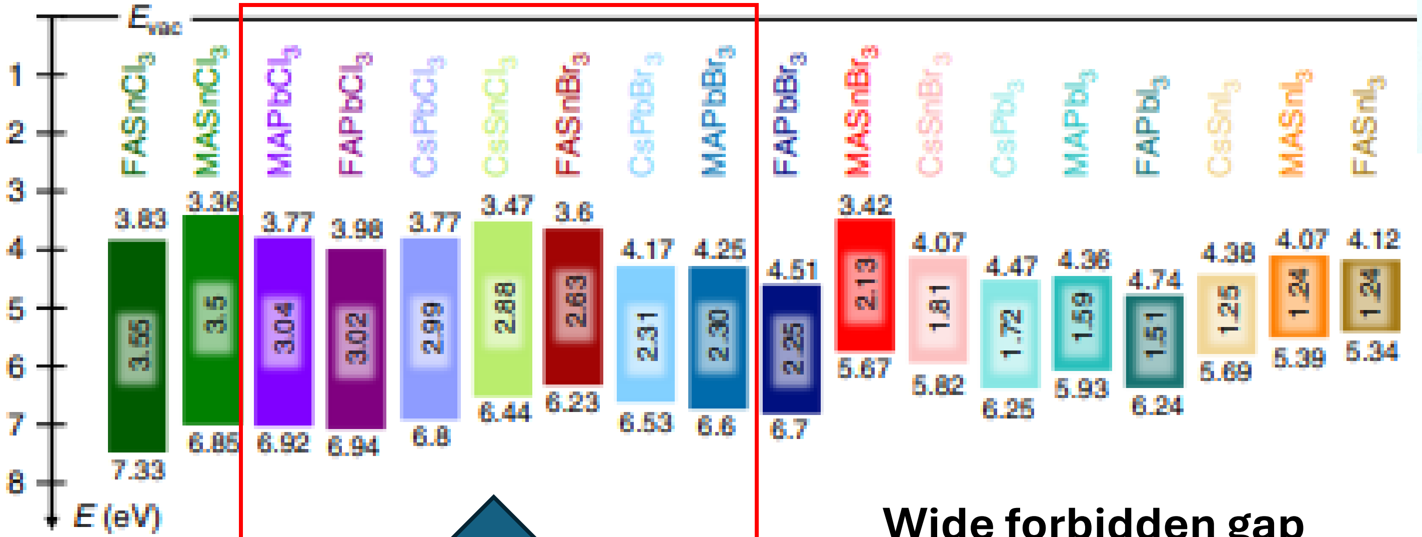

Gap: 2.4- 3.0 eV

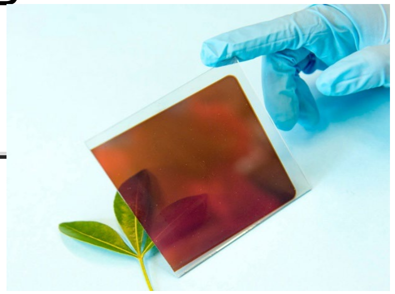

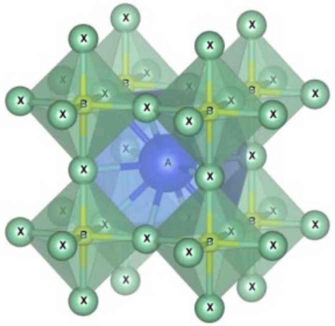

Main application :

- Solar cells

Wide forbidden gap
→ lower dark current – noise

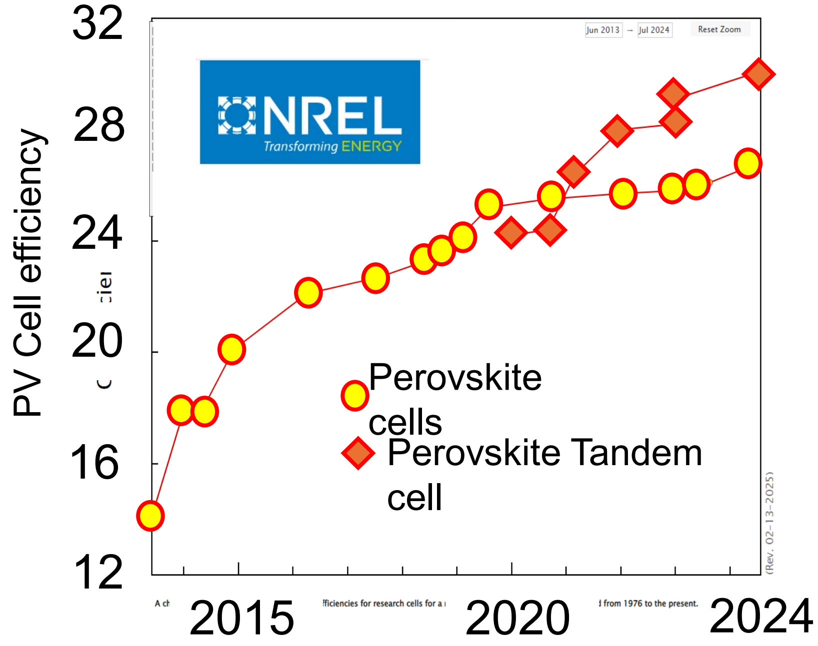

INFN Istituto Nazionale di Fisica Nucleare

Advantages of Metal Halide Perovskites for Radiation Detection I

High attenuation coefficients
→ Thinner

Low mean ionization energies to create an e-h pair
→ Higher efficiency, high sensitivity per unit volume

Shaded areas
Green - projectional radiography (20–100 keV)
Purple - nuclear medical imaging (50–511 keV)
Orange - industrial inspection (80–450 keV)
Blue - homeland security (0.1–3 MeV)

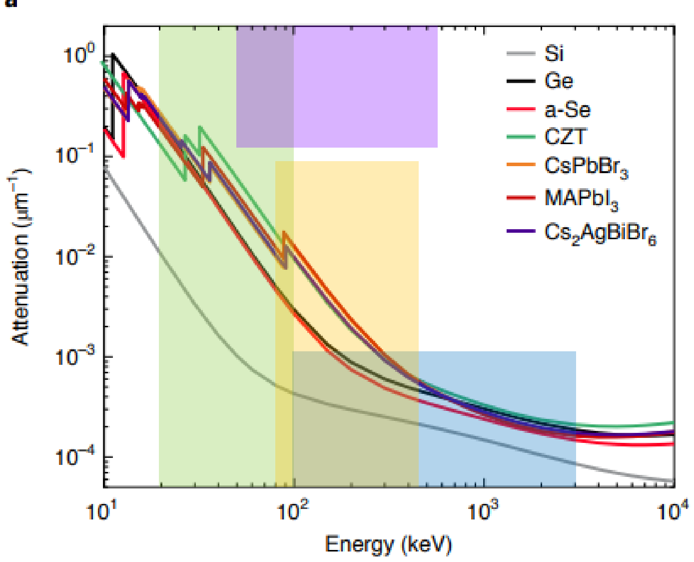

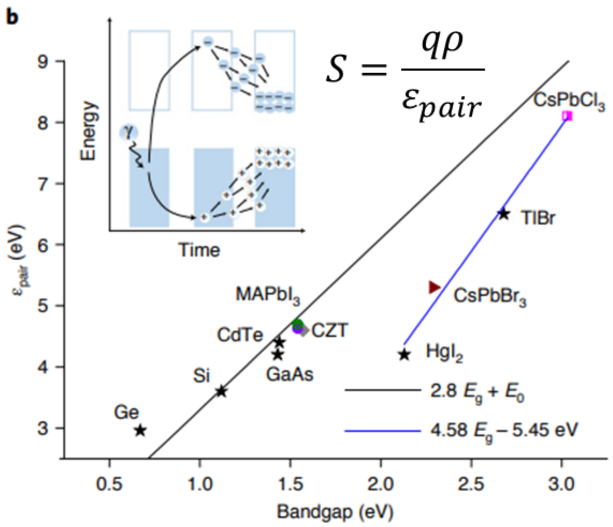

	IC(AIR)	Si	SiC	DIAMOND	CsPbBr3
ρ [g/cm³]	1.29×10^{-3}	2.33	3.21	3.52	4.55
Eg [eV]		1.12	3.26	5.5	2.40
E_i [eV]	34.00	3.60	7.80	16.20	5.30
Sensitivity [nC/Gymm³]	0.038	647	412	217	860

Good optoelectronic properties
- efficient carrier mobility 1–10 cm^2 /(Vs)
- long charge diffusion length

Physical vapour deposition and solution methods

- **Easy, low-cost manufacturing process**
- **Low temperature (RT < 100°C, RT)**

- **Easy scalability, driven by massive solar cell production**
- **Flexible devices**

- **Direct deposition on electrode backplanes**

Solution methods

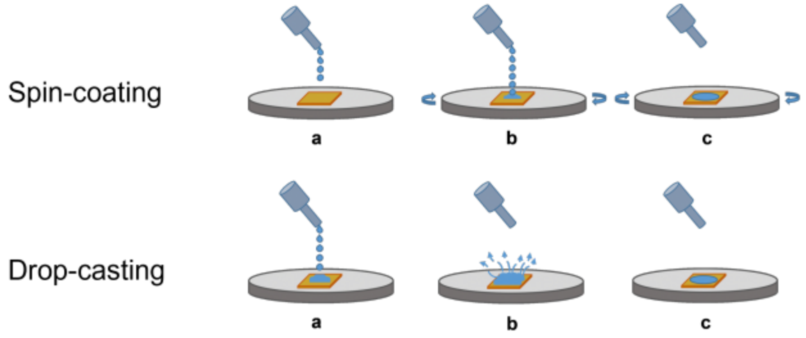

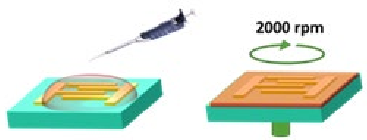

(a)

N. Falsini et al. Sensors 2023, 23, 4930

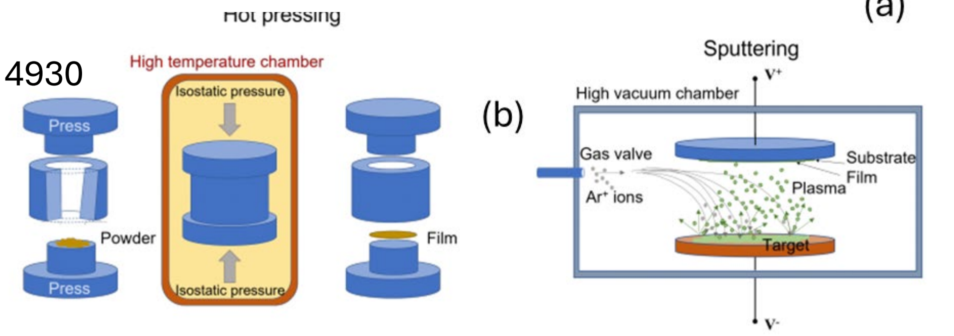

Li et al., Sci. Adv. 10, eadj8659 (2024)

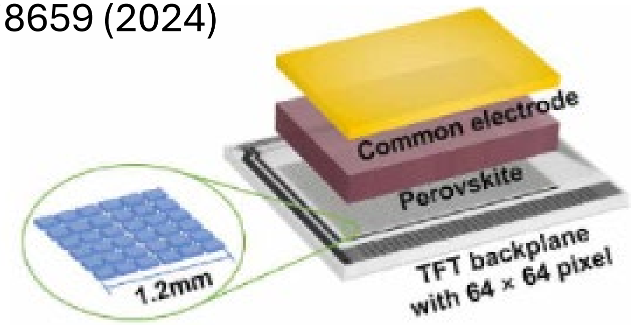

Magnetron Sputtering

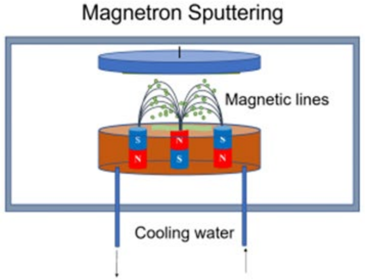

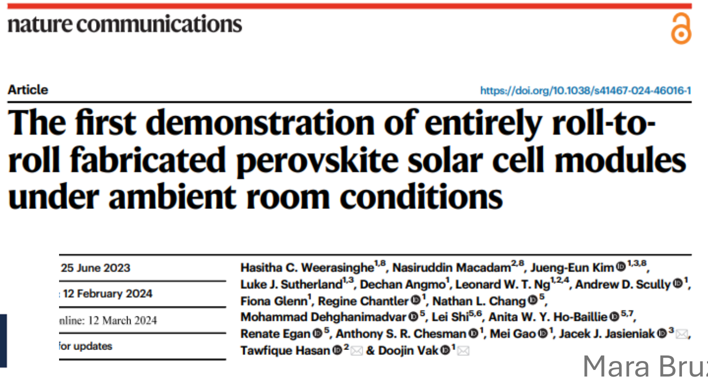

nature communications

Article https://doi.org/10.1038/s41467-024-46016-1

The first demonstration of entirely roll-to-roll fabricated perovskite solar cell modules under ambient room conditions

25 June 2023
12 February 2024
nline: 12 March 2024
for updates

Hasitha C. Weerasinghe[1,8], Nasiruddin Macadam[2,8], Jueng-Eun Kim[1,3,8], Luke J. Sutherland[1,3], Dechan Angmo[1], Leonard W. T. Ng[1,2,4], Andrew D. Scully[1], Fiona Glenn[1], Regine Chantler[1], Nathan L. Chang[5], Mohammad Dehghanimadvar[5], Lei Shi[5,6], Anita W. Y. Ho-Baillie[5,7], Renate Egan[5], Anthony S. R. Chesman[1], Mei Gao[1], Jacek J. Jasieniak[3], Tawfique Hasan[2] & Doojin Vak[1]

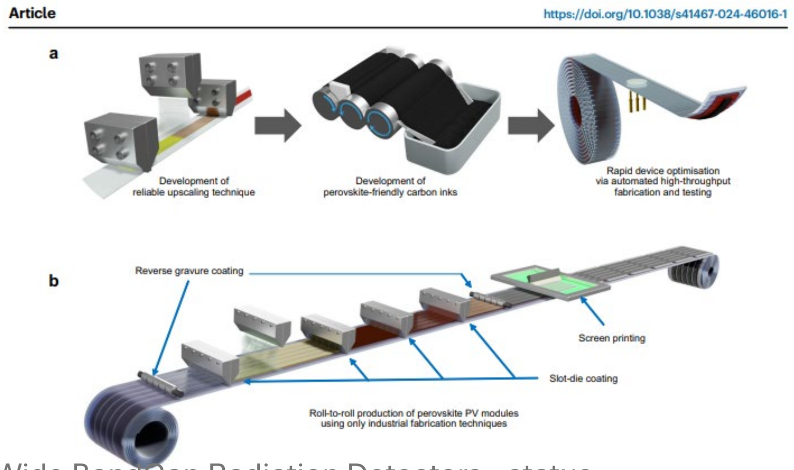

Istituto Nazionale di Fisica Nucleare

Perovskite flexible thin film radiation detectors

Flexible $CsPbBr_3$ QDs perovskite-based detector arrays on PET

Adv. Mater. 2019, 31, 1901644

thin film perovskite ultraflexible detector fabricated on 1.4 µm PET

66 Adv. Sci. 2020, 7, 2002586.

Detectors on flexible polyethylene naphthalate (PEN) substrates inkjet-printed layers of triple cation perovskite (TCP) as X-ray conversion layers

ACS Appl. Mater. Interfaces 2020, 12, 15774–15784

($400\ cm^2$) flexible nylon membrane after loading perovskites

74 Nat. Photonics 2020, 14, 612–617.

multiplexed detector consisting of pressure-sensitive IGZO TFTs and X-ray detectors

Adv. Mater. 2019, 31, 1901644

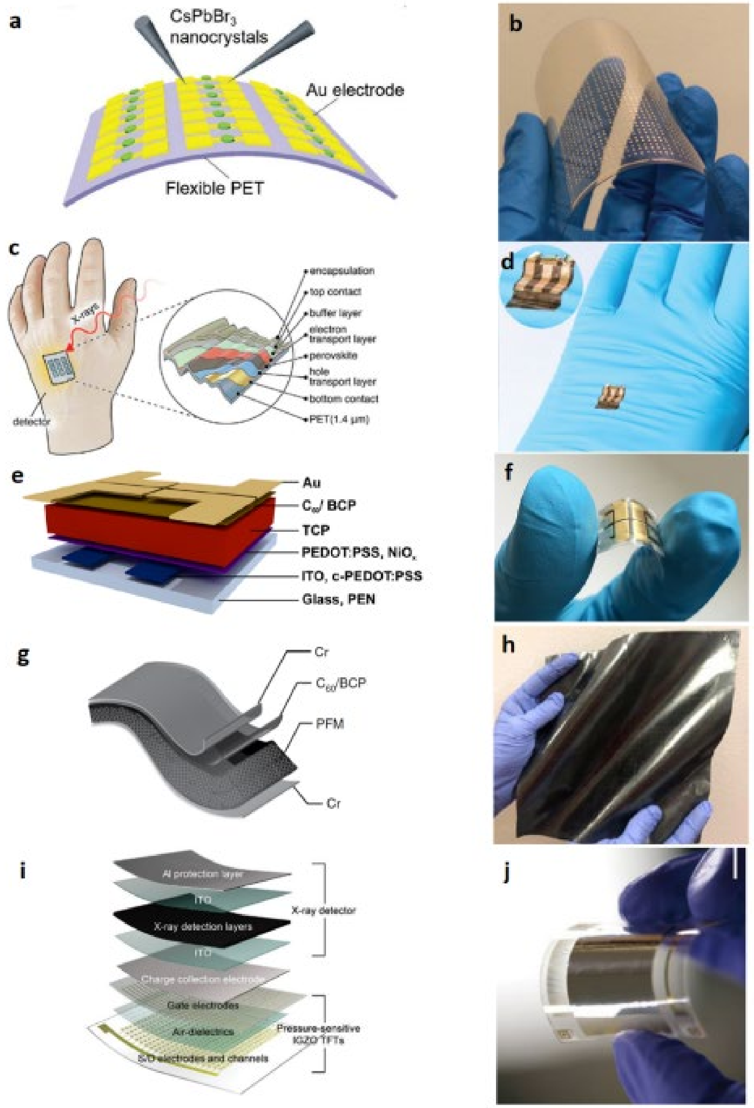

INFN
Istituto Nazionale di Fisica Nucleare

UNIVERSITÀ DEGLI STUDI FIRENZE

Perovskite thin film deposition UNIFI –INFN Firenze I

RF magnetron sputtering @ UNIFI – INFN Firenze

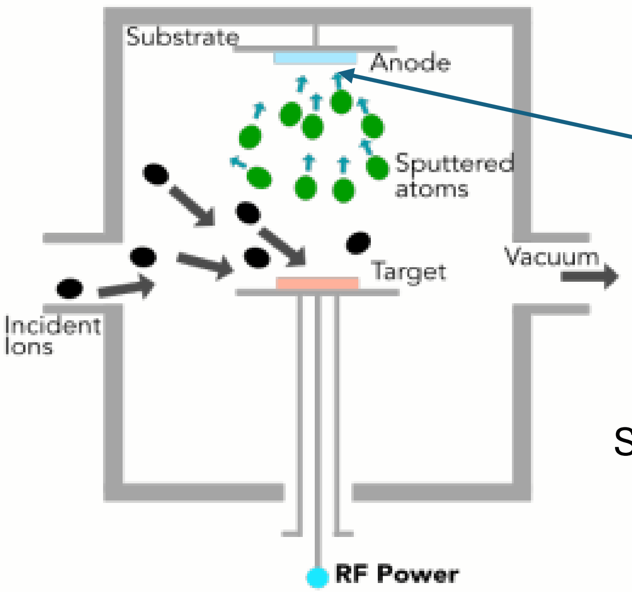

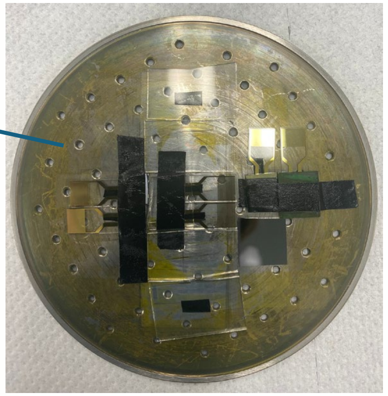

Substrates mounted on anode

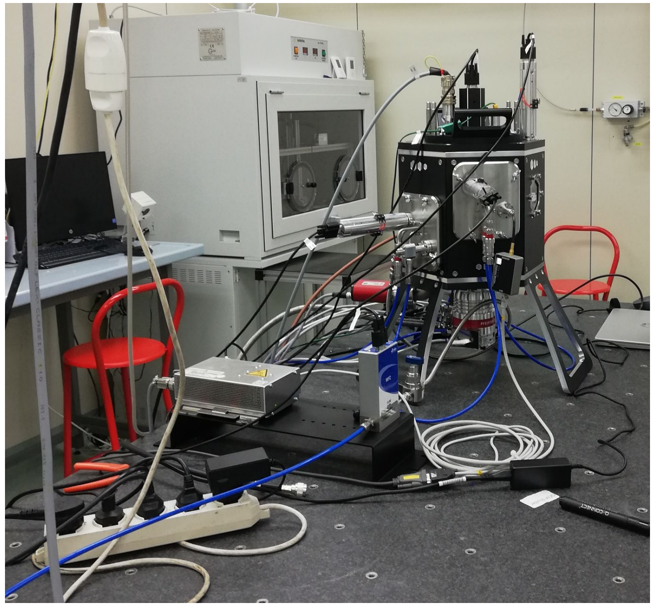

- magnetron sputtering equipment, Korvus HEX system
- RF source 13.56MHz,
- 18W power Ar gas flow 18sccm.
- Room temperature.
- Dynamic working pressure 4×10^{-6} atm, deposition rate 0.5Å/s.
- Film thickness monitored using quartz crystal nanobalance

SEM image @ 100 K magnification of a 500nm $CsPbBr_3$ sample

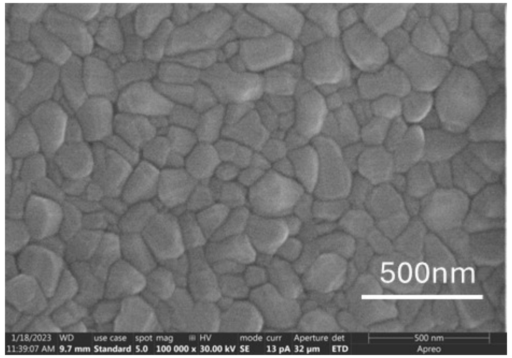

Compact film composed of crystallites of about 100nm size

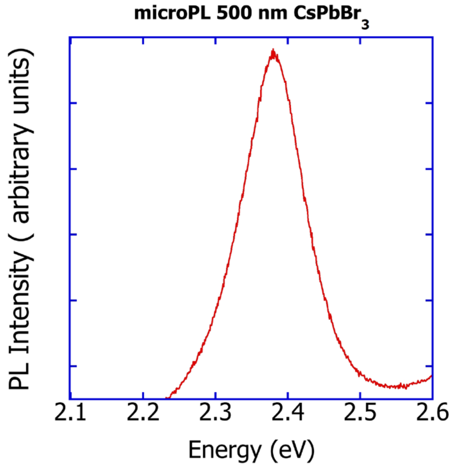

Target production stages of grinding process of two salts CsBr and $PbBr_2$

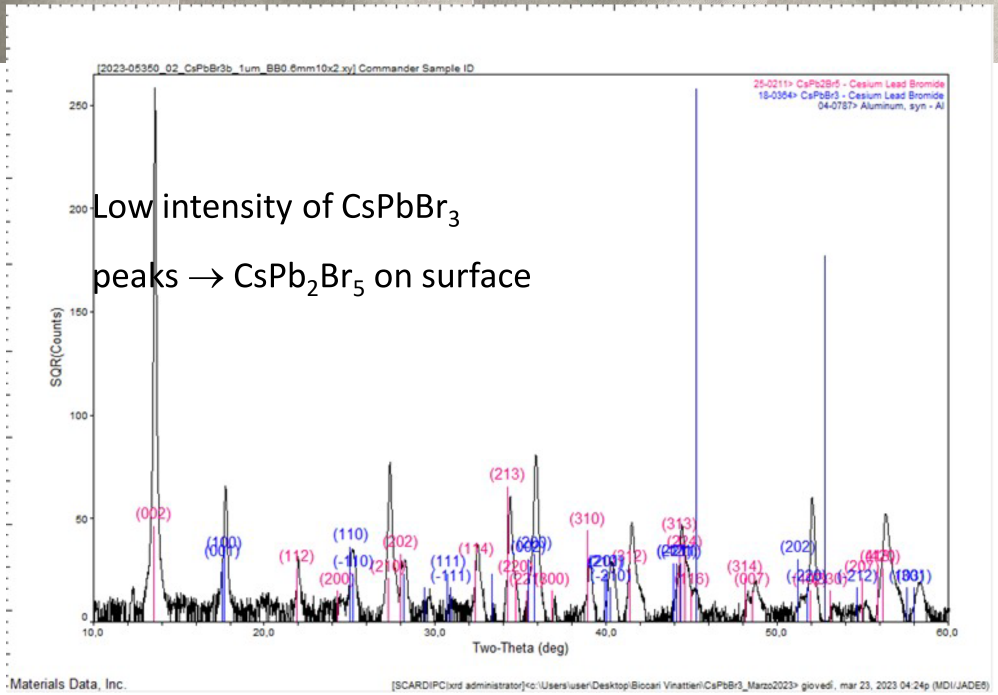

Low intensity of $CsPbBr_3$

peaks $\rightarrow$ $CsPb_2Br_5$ on surface

XRD phase identification for 1 µm at 0.3Å/s

press and obtained target

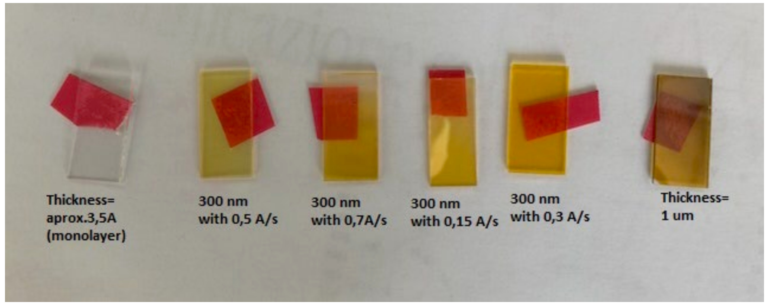

left to right: from crystal monolayer 3.5 Å to 1 µm thickness

Outline

- Introduction : electronic properties of WBG Semiconductors
- Growth processes
  - Beyond wafers: the perovskite family
- **Lattice disorder, defects and energy levels; how to detect**
- Research on WBG Radiation Detectors
  - Explorative studies (blue sky research) in the HEP community
  - Applications in medical field: proton and Flash therapy

Crystalline vs Amorphous

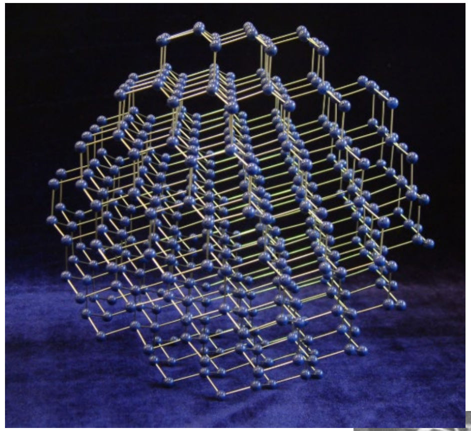

Crystalline : Long-range order and periodic structure

Low lattice disorder → high mobility and lifetime of e-h pairs generated by the incoming particle → complete charge collection.

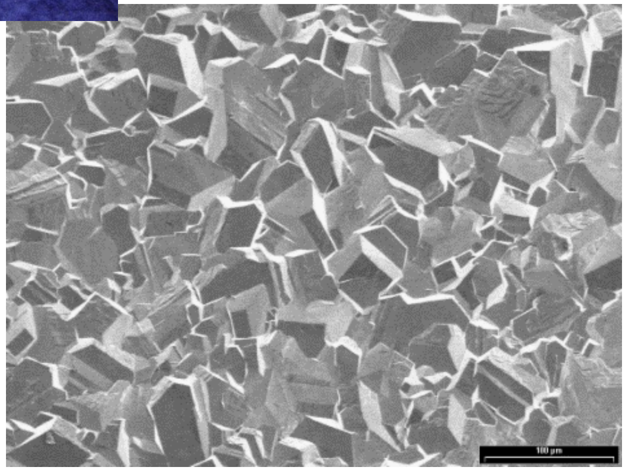

Polycrystalline: crystal organization on the order of micron to mm: grains with different orientation and dimension are surrounded by grain boundaries. E-h suffer of trapping and recombination means at defects,
→ reduced mobility and lifetime → incomplete charge collection.

Amorphous: short-range ordered structure.
→ low mobility, lifetime → incomplete charge collection
→ Less effect on radiation-damage

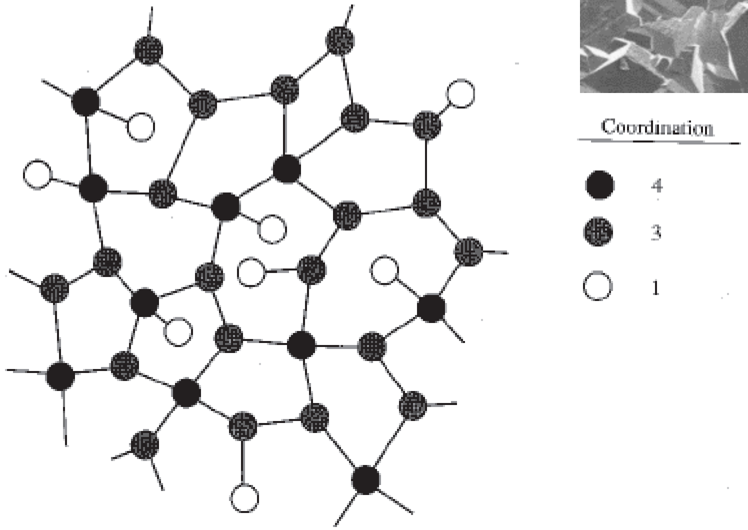

Crystalline vs amorphous

E_g comes as a result of the short-order coordination (molecular bonding)

Anderson model (1958) Perfect crystal: array of equal potential wells. Amorphous: array plus random potential with average amplitude V_0.

Crystalline

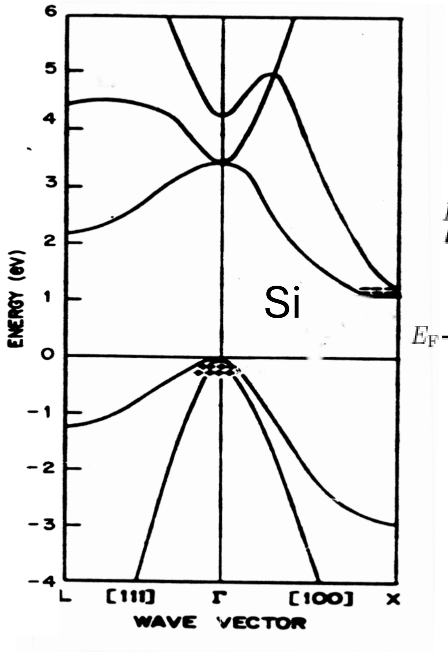

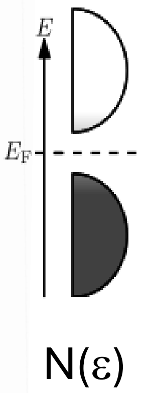

Chelikowsky & Cohen,
Phys Rev B14, 556 (1976)

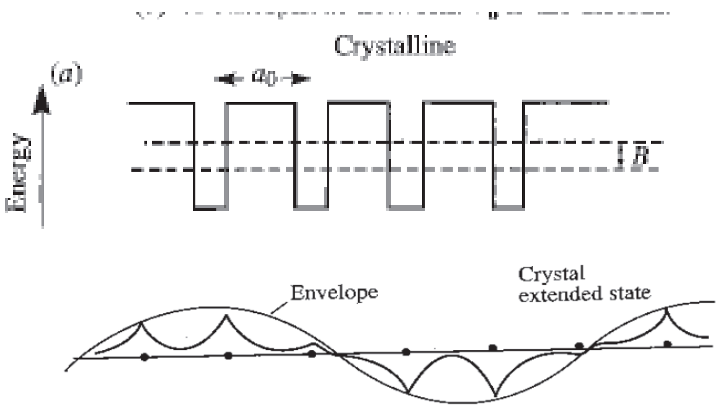

Crystalline: Energy bands described by:

- Energy *vs* k plots
- Density of States (DoS) + Fermi-Dirac
- Electronic properties depend on E(k)

$$m^*_{n,p} = \frac{\hbar^2}{\left(\frac{d^2E}{dk^2}\right)} \qquad \mu_{n,p} = \frac{e\tau}{m^*_{n,p}} \qquad v_{drift} = \mu E$$

amorphous

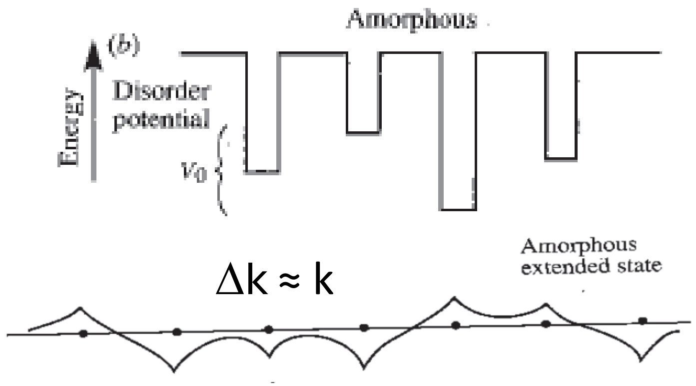

$\Delta k \approx k$

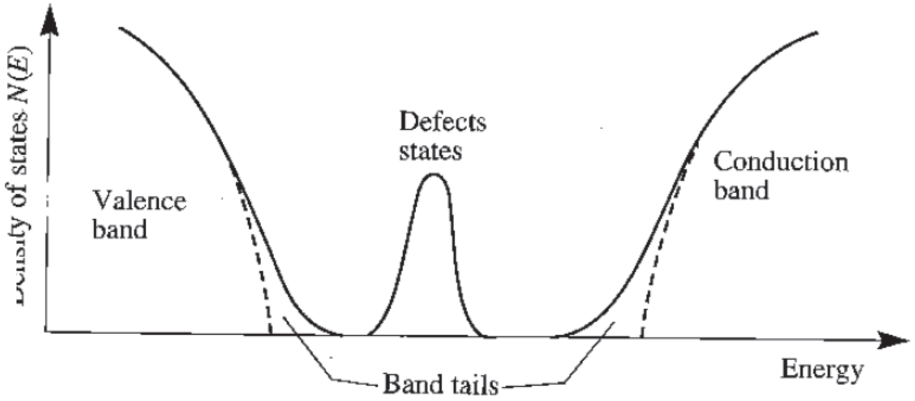

- Energy bands **not described as a function of k** , only by DoS + F-D
- Band tails due to defects settle free carriers mobility edges, low mobility

The effect of crystalline quality : Native / Radiation Induced Defects

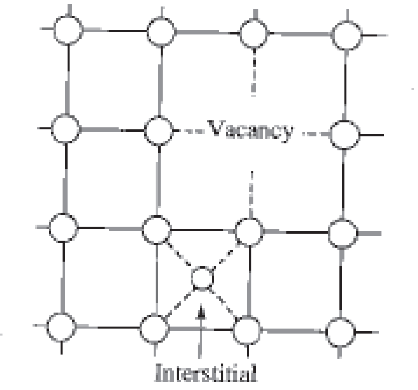

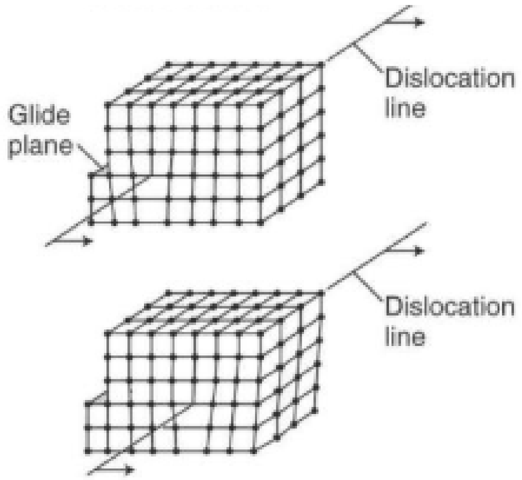

Lattice Disorder	Impurities
Point defects o **Vacancy** o **interstitial**	**Point Defects** o **substitutional (e.g. Dopants)** o **interstitial**
Linear defects o **dislocations**	**Bulk defects** o **precipitates**
Extended defects o **grain boundaries** o **Interfaces** o **Surface**	

Monocrystalline bulk

Polycrystalline structures
example: synthetic (Chemical Vapour Deposited) Diamond

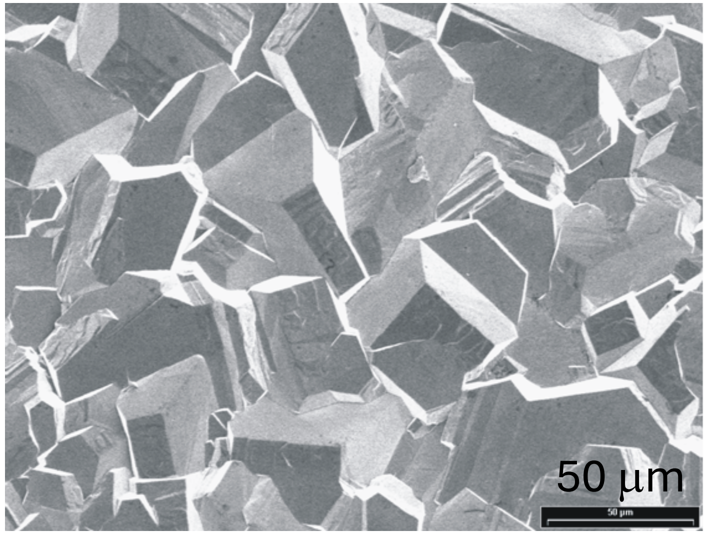

After polishing and
Material removal

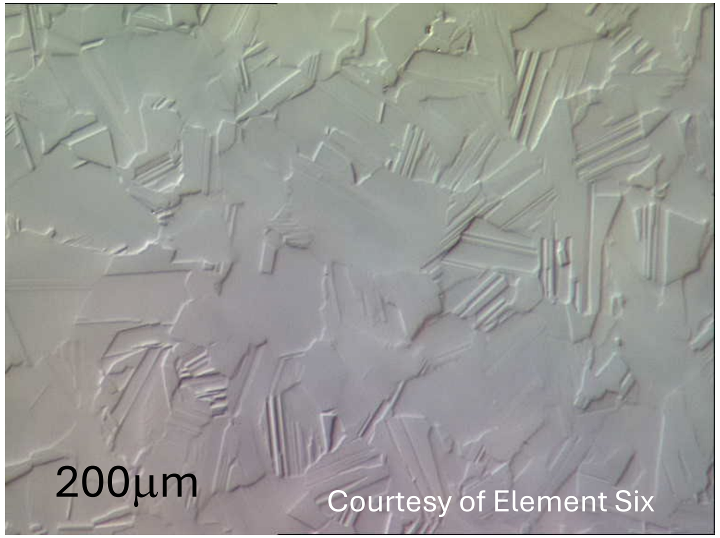

Presence of grain – boundaries around the crystallites

- Columnar growth – increased quality at growth side

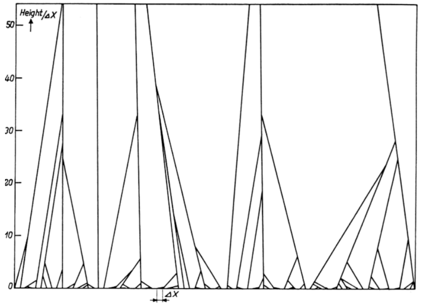

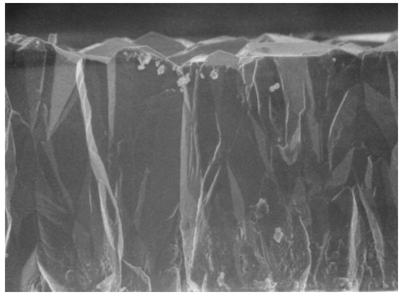

CVD diamond made in 1998

by UNIFI / INFN Florence

INFN Istituto Nazionale di Fisica Nucleare

UNIVERSITÀ DEGLI STUDI FIRENZE

Epilayer grown on substrates: need of single crystals with matching lattice constant and thermal expansion coefficient.

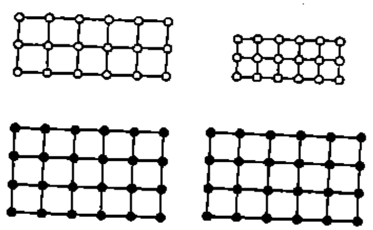

Lattice matched   Lattice mismatched

Dislocations due to lattice mismatch

Threading dislocation $\rightarrow$ extends from strained layer system, going through layer or bending at interface into misfit dislocation

Misfit dislocation: **crystal defect localized at the substrate/layer interface**, generated during the growth process and associated with the ending or starting of an atomic plane in the crystal in case of compressive or tensile system

GaN-on sapphire vs GaN-on-GaN epilayers

Table 2. Lowest reported threading dislocation density (TDD) in GaN drift layers on different substrates.

Parameter	Si	Sapphire	SiC	GaN
Lattice mismatch	−17%	−33%	3.5%	0
Thermal Mismatch	116%	−23%	24%	0
TDD (/cm^2)	~10^9	~10^9	~10^7	~10^4

Micromachines 2020, 11, 519

dislocation

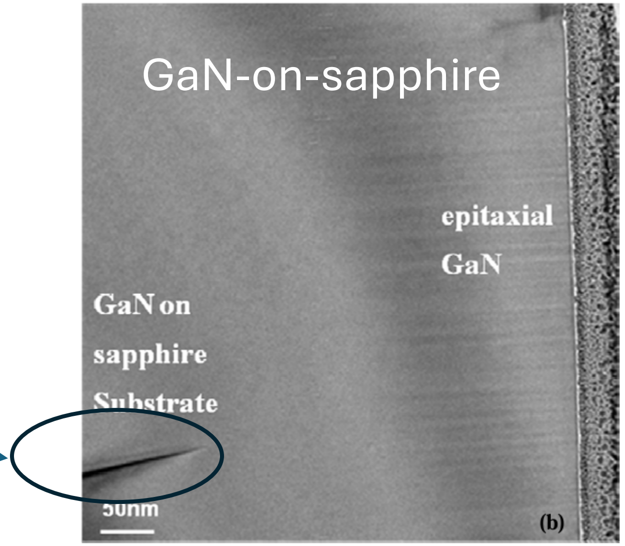

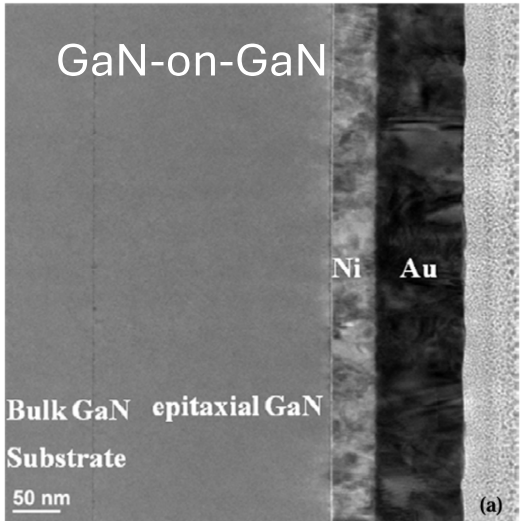

CS MANTECH Conference, 2013, TEM pictures

Energy levels related to Defects

Shallow Levels

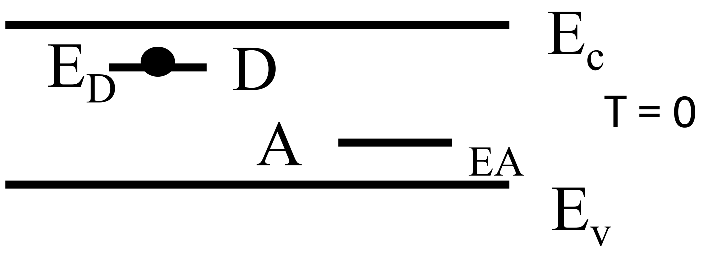

→ **fully ionized at moderate temperatures**
→ **Doping and avalanche layers**

Deep Levels

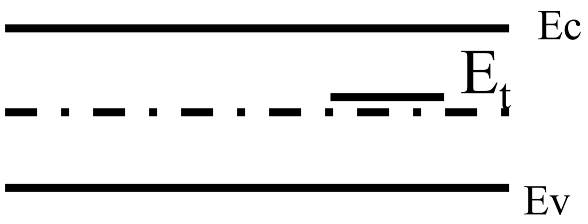

$E \approx E_g/2$

close to midgap

- **Charge trap**
- **Generation/ recombination centres**
- **Dopant removal / compensation**

Main doping shallow levels in Si and WBGSs

	4H-SiC	GaN	Diamond	Si
E_D [meV]	60 (N)	22 (Si)	570 (P)*	45 (P)
E_A [meV]	250 (Al)	160 (Mg)	500 (B)	44 (B)

*n-type doped diamond is still a challenge, many promising elements (Li,Na, N, P, O, S). P is regarded as the most promising dopant, however, the doping efficiency of phosphorus in diamond at room temperature is low (50–90% compensation rate). Electronics **2024**, 13, 1703. https://doi.org/10.3390/electronics13091703

Generation / recombination due to deep levels in gap

$E_t = energy\ level$

$N_t = trap\ concentration$

$\sigma = capture\ cross\ section$

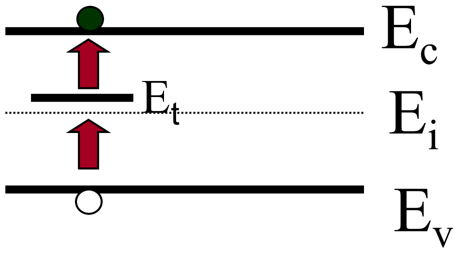

SRH model

$$U = -\frac{\sigma_n \sigma_p v_{th} N_t}{\sigma_n \exp\left(\frac{E_t - E_i}{K_B T}\right) + \sigma_p \exp\left(\frac{E_i - E_t}{K_B T}\right)} n_i = -\frac{n_i}{\tau}$$

Depletion region: generation of free carriers

- Affecting noise
- Need for cooling

$$J_{gen} = q|U|W = q\frac{n_i}{\tau}W$$

W = depletion depth

if $E_i \approx E_t\,;\sigma_n \approx \sigma_p \quad \rightarrow \tau \cong \frac{1}{\sigma v_{th} N_t}$

Neutral region: Recombination of carriers due to deep levels

→ Bulk resistivity go to intrinsic

→ Free cariers removal

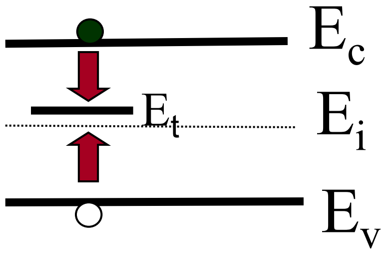

Si : linear increase of midgap level N_t with fluence →→ linear increase of leakage current per unit volume

$J(\varphi) = \alpha\varphi W$ α = damage constant

W = depletion depth

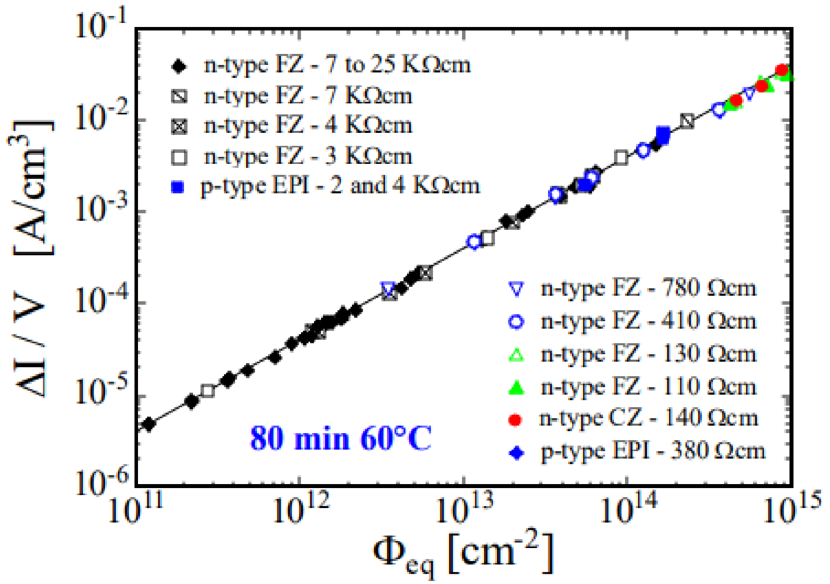

Generation of leakage current due to midgap defects is not present in WBG semiconductors

The radiation induced lattice disorder is not affecting the leakage current

WBGs
→ low leakage current @ RT
→ even after very high fluence

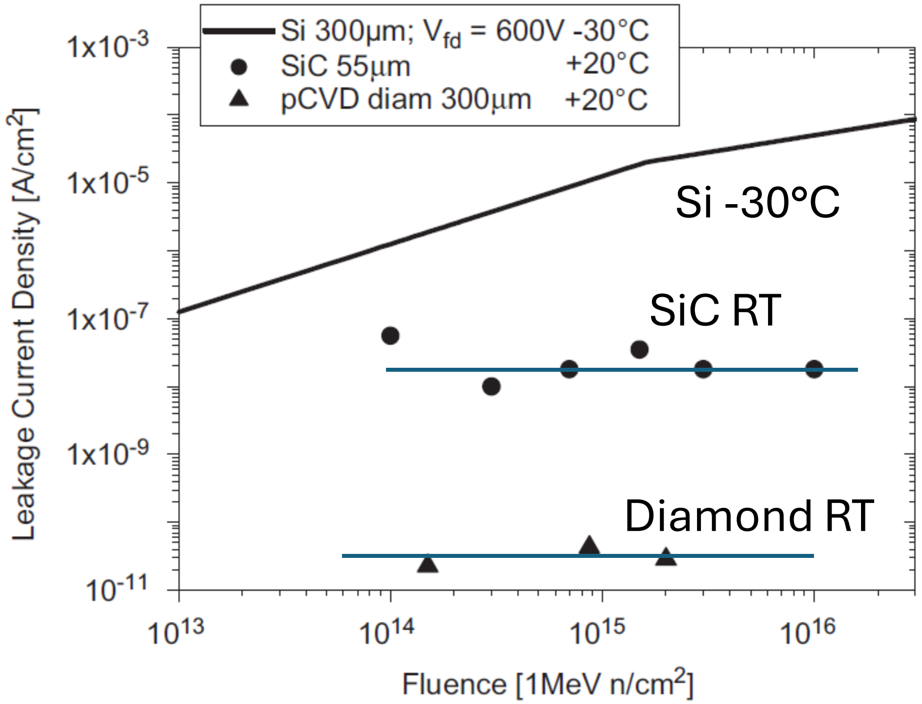

SiC and Diamond leakage current compared to Si

Comparing radiation tolerant materials and devices for ultra rad-hard tracking detectors

Mara Bruzzi[a,*], Hartmut F.-W. Sadrozinski[b], Abraham Seiden[b]

[a]INFN Florence—Dipartimento di Energetica S. Stecco, Via. S. Marta 3, Firenze, Italy
[b]SCIPP, University of California Santa Cruz, Santa Cruz, CA 95064, USA

Available online 11 June 2007

Radiation induced Defects

particle → Si_S → E_K>25 eV

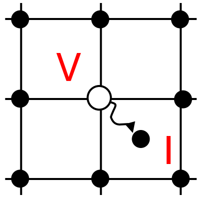

Vacancy + Interstitial → *point defects (V-O, C-O, ..)*

E_K > 5 keV *point defects and clusters of defects*

♦ ^{60}Co-gammas
- Compton Electrons with max. $E_\gamma \approx$1 MeV (no cluster production)

♦ Electrons
- E_e > 255 keV for displacement
- E_e > 8 MeV for cluster

♦ Neutrons (elastic scattering)
- E_n > 185 eV for displacement
- E_n > 35 keV for cluster

Displacement energy - energy needed to displace an atom from the lattice site: 13-20 eV Si , 43eV Diamond .

Initial distribution of vacancies in (1µm)^3 after 10^{14} particles/cm^2
[Mika Huhtinen ROSE TN/2001-02]

10 MeV protons 24 GeV/c protons 1 MeV neutrons

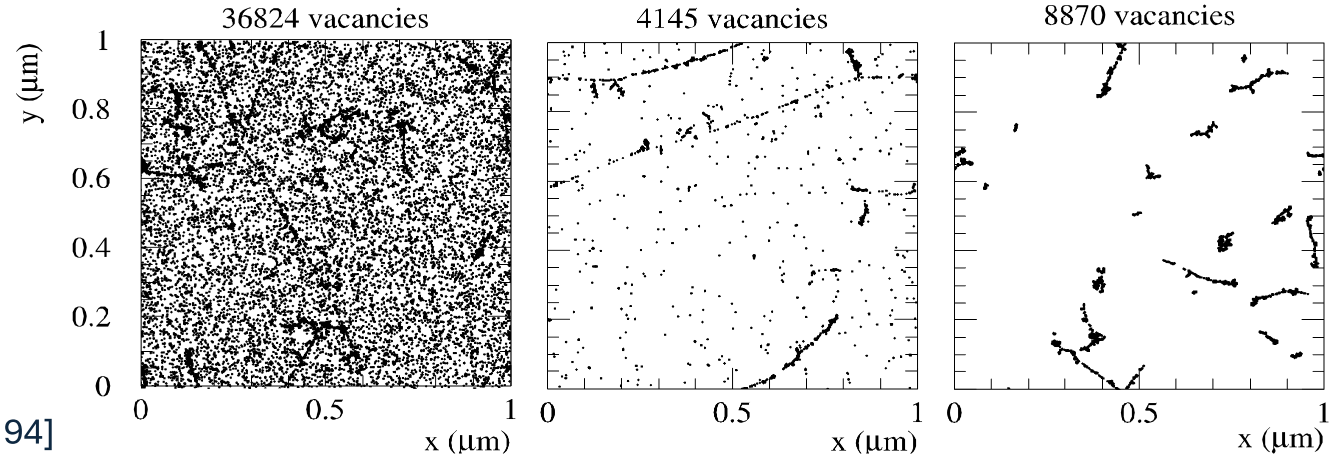

[Mika Huhtinen NIMA 491(2002) 194]

Threshold displacement energy in WBGS

particle → *Lattice atom* $\xrightarrow{+\ Td}$ **Frenkel pair** Vacancy + Interstitial

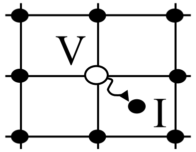

Diamond, SiC, GaN semiconductors are supposed to be RADIATION HARDER then Si due to their **higher displacement energy**

	Td (eV)	
Si	13-20	
SiC	16(Si) / 40 (C)	*AIP Advances* 9, 055007 (2019)
GaN	73.2(Ga) / 32.4 (N)	*J. Appl. Phys.* 105, 123527 (2009)
Diamond	70	Jour Nuclear Materials 419 (2011) 32–38

4H-SiC

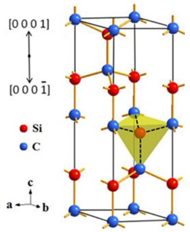

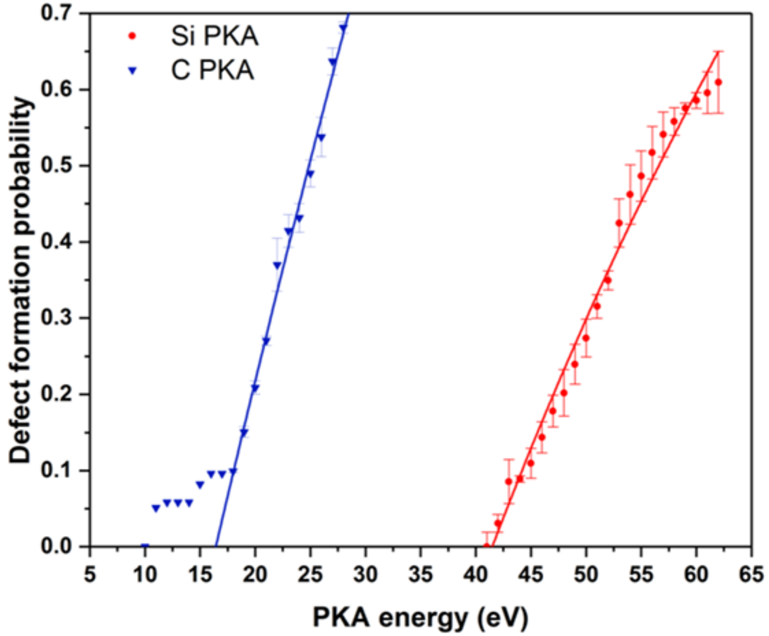

FIG. 4. Defect formation probabilities for both Si and C PKA.

How to detect electrically active defects ?

Defect Spectroscopy in semiconductors

1. Thermally Stimulated Currents TSC
2. Deep Level Transient Spectroscopy DLTS
3. Photo Induced Current Transient Spectroscopy PICTS

Thermally Stimulated Current: TSC

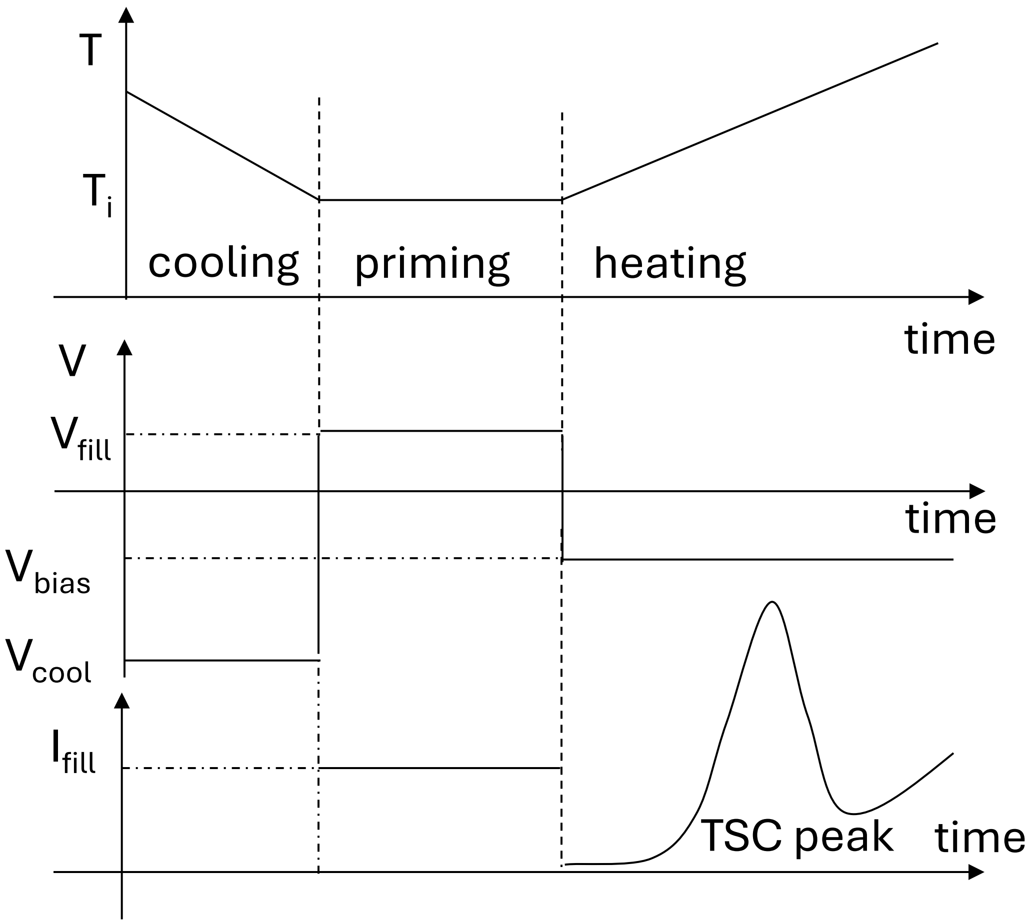

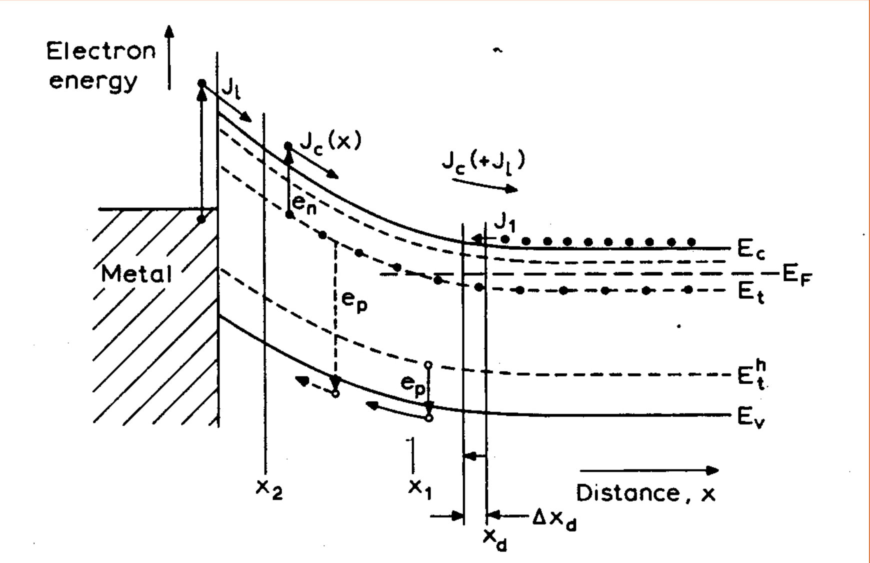

$$\frac{dn_t}{dt} = -e_n \cdot n_t$$

$$e_n = N_c \sigma_n v_{th} \cdot e^{-\frac{E_c - E_t}{KT}}$$

$$I_{TSC}(T) = -\frac{1}{2} q \cdot A \cdot N_t \cdot W \cdot e_n(T) \exp\left(-\frac{1}{b}\int_{Ti}^{T} e_n(T) dT\right)$$

TSC

Low Temperature Shallow Donor Removal in n-type Si irradiated with neutrons

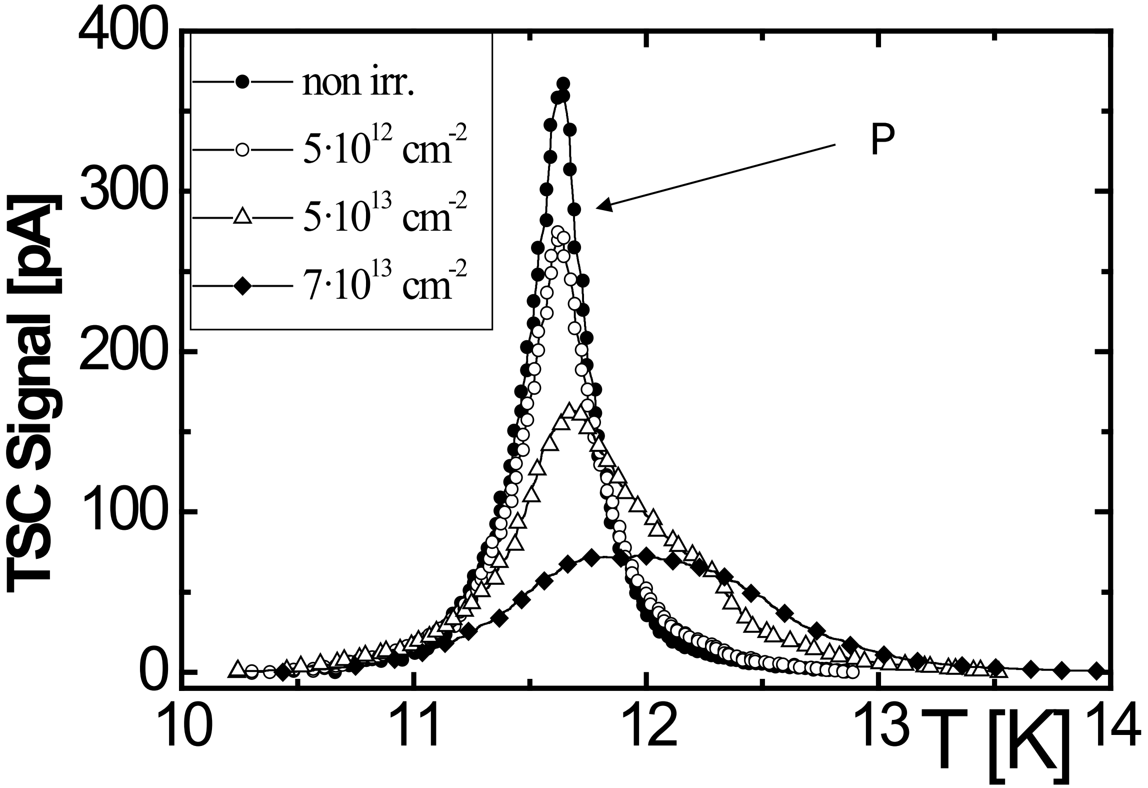

J. Phys. D: Appl. Phys. 33 (2000) 299–304. Printed in the UK PII: S0022-3727(00)06399-3

Thermally stimulated currents analysis of the shallow levels in irradiated silicon detectors

E Borchi†‡, M Bruzzi†‡, Z Li§ and S Pirollo†‡

High Temperature: Deep levels due to Native defects in CVD Diamond

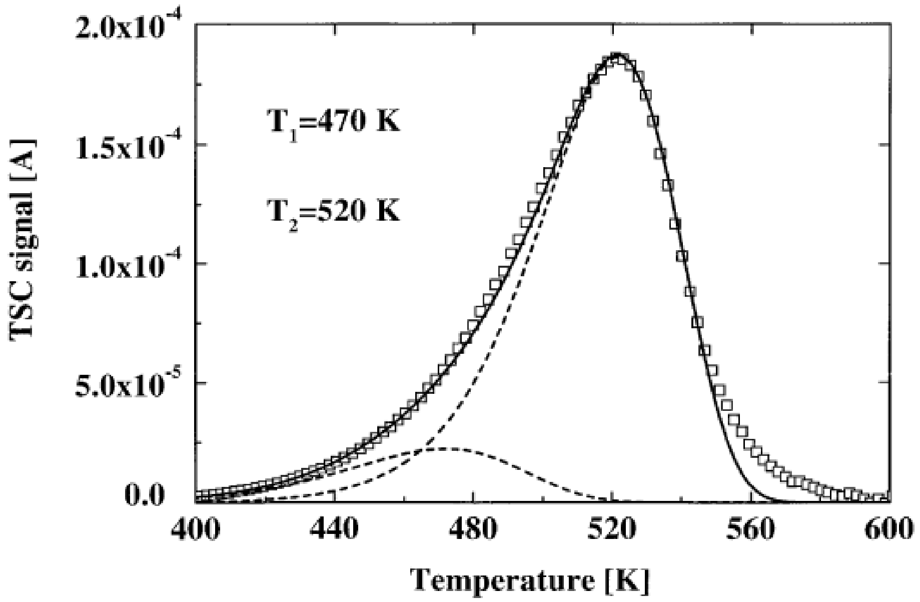

Nuclear Instruments and Methods in Physics Research A 426 (1999) 181Ð184

Deep Level Transient Spectroscopy DLTS

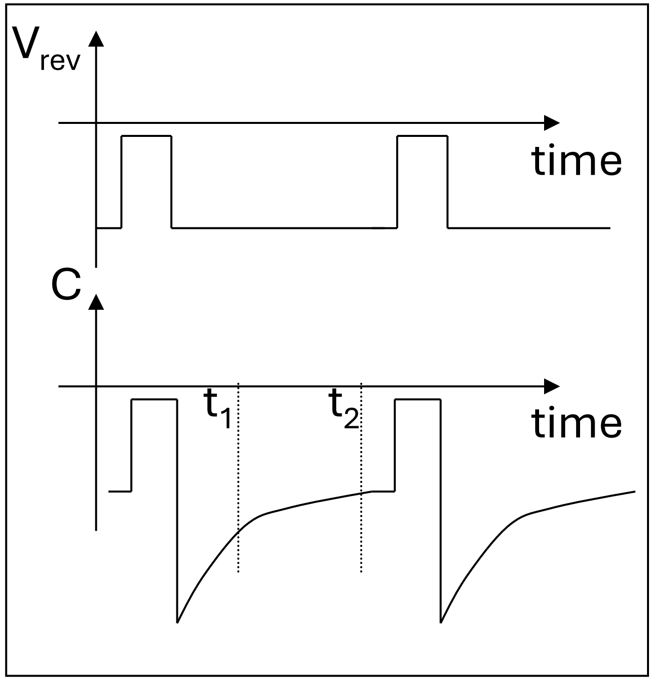

$$S = \Delta C_0 \left(e^{-e_n(T)t_1} - e^{-e_n(T)t_2} \right)$$

$$e_n(T_{\max}) = \frac{t_2 - t_1}{\ln(t_2 / t_1)} \alpha T_{\max}^2 \cdot e^{-E_t / KT_{\max}}$$

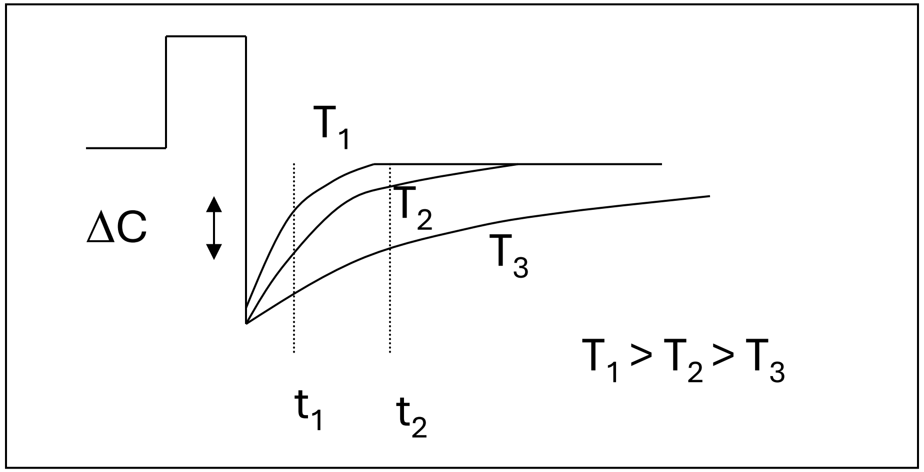

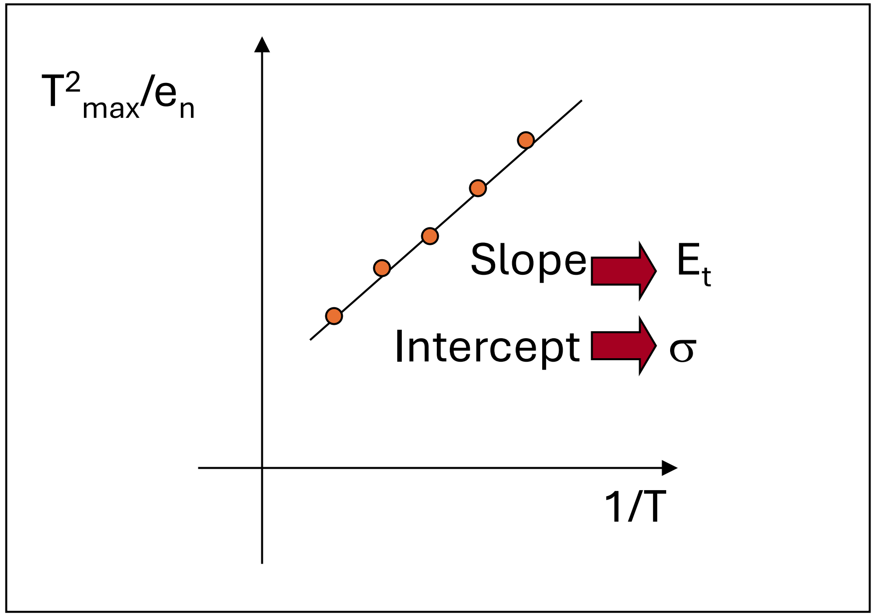

Example: DLTS in Silicon f =10^{11} cm^{-2} 5.3MeV neutrons
ROSE Coll. NIM A 466 (2001) 308-326

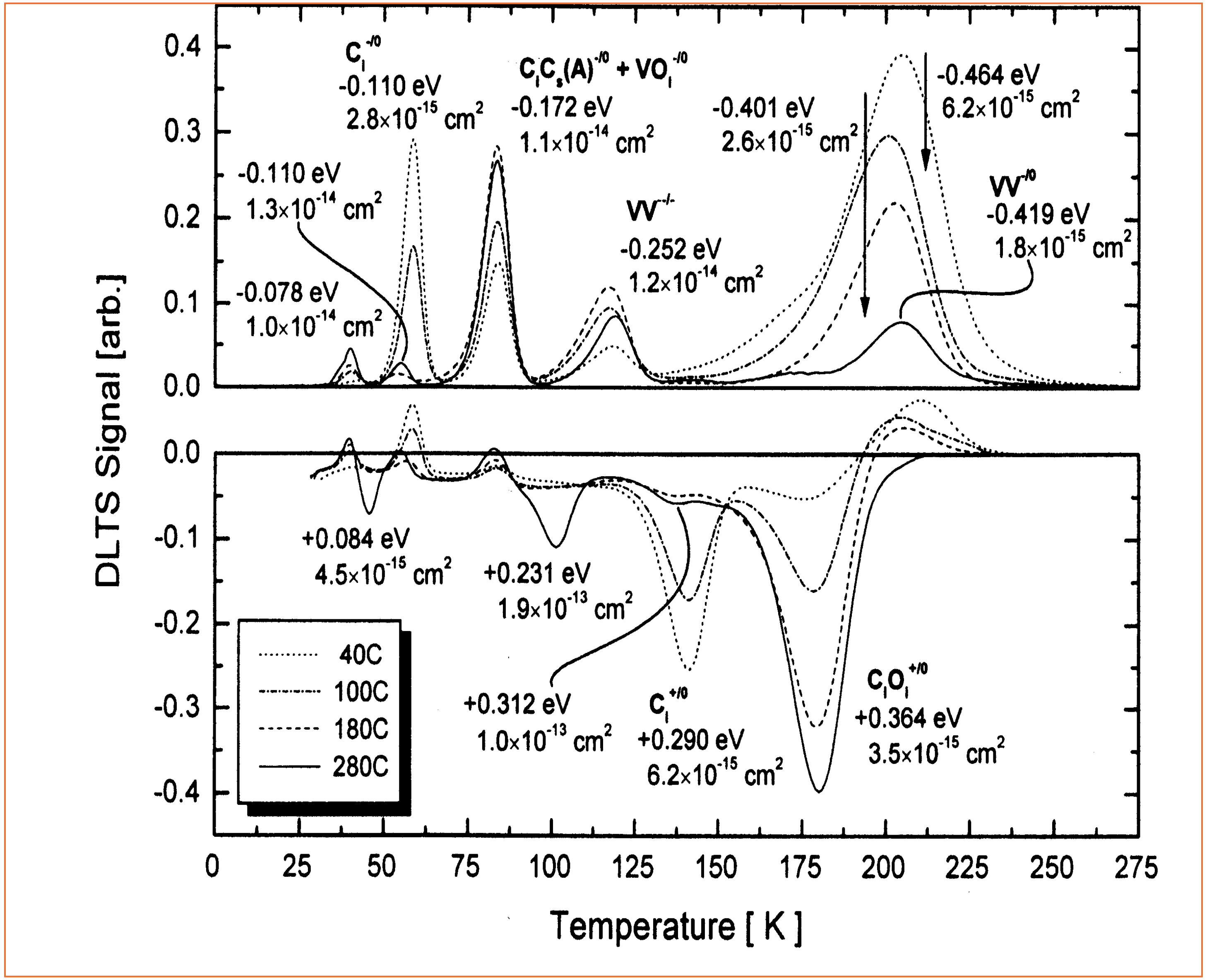

Example: DLTS in 4H-SiC

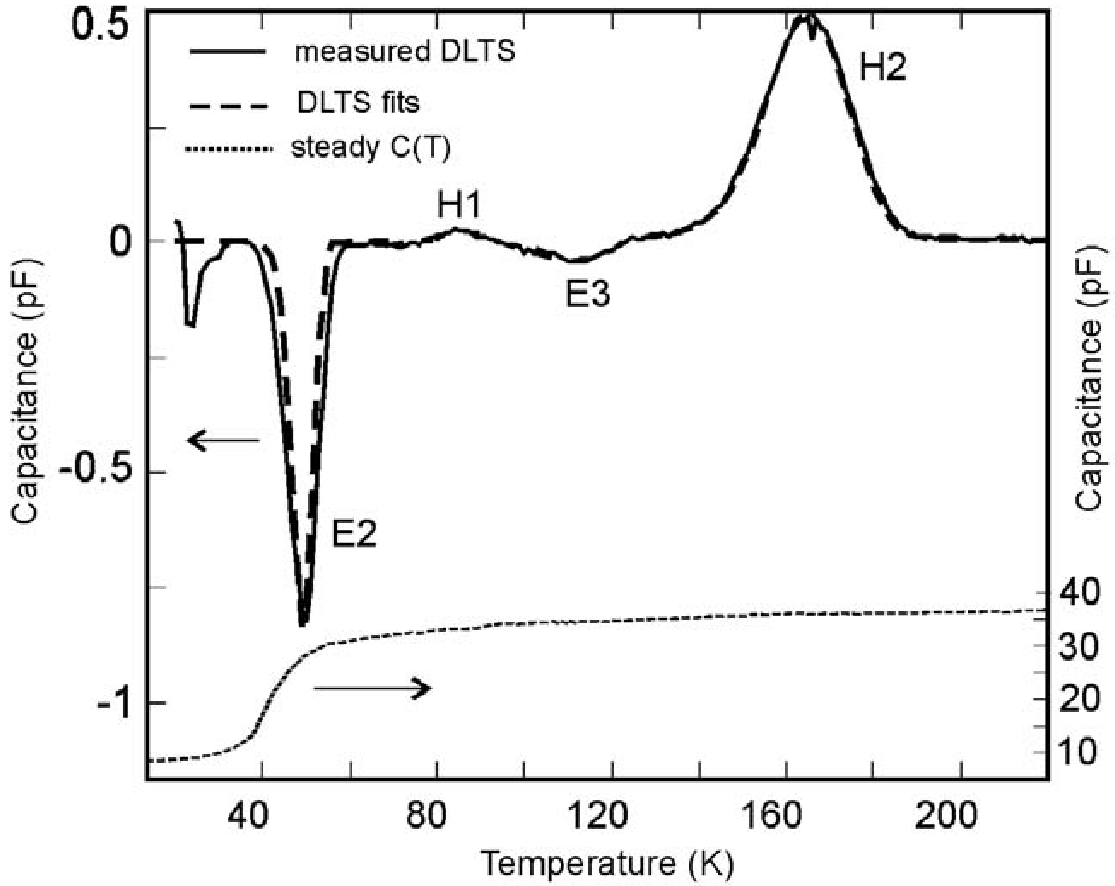

Level	Defect	E (eV)	σ ($\cdot 10^{-15}$ cm^{-2})	N_t ($\cdot 10^{15}$ cm^{-3})	Notes
E_1	Shallower N	~0.05[a]	–	1.1	Observed only by current techniques.
E_2	Deeper N	0.1±0.01	10–200		(E,σ) deduced from Arrhenius plot. Overall N_t from $C(V)$ at 300 K.
E_3	–	0.15±0.01	~0.01	<0.1	
E_4	$Z_{1/2}$	0.63–0.67[a]	3–20[a]	<0.01	
H_1	–	0.11±0.01	0.01–0.1	0.2	Data from I-DLTS, TSC and TSCAP correlation. Not observed by C-DLTS.
H_2	Shallower B	0.28±0.01	0.2–1	0.04–0.1	(E,σ) from Arrhenius plot.
H_3	Deeper B	0.58–0.63[a]	10–100[a]	<0.01	

The superscript a indicates data taken from literature—these cases were checked for agreement with our measurements.

4H-SiC n-type epitaxial wafer p^+n junction
p+ Al implantation in the epilayer 40 µm thick,
n (nitrogen N) doped with density $N_D=1.1\times10^{15}$ cm^{-3}

D. Menichelli et al. / Diamond & Related Materials (2006)

Outline

- Introduction : electronic properties of WBG Semiconductors
- Growth processes
  - Beyond wafers: the perovskite family
- Lattice disorder, defects and energy levels; how to detect
- **Research on WBG Radiation Detectors**
  - **Explorative studies (blue sky research) in the HEP community**
  - Applications in medical field: proton and Flash therapy

DRD3: Semiconductor Detectors

- DRD3 benefits from previous RD50 and
- RD42 communities

- realization of the strategic developments outlined by Task Force 3 (TF3) in the ECFA road map
- promoting blue-sky R&D in the field of solid-state detectors.

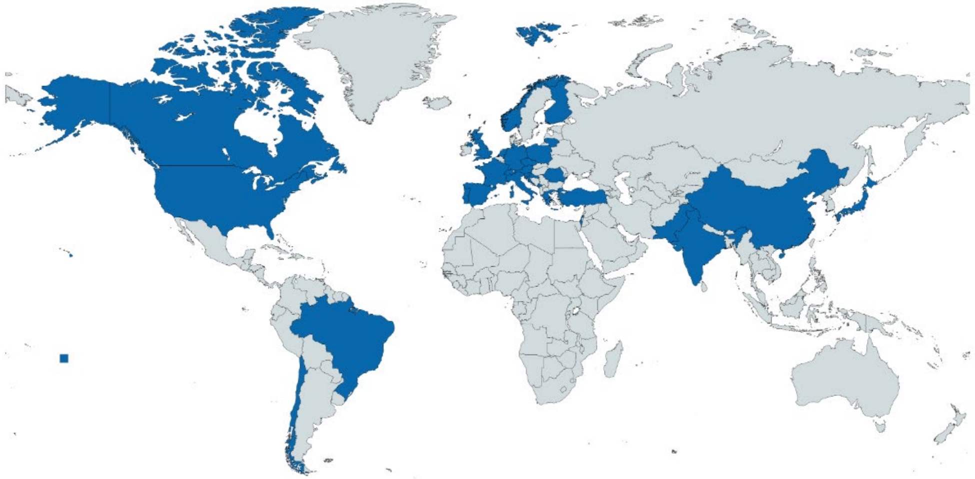

- CB Board chair : Giulio Pellegrini (CNM Spain)
- Spokesperson: Gregor Kramberger (JSI Slovenia) deputies
- Webpage: https://drd3.web.cern.ch/

- Large Collaboration: 143 institutes
  - 600+ interested people
  - ~ 70% are from Europe, 15% from North America

- 1st DRD3 collaboration meeting (17-21 June 2024);
- 2nd collaboration meeting (3-6 Dec 2024)

- Focus widened from pure radiation hardness (HL-LHC Ph-2 upgrades) to lepton collider needs
- Large interest in CMOS (DMAPS) sensors
- **Blue sky → Non-silicon-based detectors**

DRD3: Research Structure

WP - DRDTs
WP1 - DRDT 3.1 Monolithic CMOS sensors
WP2 - DRDT 3.2 Sensors for 4D-tracking
WP3 - DRDT 3.3 Sensors for extreme fluences
WP4 - DRDT 3.4 3D-integration & interconnections

Working Groups - WGs
WG1 Monolithic silicon technologies
WG2 Hybrid silicon technologies
WG3 Radiation damage characterization and sensor operation at extreme fluences
WG4 Simulations
WG5 Characterization techniques, facilities
WG6 Wide band-gap and innovative sensor materials
WG7 Interconnections and device fabrication
WG8 Dissemination and outreach

DRD3___Silicon_Detectors___Scientific_Proposal_27052024_V3.1.pdf

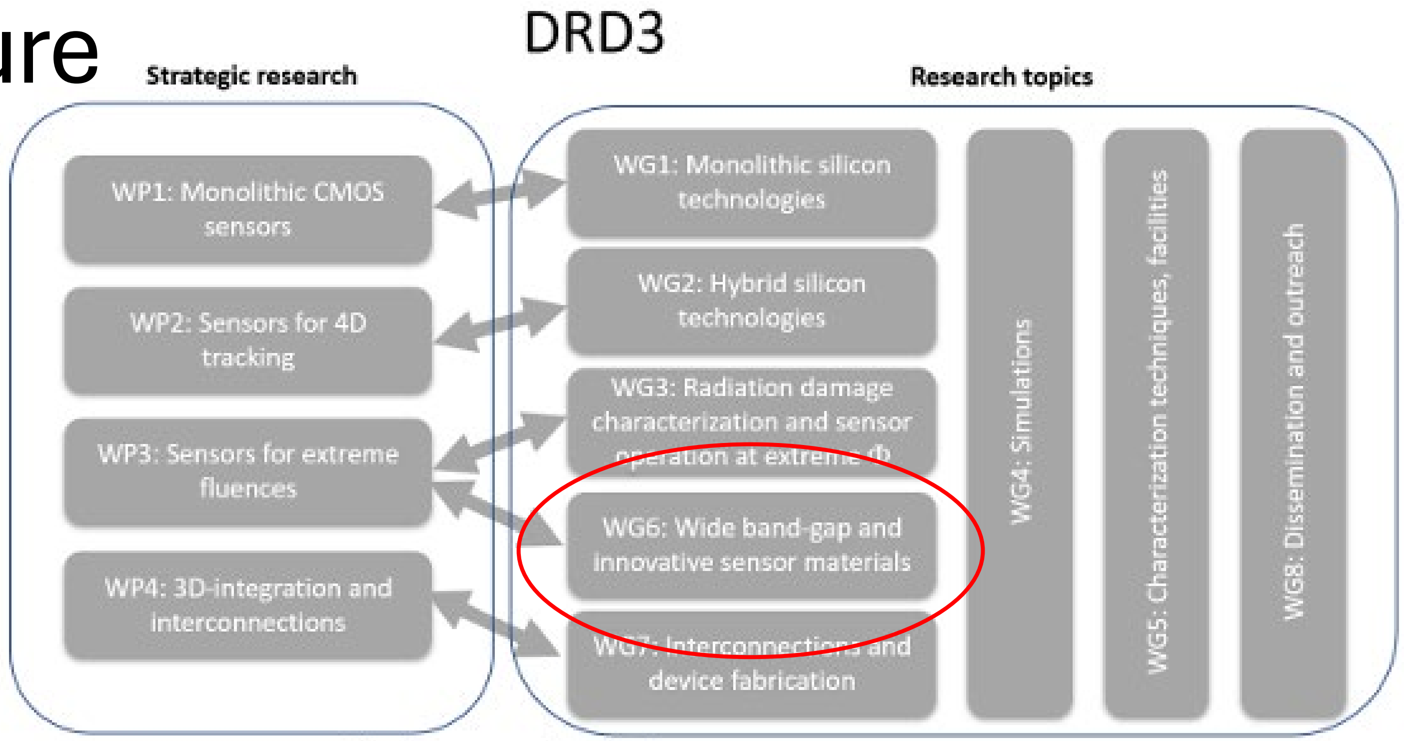

Close but not exclusive links
between corresponding WP and WG

WG 6 - Wide Bandgap and Innovative Sensor Materials

→ GaN / SiC / Diamond

Convenors:
Alexander Oh (alexander.oh@cern.ch)
Xin Shi (xin.shi@cern.ch)

Meetings:

WG6 General Meetings: https://indico.cern.ch/category/18202/

Proposals:

- GaN for MIP detection - CERN-DRD3-PROJECT-2024-001
- SiC LGAD Detector - CERN-DRD3-PROJECT-2024-002
- 3D diamond detectors - CERN-DRD3-PROJECT-2024-003

Contacts:
Email: drd3-wg6-conveners
Meetings: Indico Page
E-group subscription: drd3-wg6-non-silicon
Mattermost: WG6 channel

Materials under investigation in WG6:

- Silicon Carbide
- Diamond
- Gallium Nitride

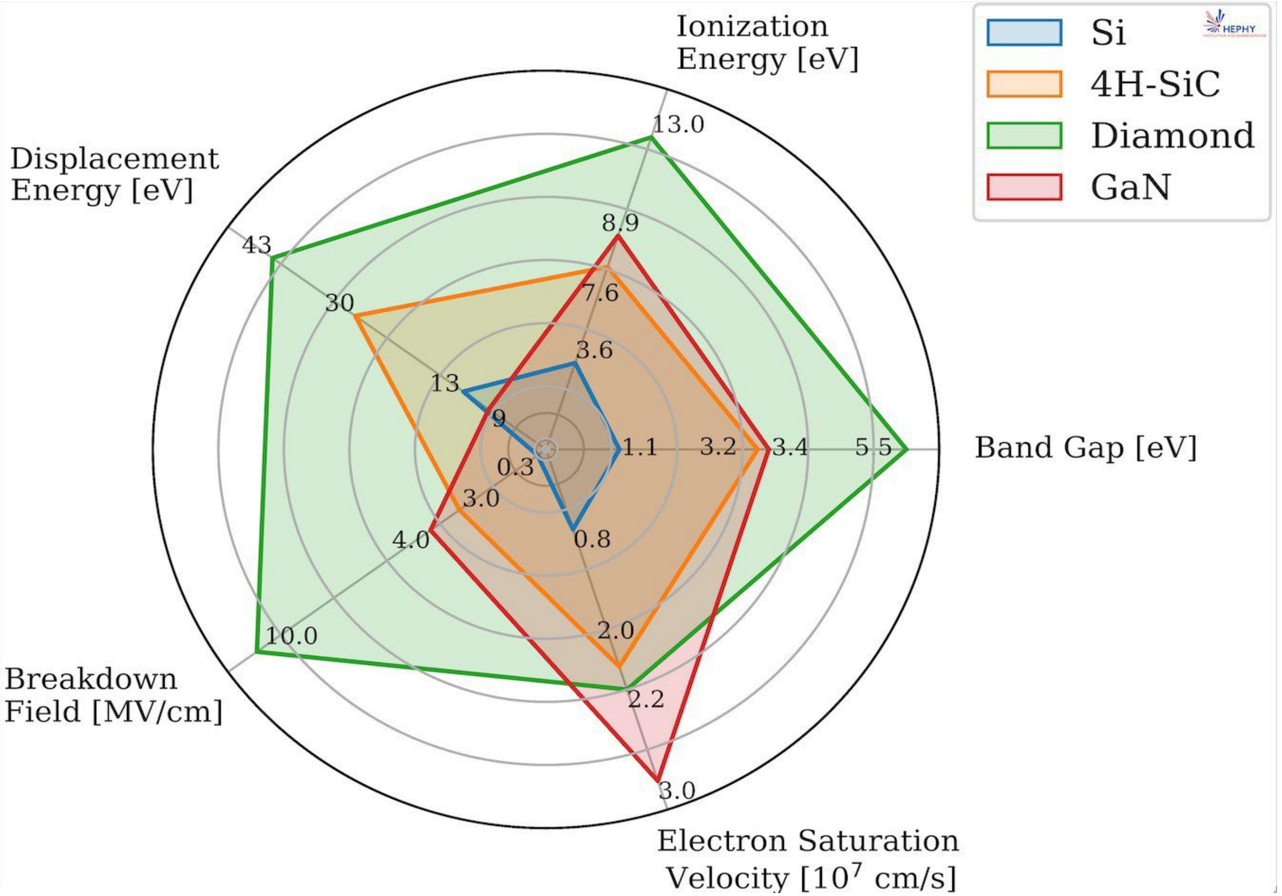

Gallium Nitride

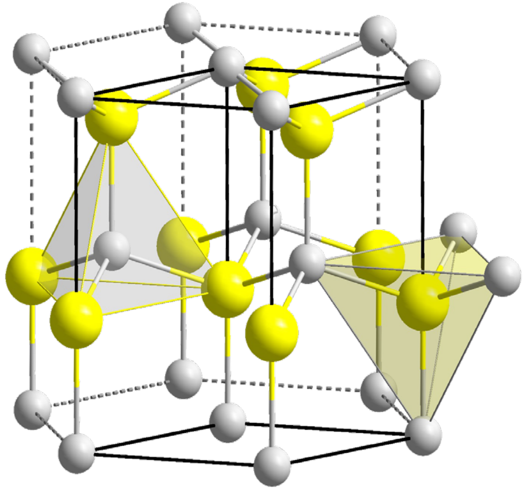

- Wide direct bandgap semiconductor, E_g = 3.4 eV wurtzite crystalline structure
- High electron mobility (up to 2000 cm^2/Vs)
- High breakdown voltage (600-1200 V/µm)
- High atomic bond energy (~9 eV/atom)
- Higher power density and faster switching speed compared to silicon, use in power electronics

DRAWBACKS: less mature technology, typically with high dislocation density >10^6 cm^2

Loss of carriers due to deep traps at dislocations

Impact on mobility of charge carriers

Better GaN growth methods holds the key to the future (GaN-on-GaN)

Neutron irradiation to 10^{18} neq/cm^2 in August 2024 at JSI

- **Note: GaN FETs still functional after >10^{17} neq/cm^2 protons irradiation**

Gallium Nitride: α detection

DRD3

- Sandwich structure grown on HVPE free-standing bulk GaN

- Schottky contact on Ga side by depositing circular Ni/Au pads

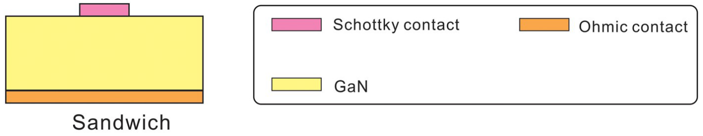

https://doi.org/10.1116/1.3690644

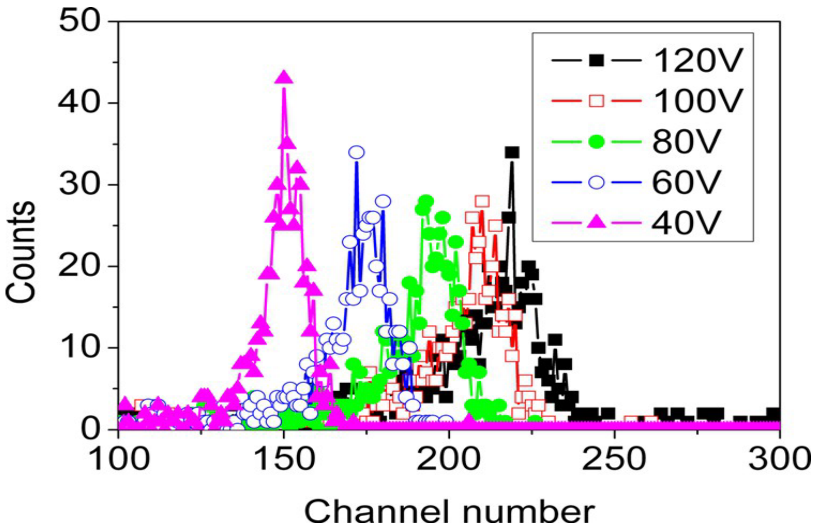

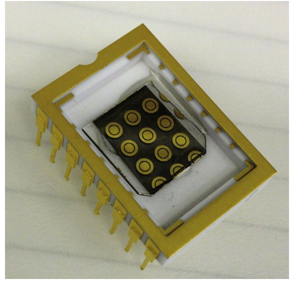

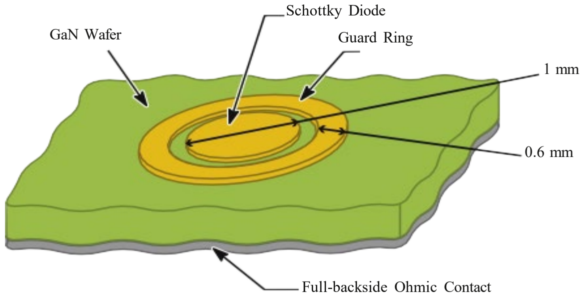

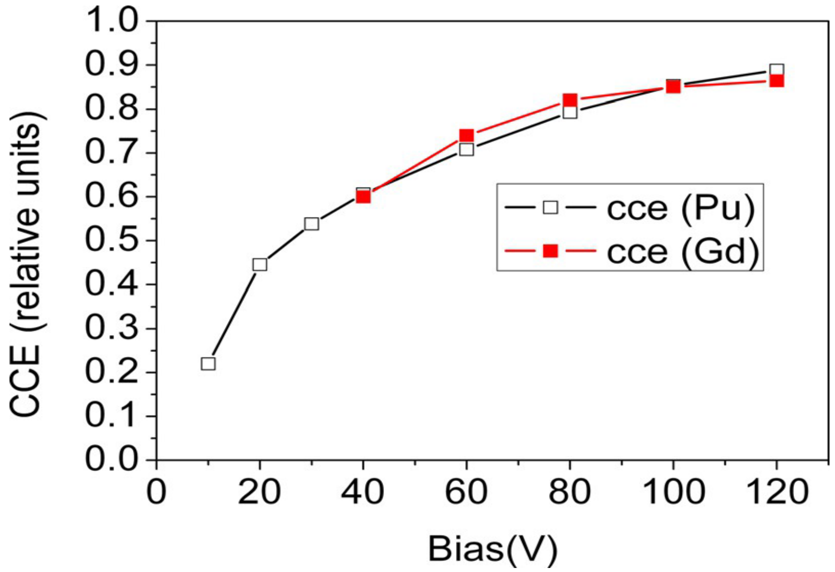

- charge collection efficiency (CCE) close to 100% for α-particles with energy up to 5.1 MeV.

GaN Schottky device

Fabricating GaN Schottky devices using 8 µm GaN epi-layer on GaN native substrate

- At the Canadian National Research Council (NRC) and CNM-Barcelona

- 2” wafer
- rear-side Ohmic metal with high T anneal
- front-side Ni/Au Schottky metal with ~0.8 eV barrier after rapid thermal anneal
- Variable area devices with & without guard rings to suppress surface leakage
  - significantly improved GaN material quality when epitaxial layer is grown on native substrate

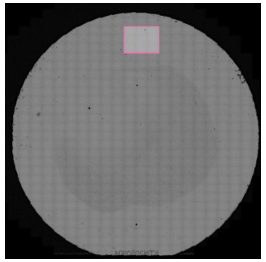

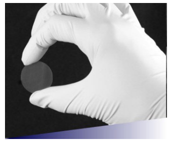

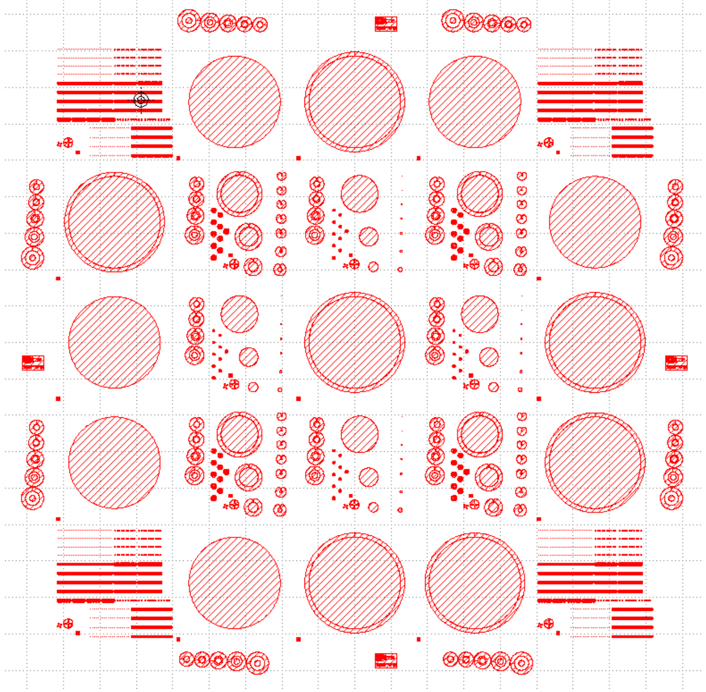

See 43rd RD50 Workshop

GaN future work

- Continue with Schottky device fabrication at NRC and CNM
  - More irradiations, material defects measurements, CCE
  - Many GaN radiation damage issues still not understood
    - Poor understanding of interaction of radiation defects with dislocations
    - Effect of defect transformation upon annealing not understood
- Assess GaN devices as potentially high-rate, high timing precision devices

- **Identify industrial partners**
  - **Investigate possibility of large-scale production, e.g. ≥6” wafers**
    - **Main issue: particle physics a low-priority customer due to small size**

Silicon Carbide

- **Wide bandgap semiconductor (3.26 eV)**
  Low leakage currents, insensitivity to visible light
- **Renewed interest:**
  High quality wafers for power electronics industry

+ **High breakdown field and saturation velocity** :
  Timing applications
+ **Potentially higher radiation hardness** (displacement energy)
  no cooling needed after irradiation
- **Higher ionization energy** (~30% less signal per μm) [9]
- **Limitations in wafer thickness and resistivity**

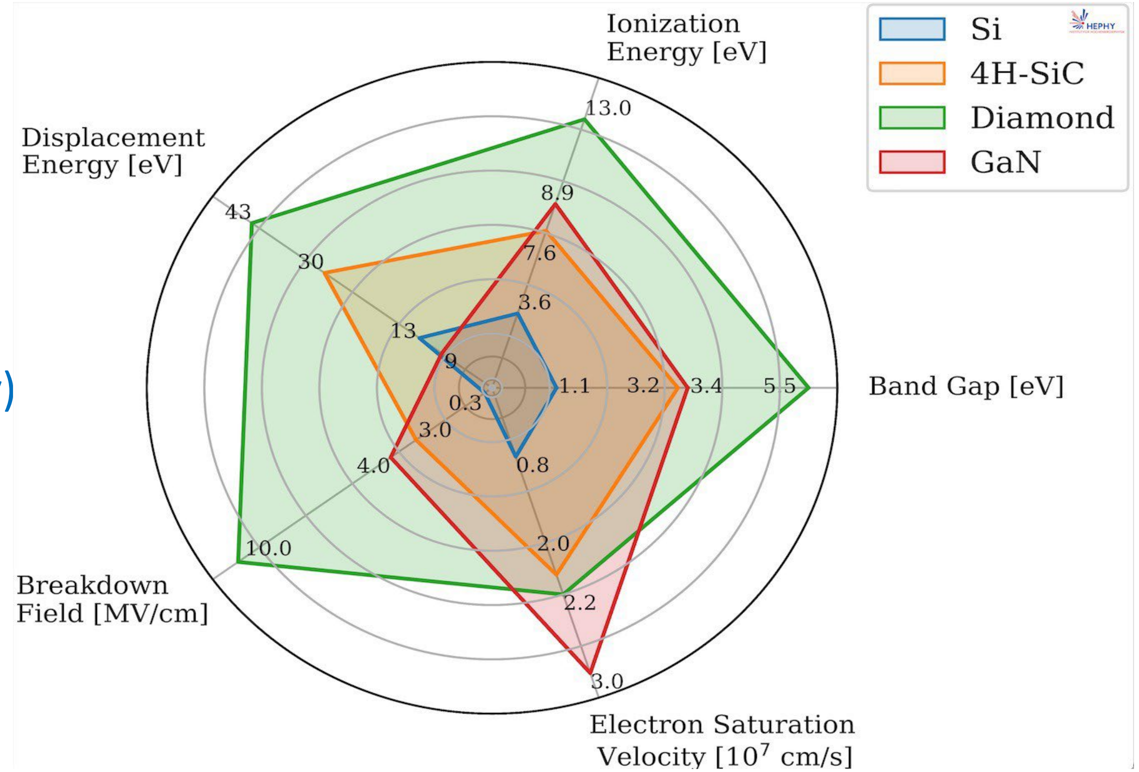

SiC-LGAD RD50 Common Fund Project DRD3

- **RD50, now DRD3 project started about a year ago**
- Aiming to produce planar diodes and LGADs on 6-inch wafers at CNM

- First results from planar run
- Update on LGAD progress

Activity	Institute	Year 1				Year 2				Year 3			
		Q1	Q2	Q3	Q4	Q1	Q2	Q3	Q4	Q1	Q2	Q3	Q4
TCAD simulations	*HEPHY, CNM*	Planar			LGAD run1			LGAD run2					
Wafer layout	*HEPHY, CNM*												
Production	*CNM*												
IV, CV characterization	*HEPHY, CNM, Perugia, NIKHEF*												
UV-TCT Measurements	*HEPHY, CNM*												
TPA-TCT Measurements	*Santander*												
Alibava	*CERN*												
Neutron Irradiations	*HEPHY*												
X-Ray irradiations	*Perugia*												

Silicon Carbide

- 4H-SiC p-n planar diodes from Run 13575 of CNM [5]
- 3 x 3 mm² active area, 50 µm epi

Full depletion voltage : 400 V, C_{det} = 18 pF

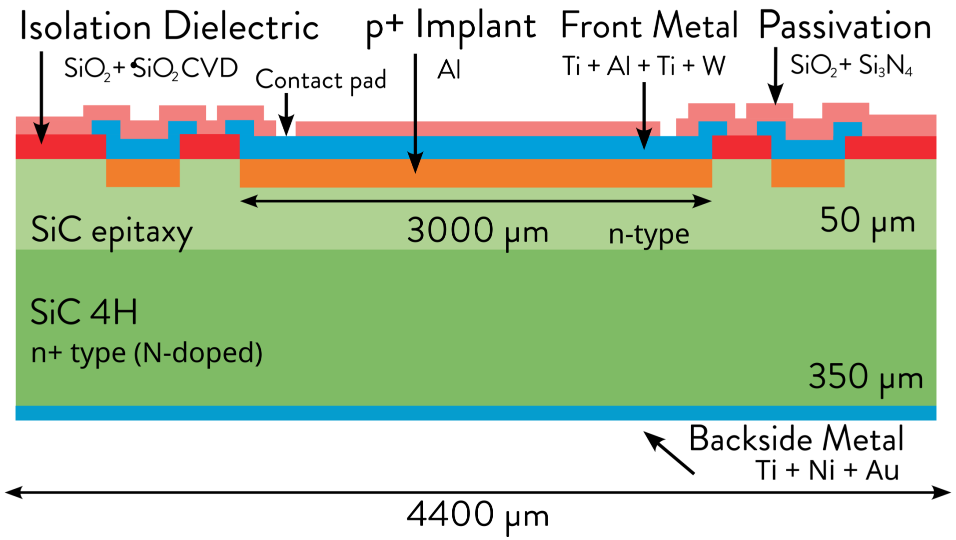

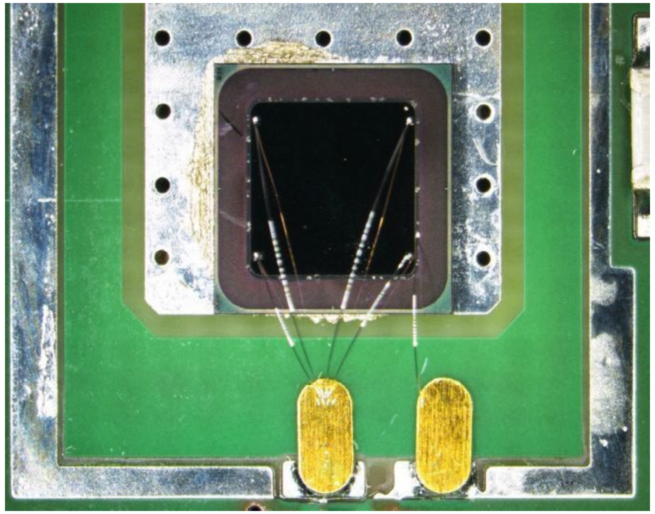

4H-SiC pad diode on readout board

material from HEPHY

Rafí et al. Electron, Neutron, and Proton Irradiation Effects on SiC Radiation Detectors. IEEE TRANSACTIONS ON NUCLEAR SCIENCE 67, 9 (2020).

Silicon Carbide:
Neutron Irradiation studies

DRD3

- Neutron irradiated (**$5 \cdot 10^{14} – 1 \cdot 10^{16}$ n_{eq}/cm^2**) at ATI Vienna [6] (previous studies [7,8])

Fluence n_{eq}/cm^2	CCE %
5×10^{14}	64
1×10^{15}	51
5×10^{15}	15

Old studies (2006)

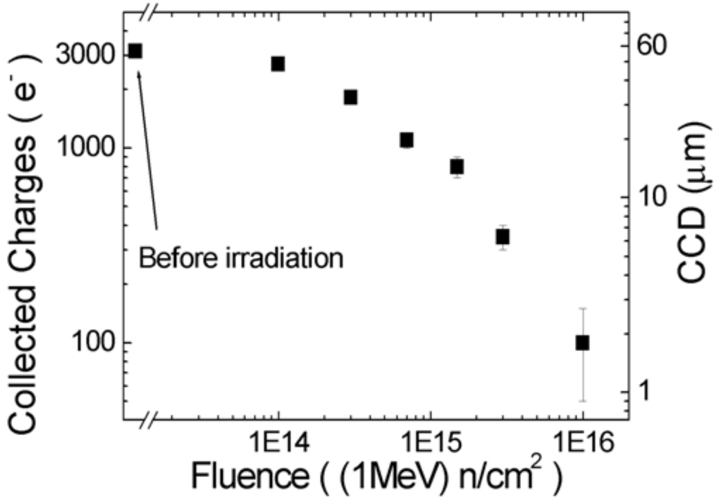

https://doi.org/10.1109/TNS.2006.872202

[7] : Gaggl et al., Charge collection efficiency study on neutron-irradiated planar silicon carbide diodes via UV-TCT, 10.1016/j.nima.2022.167218

[8] : Gaggl et al., Performance of neutron-irradiated 4H-silicon carbide diodes subjected to alpha radiation, J. Inst.18, C01042 (2023)

Silicon Carbide:
CCE characterisation

DRD3

Alpha measurements

- Signals obtained even at highest fluences, in forward and reverse bias
- Bias voltage limited by readout
- At highest fluences, forward and reverse bias identical

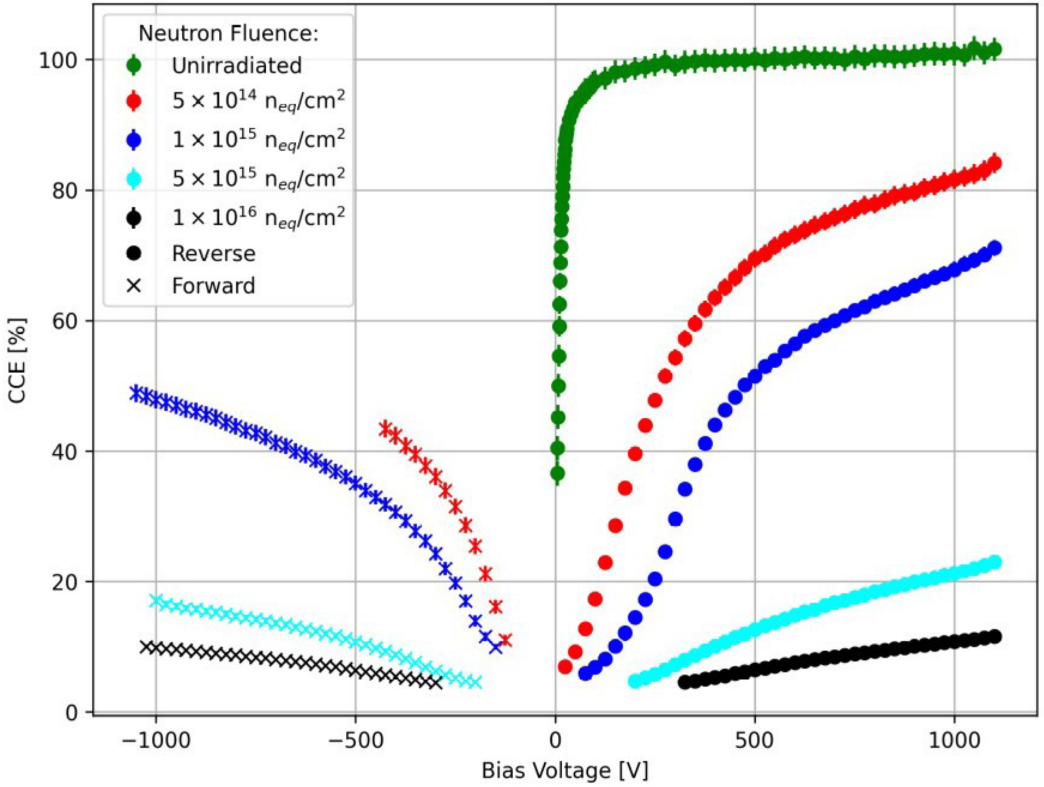

Silicon Carbide: LGAD

- LGAD : Low Gain Avalanche Diode [16], wide-spread usage for Si
- Attractive for SiC (large signal from thin detectors, timing)
- RD50 common project [17], ongoing work at IHEP / NJU [18-20]
- TCAD studies to optimize design

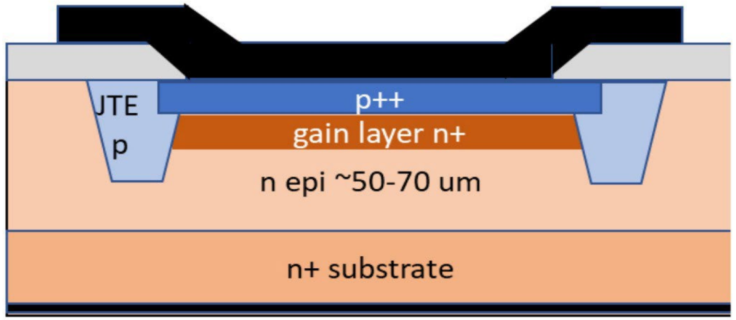

Idealized 4H-SiC LGAD structure [20]

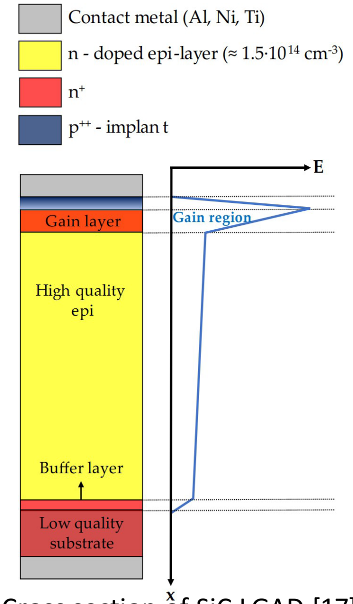

Cross section of SiC LGAD [17]

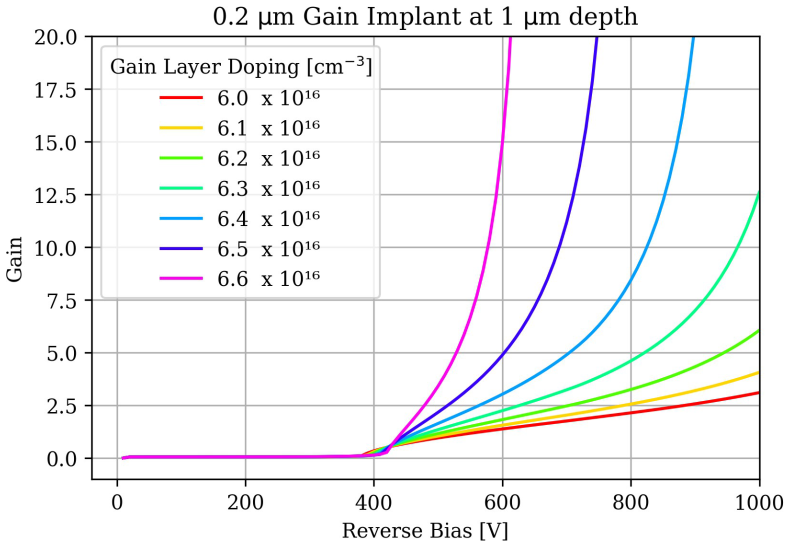

TCAD Simulation of 4H-SiC LGADs with different gain doping

material from HEPHY

Design and Simulation of 4H-SiC LGAD

TCAD

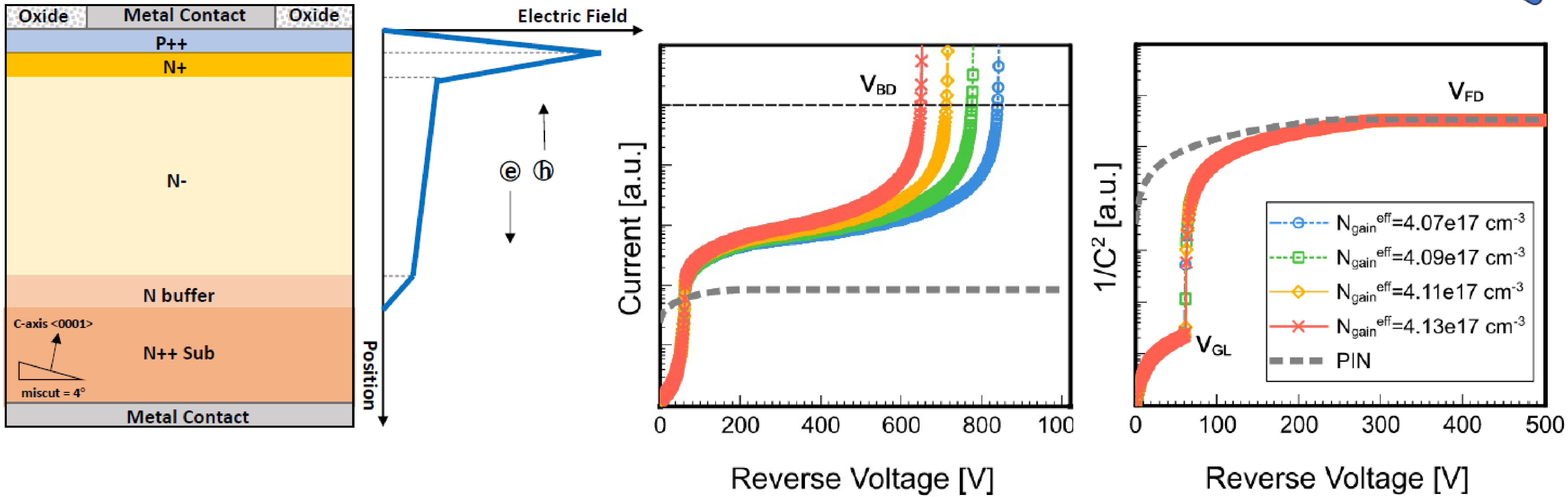

- "Triangle" Electric Field determined by gain layer doping concentration or depth
- Could reach full depletion less than 500V, with gain larger than 10

https://doi.org/10.1016/j.nima.2023.168677

Silicon Carbide: Summary

DRD3

- 4H-SiC features extremely low leakage currents even after irradiation up to $1 \cdot 10^{16}$ n_{eq}/cm^2
- CCE scales with fluence $\propto \Phi_{eq}^{-0.56}$
- Unirradiated devices can be accurately simulated using TCAD
- Ongoing work on SiC LGAD, promising for timing applications
- New wafer production in the pipeline.

This work was supported by the Austrian research promotion agency FFG, project number 883652.

Production and development of the 4H-SiC samples was supported by the Spanish State Research Agency (AEI) and the European Regional Development Fund (ERDF), ref. RTC-2017-6369-3.

material from HEPHY

Diamond

DRD3

Property	Diamond	Silicon
band gap	5.47	1.12
mass density [g/cm^3]	3.5	2.33
dielectric constant	5.7	11.9
resistivity [0cm]	>10^{11}	2.3e5
breakdown [kV/cm]	1e3...20e3	300
e mobility [cm^2/Vs]	2150	1350
h mobility [cm^2/Vs]	1700	480
therm. conductivity [W / cm K]	10..20	1.5
radiation length [cm]	12	9.4
Energy to create an eh-pair [eV]	13	3.6
ionisation density MIP [eh/mm]	36	89
ion. dens. of a MIP [eh/ 0.1 ‰ X_0]	450	840

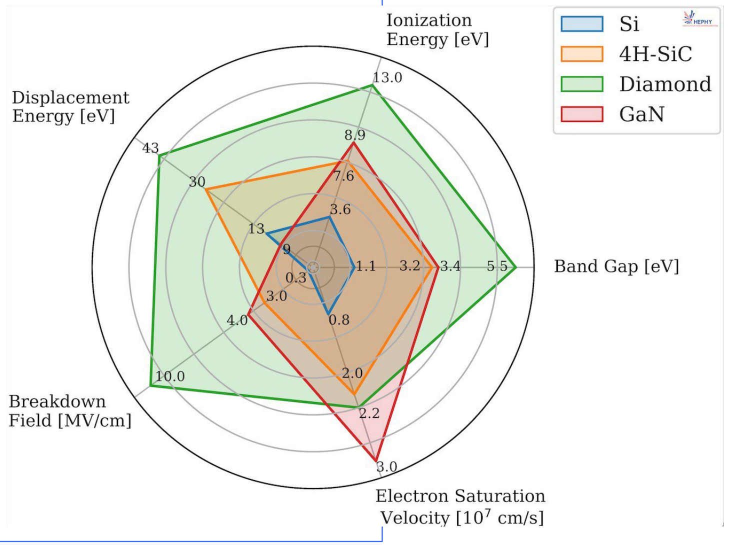

- Low dielectric constant ➔ low capacitance
- Low leakage current ➔ low noise
- Room temperature operation
- Fast signal collection time

–MIP signal ~2 smaller at same X_0

–Efficiency < 100% (pCVD)

Diamond

- Today two <u>main manufacturers</u> of detector grade diamond
  - **ElementSix Ltd**
    - large **polycrystalline** wafers
    - **single crystal** diamonds
  - **II-VI Semiconductors**
    - large **polycrystalline** wafers
    - relatively recent entry

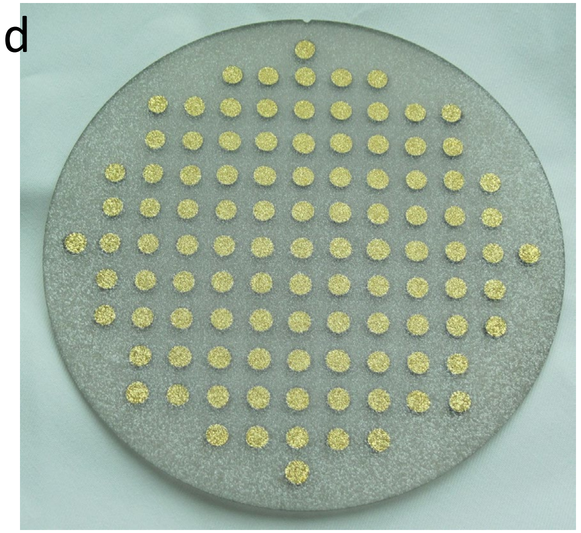

- <u>Alternative sources</u>
  - Diamond on Iridium (DoI) (Audiatec, Germany)
  - Hetero-epitaxially grown -> **large area**
  - **Highly oriented crystallites**.

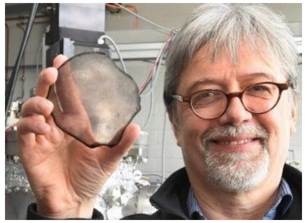

Diamond

DRD3

- Impressive progress over the last 25 years.
- Current state of the art for **polycrystalline** CVD diamond **8 ~ 320 μm in 500um thickness**
  - **(~11500 e/MIP)**
  - **commercially available.**

  - 1995: 8 ~ 50 μm
  - 2000: 8 ~ 180 μm
  - 2020: 8 ~ 320 μm

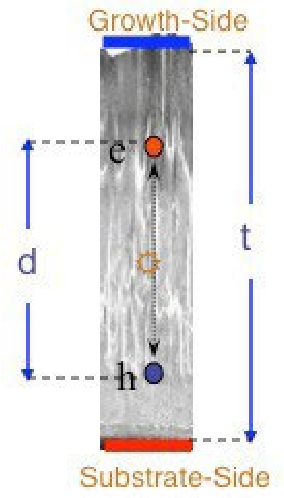

Diamond

3

- Summary of RD42 irradiation results:

Irradiation Species	k_i
200 MeV pions	3.2 ± 0.8
Fast neutrons	4.27 ± 0.33
70 MeV protons	2.60 ± 0.27
800 MeV protons	1.67 ± 0.09
24 GeV protons	1

"Back-of-an-envelope calculation, expect Schubweg of:
ℵ~ 16µm at 10^{17} cm^{-2} protons_24 GeV_eq

*normalized to 24GeV protons

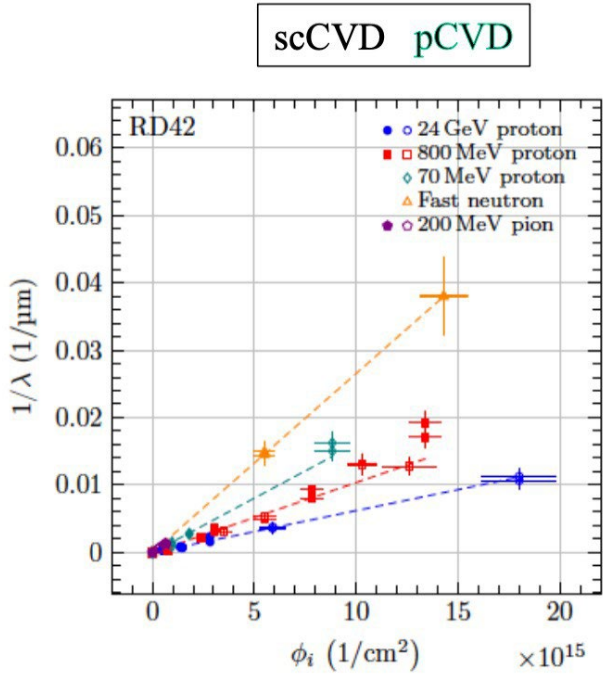

Radiation damage is fitted with simple damage model:

$$\frac{1}{\lambda} = \frac{1}{\lambda_0} + k_\lambda \Phi$$

damage constant

particle fluence

Carrier lifetime challenge – 3D diamond detectors

- After large radiation fluence all detectors are trap limited
- Mean free paths λ< 50μm
- Need to keep drift length (L) smaller than mfp(λ)
- Build **3D detectors** to reduce transit time.
- Huge progress made in fabrication of 3D diamond detectors in the last 10 years.

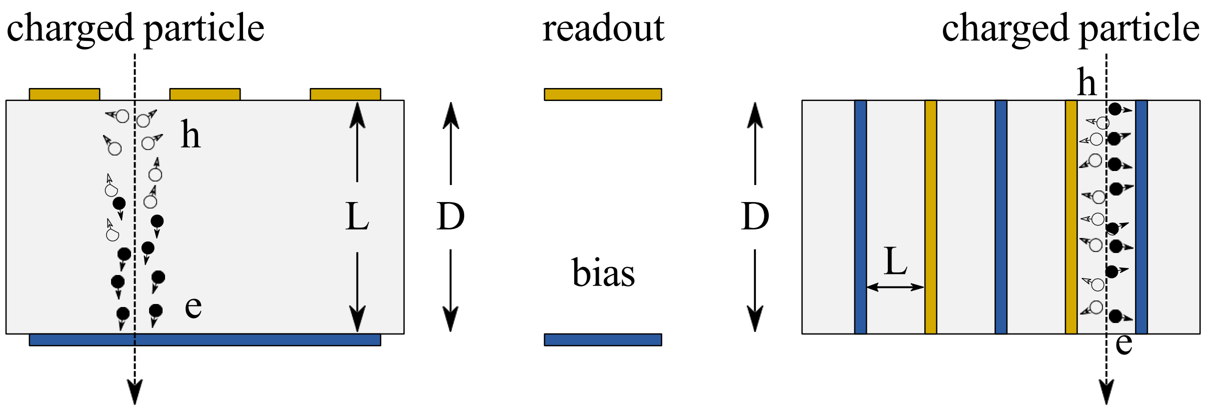

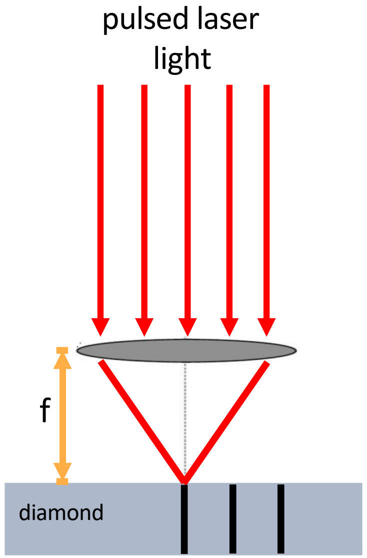

3D diamond? (2008)

Lasered graphitic structures in pCVD ('10)

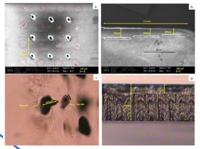

Single crystal with column structure ('11) [30]

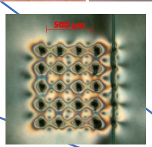

Pico second laser for improved graphitic electrodes ('12)

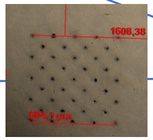

Femto second laser processing and **TCAD simulation ('13,'14)**

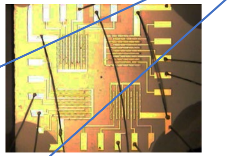

Phase modulated laser processing ('15,'16)

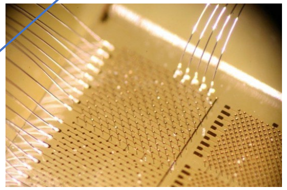

Polarised & Phase modulated laser processing ('17,'18)

Prototypes with poly and single crystal diamond (2019 ++.

Several Prototypes tested at
Diamond Light Source [30]
CERN test beam [31]
RBI proton beam [32]
Clinical Photon beam [33]

3D Diamond prototypes

- CMS and ATLAS pixel prototypes tested:

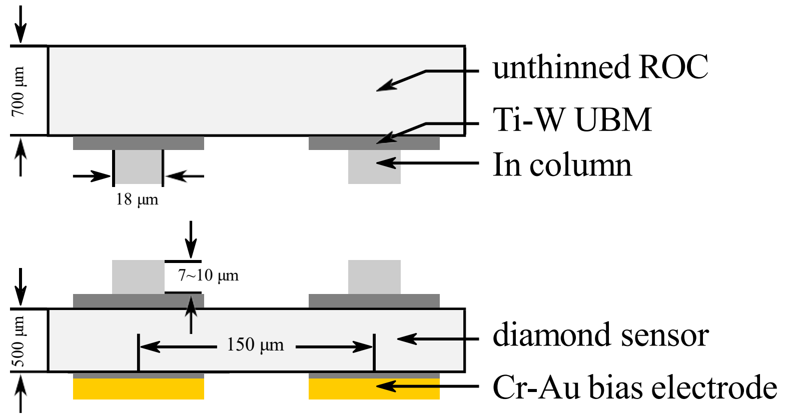

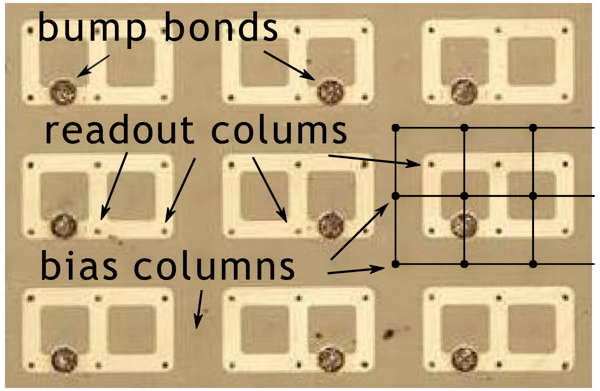

3D Diamond prototypes

- CMS and ATLAS pixel prototypes tested:

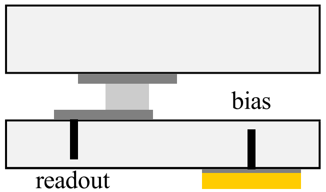

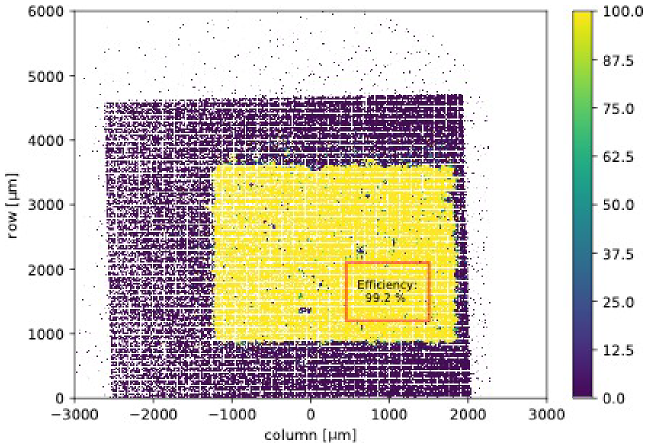

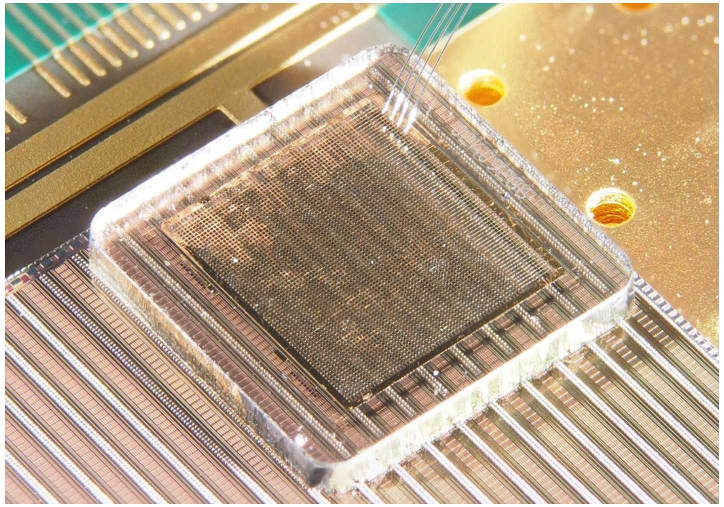

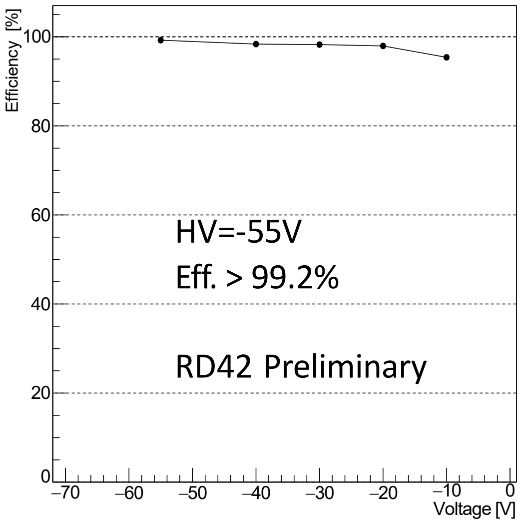

3D Diamond Radiation Hardness

Sensors **2022**, *22*(22), 8722; https://doi.org/10.3390/s22228722

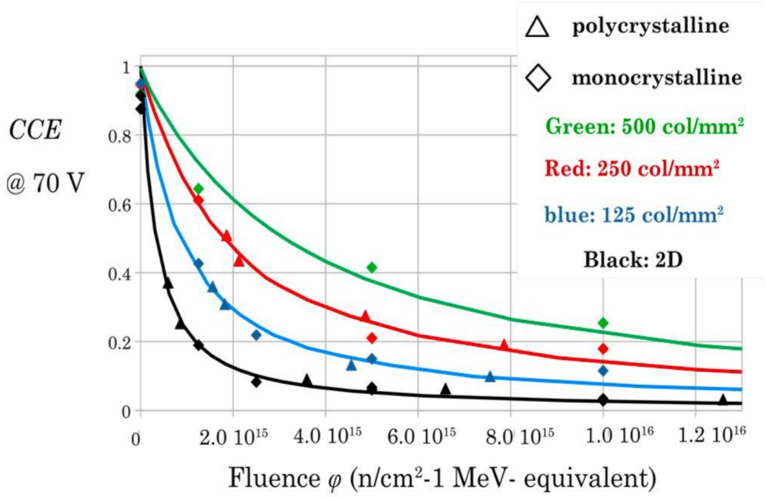

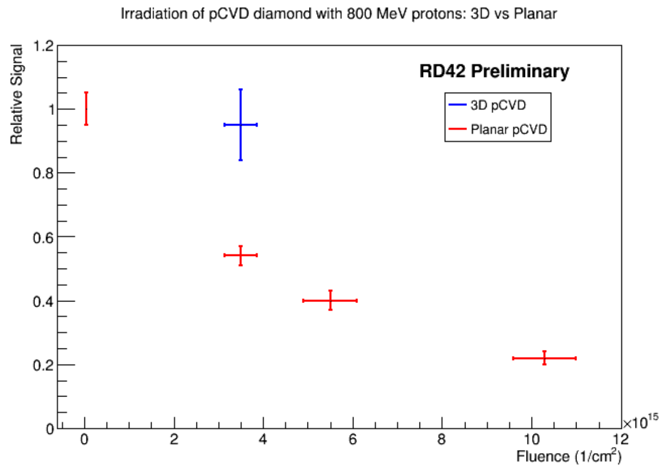

- Few radiation hardness data available, but promising:
  - Compare signal loss in 3D pixels to published results from planar
  - **3D sensors collect twice as much charge when unirradiated**
  - **3D sensors see 5±10 % reduction** in signal at 3.5 x10^{15}
  - **Planar sensors see 45±5 % reduction** for 3.5 x10^{15}

Outline

- Introduction : electronic properties of WBG Semiconductors
- Growth processes
  - Beyond wafers: the perovskite family
- Lattice disorder, defects and energy levels; how to detect
- **Research on WBG Radiation Detectors**
  - Explorative studies (blue sky research) in the HEP community
  - **Applications in medical field: proton and Flash therapy**

Istituto Nazionale di Fisica Nucleare

UNIVERSITÀ DEGLI STUDI FIRENZE

Radiotherapy
A technological solution to a biological problem

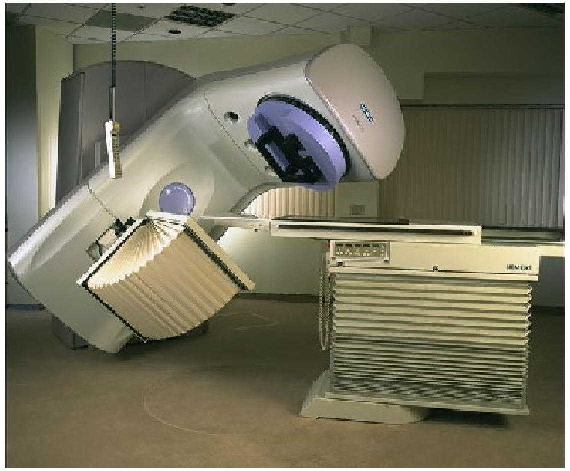

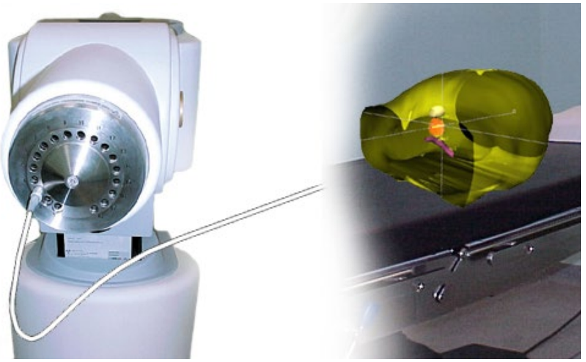

External beam radiotherapy (EBRT)

Radiation beams with high energy (X, γ, electrons, protons, ions) produced by radionuclides or particle accelerators

→ This lesson

Brachytherapy
Sealed radioactive sources introduced in the body

Methabolic radiotherapy
Non-sealed radioactive sources vehicolated within the body

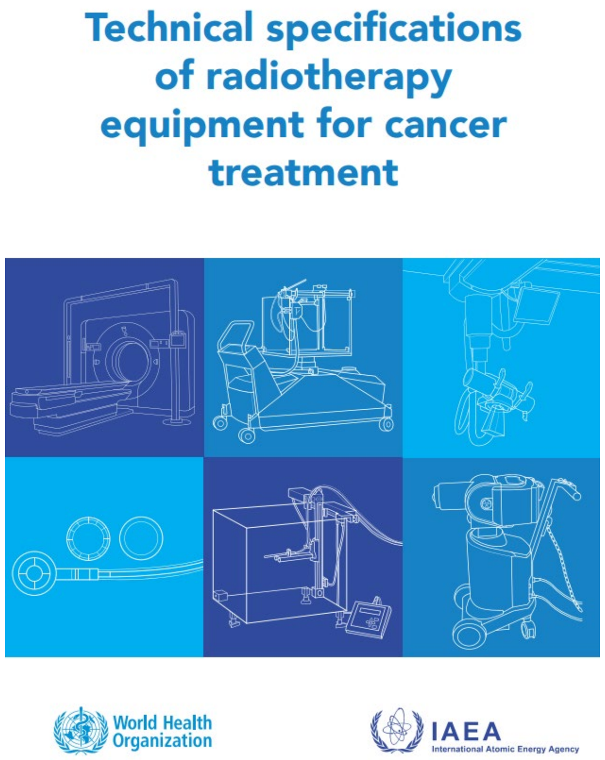

LINAC radiotherapy facility

- LINAC (Linear Accelerator) by means of high frequency (~ 3 GHz) electromagnetic waves accelerates charged particles at high energy along a linear path

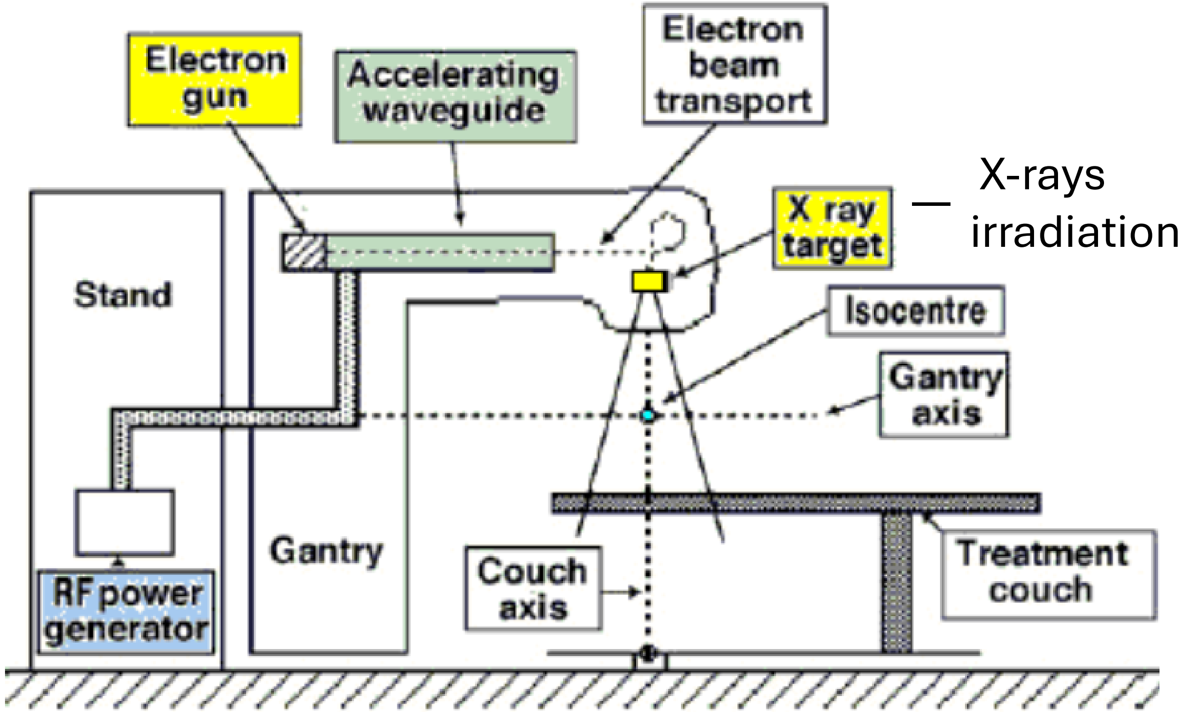

— X-rays irradiation

Figure 2. Features of a conventional LINAC with gantry stand

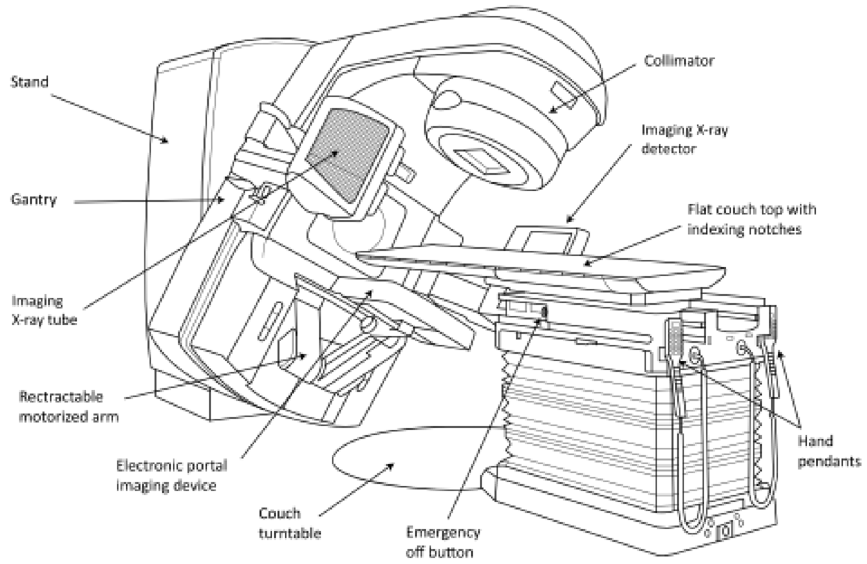

Intensity Modulated Radiation Therapy (IMRT)

Intensity Modulated Radiation Therapy (IMRT) consists in using a few radiation beams, generally from 2 to 9, produced by the same linear accelerator and directed towards the tumor from different angles, in order to concentrate the dose released on the volume of the tumor.

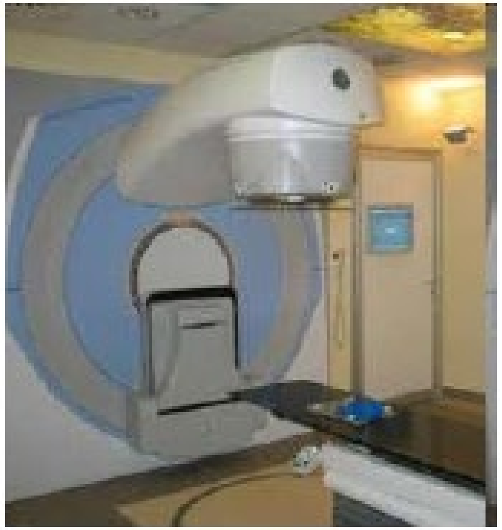

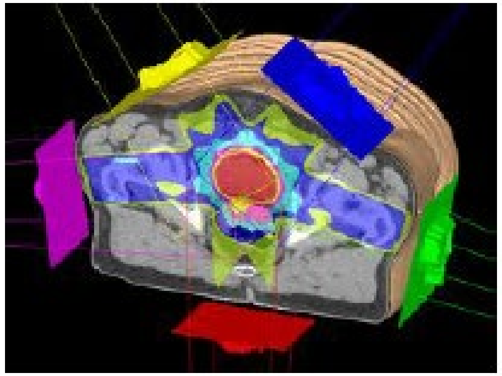

To spare at best surrounding healthy tissues the dose released to the tumor needs to be shaped along an irregular field to be best conformed to the

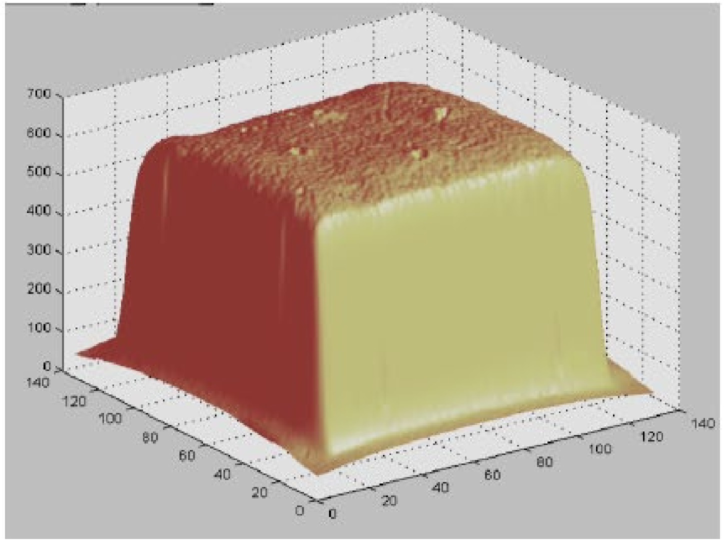

Flat Dose Map

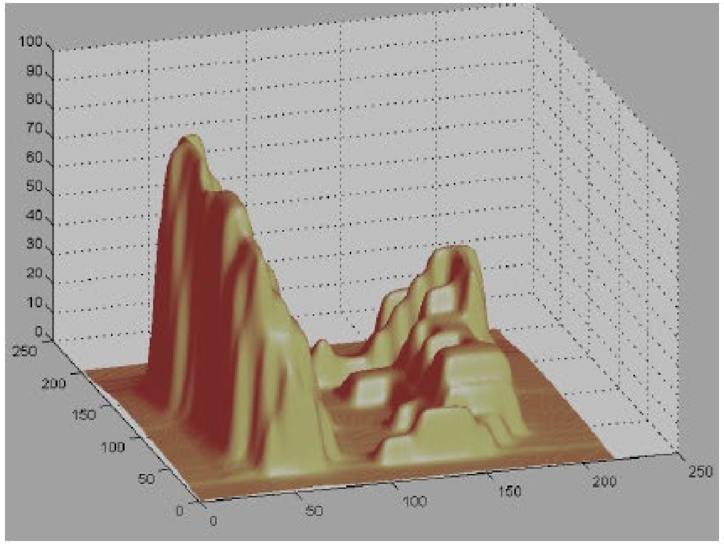

Modulated Intensity Dose Map

Multi Leaf Collimators (MLC)

The dose conformation is obtained using Multileaf Collimators with sets of mobile lamellas in W mounted externally on the LINAC head

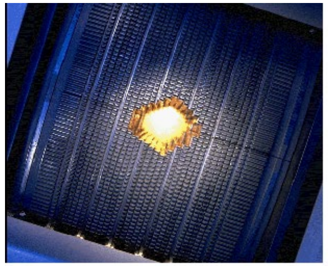

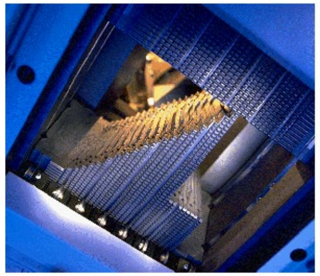

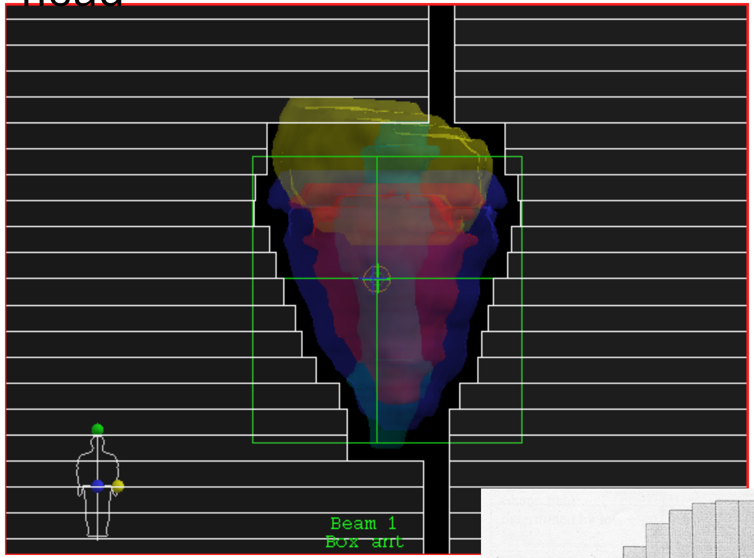

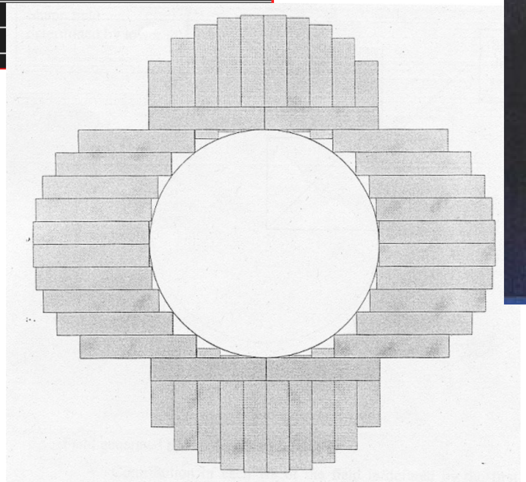

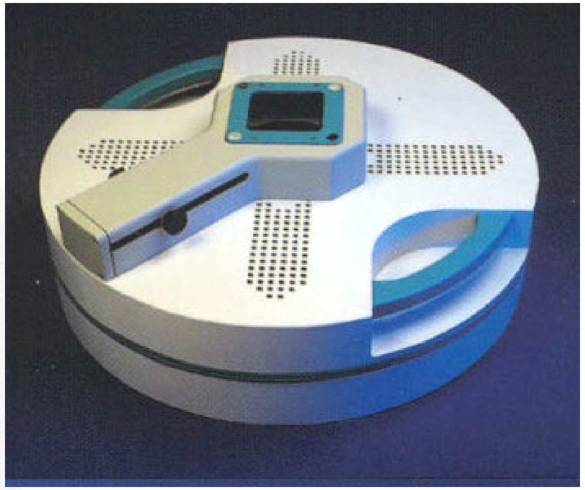

Example: IMRT irradiation in step and shoot modality, the total dose is released as a sum of nine segments. Each segment corresponds to a particular arrangement of the MLC lamellas (left). Beam is off during their movement.

Total dose is obtained as the sum of the dose released by each segment (right).

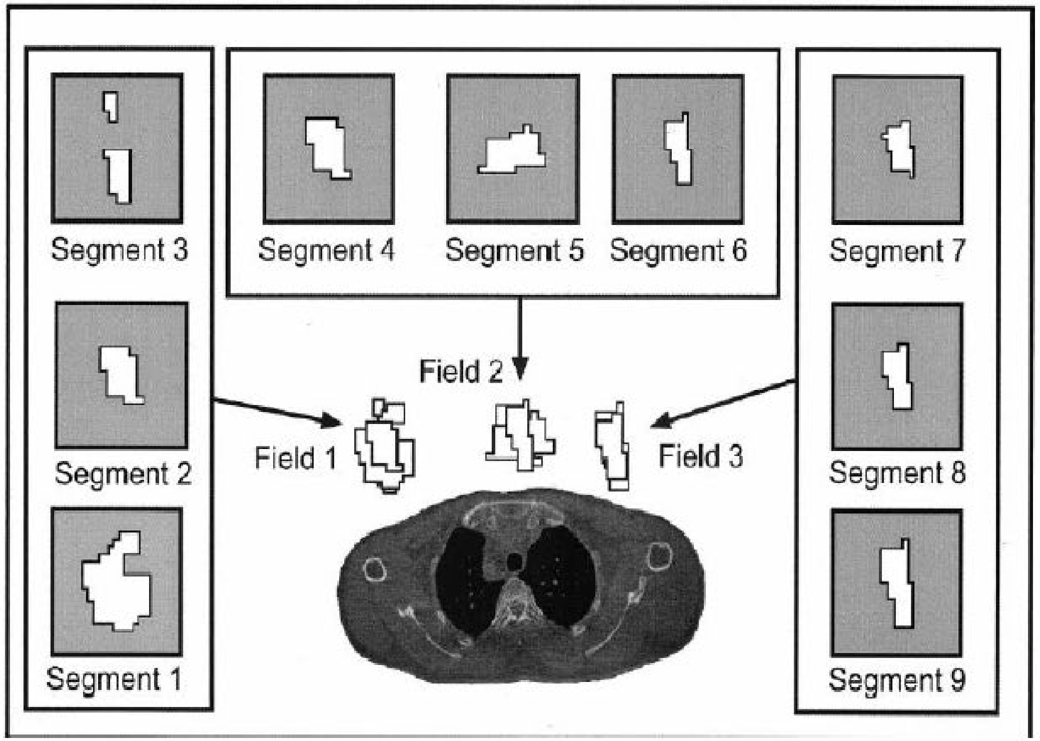

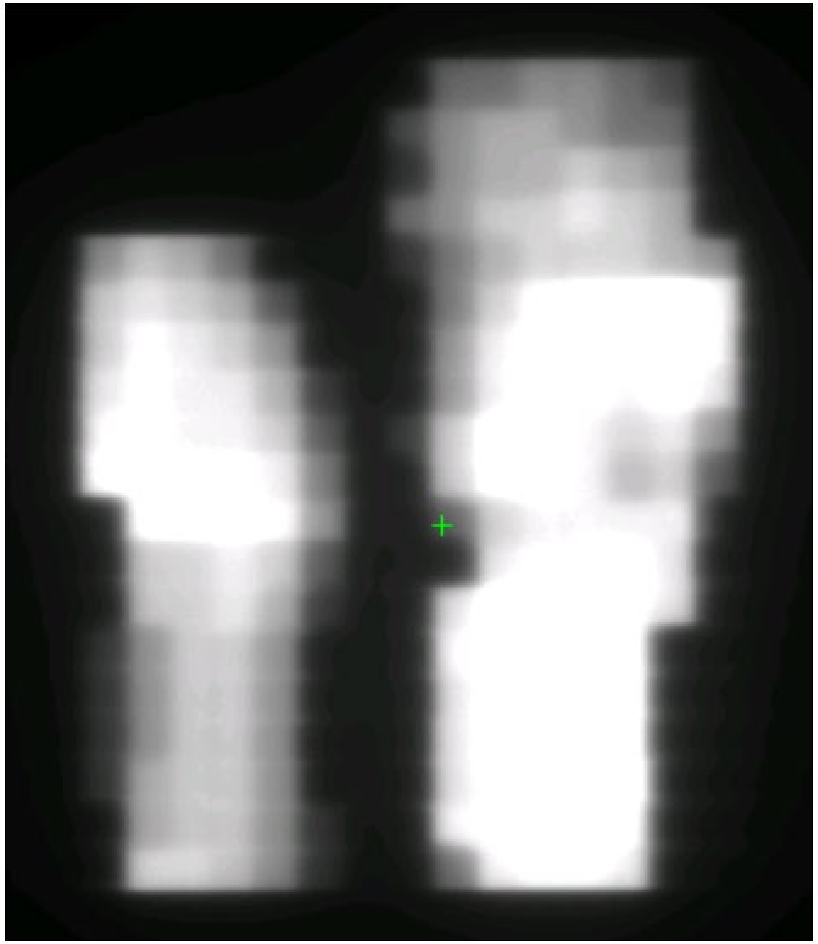

VMAT (*Volumetric Modulated Arc Therapy*)

- ❑ Able to focus more accurately at tumor tissues, ensuring greater preservation of healthy ones.
- ❑ Modulating not only the amplitude and velocity of the MLC, but also **rotation speed of the Gantry and Linac dose-rate**.
- ❑ **continuous rotation of the accelerator head during irradiation for maximum focusing** of radiation on tumor tissues, which are thus affected by all possible angles.
- ❑ **significantly reducing duration of treatments** compared to IMRT: about 5-7 minutes compared to traditional times which are around 20 minutes per session.
- ❑ **useful when treatment focus must be maximum to preserve nearby organs**: tumors of the head / neck, as larynx, pharynx and oral cavity; tumors of the pelvis, as prostate and rectum; tumors of the lung and breast.

Working principle of a on-line dosimeter

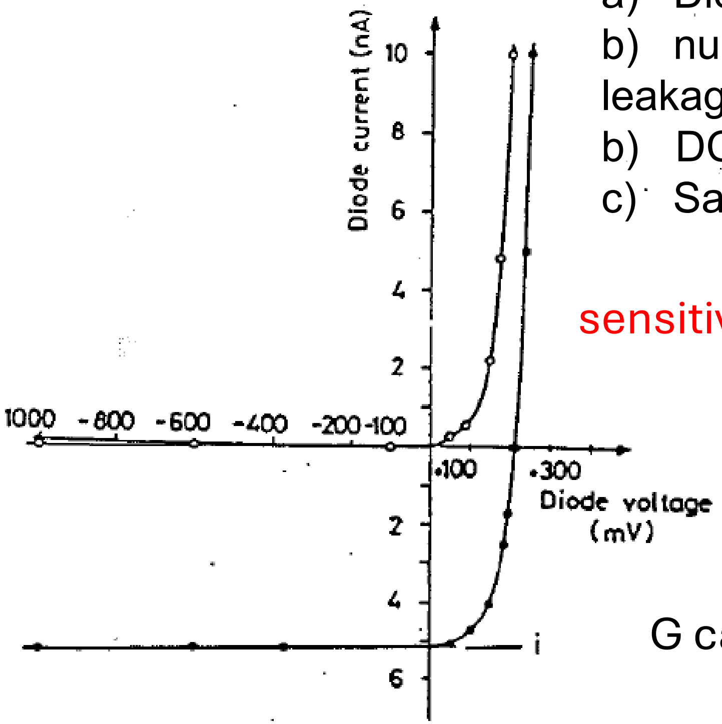

a) Diode / resistor
b) null bias or low bias (to minimize leakage current and polarization effects).
b) DC coupling.
c) Sampling time and reset fixed by digital electronics (t ≥10ms).

sensitivity $S = \frac{Q}{D\,Volume} = \frac{qG}{R}$

R,: dose rate;
Q: released charge;
D: delivered dose;
q: elementary charge

G carrier generation rate:

$$G = \frac{R\rho}{E_i}$$

→ $S = \frac{q\rho}{E_i}$.

ρ: density;
E_i: mean ionization energy.

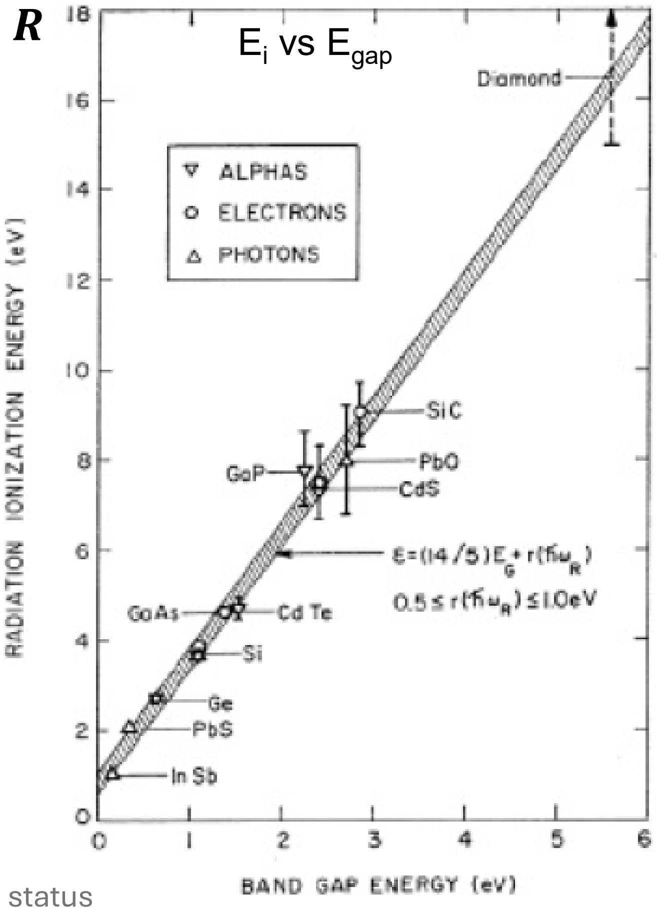

	IC(AIR)	SILICON	DIAMOND
ρ [g/cm^3]	1.29x10^{-3}	2.33	3.52
E_i [eV]	34.00	3.60	16.20
Sensitivity [nC/Gymm^3]	0.038	647.22	217.28

Dosimetry Challenges

Highly accurate imaging and dose verifications systems must match with increased accuracy of the irradiation techniques .

- **Response independent of energy**;
- **small volume and high sensitivity**;
- **response independent of dose rate,** continuously changing during VMAT;
- **Real time invivo detectors** - european community require dose delivery to be verified experimentally **directly during irradiation** (Article 56 of COUNCIL-DIRECTIVE-2013/59/EURATOM).

State-of-art commercial dosimetric devices used in cl radiotherapy

	IC (AIR)	SILICON	DIAMOND
ρ [g/cm^3]	1.29x10^{-3}	2.33	3.52
E_i [eV]	34.00	3.60	16.20
S [nC/Gymm^3]	0.038	647.22	217.28
Area [mm^2]	25.00	0.64	3.80
thickness [mm]	5.00	0.03	0.001
volume [mm^3]	125	0.019	0.0038
Array	OCTAVIUS PTW	MAPCHECK SunNuclear	-
Detector	729 PTW	SunPoint® Diode Detector	microDiamond type 60019 PTW
Reference	APL Mater. 7, 051101 (2019); doi: 10.1063/1.5083810		

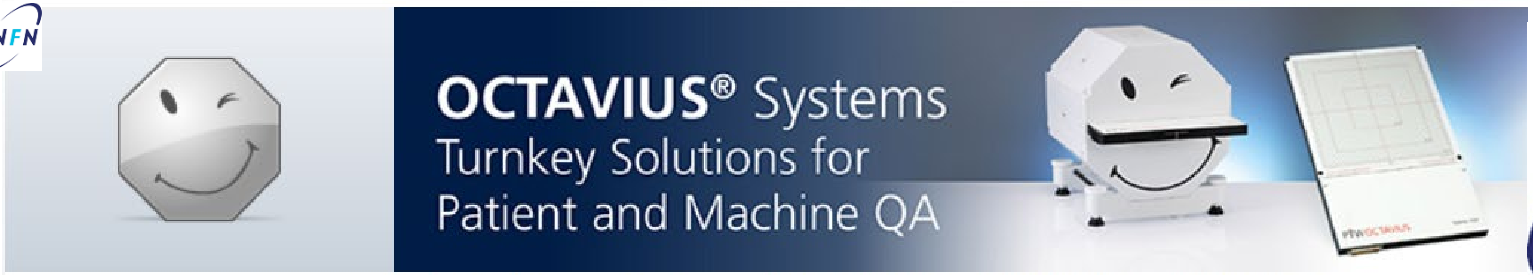

Products & Solutions > Radiation Therapy > VMAT QA, IMRT QA, OCTAVIUS, DIAMOND > OCTAVIUS 729 > Specifications

- PRODUCTS & SOLUTIONS
  - Radiation Therapy
  - Diagnostic Radiology
  - Health Physics
- SERVICES & SUPPORT
- LITERATURE
- NEWS & EVENTS
- ABOUT PTW
- REFERENCE SITES
- DOWNLOAD CENTER
- ONLINE BROCHURES
- THE DOSIMETRY SCHOOL
- CONTACT US
- LINKS
- FEEDBACK

Search

advanced search

OCTAVIUS 729 | Specifications | Learn more

OCTAVIUS Detector 729

Detector type:	Plane-parallel vented ionization chambers
Detector design:	cubic
Number of detectors:	729
Detector size:	0.5 cm x 0.5 cm x 0.5 cm ($0.125\ cm^3$)
Detector spacing:	10 mm center-to-center, 5 mm edge-to-edge
Max. field size:	27 cm x 27 cm
Reproducibility:	≤ ± 0.5%
Dead time:	zero
Repetition rate:	200 ms
Measured quantities:	absorbed dose to water (Gy), absorbed dose rate to water (Gy/min)
Resolution:	0.1 mGy or 0.1 mGy/min
Measurement range:	(0.5 ... 48 Gy/min)
Reference point:	7.5 mm below the surface of the array
Housing material:	GRP
Dimensions:	30 cm x 42 cm x 2.2 cm (W x D x H)
Weight:	5.7 kg
Power supply:	(100 ... 240) VAC; (50 ... 60) Hz
PC connection:	Ethernet, RS232
Part No.:	L981378

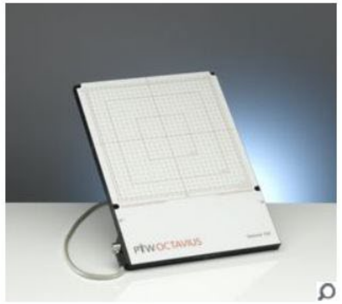

OCTAVIUS® 729 - 2D ionization chamber array for patient and machine QA with OCTAVIUS 2D/4D

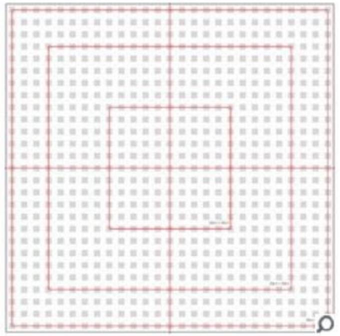

729 cubic ionization chambers uniformly arranged on 27 cm x 27 cm

ArcCHECK® & 3DVH®

The Ultimate 4D Patient QA Solution

Helical Detector Grid

Detectors are arranged on a HeliGrid™ which increases the sampling rate and reduces BEV detector overlap and shadowing.

- An ArcCHECK 10 x 10 cm² area contains 221 detectors; equivalent to the detector density in a MapCHECK® 2
- Entrance and exit dose are measured, effectively doubling the detector density in the measurement field

Beam Delivery

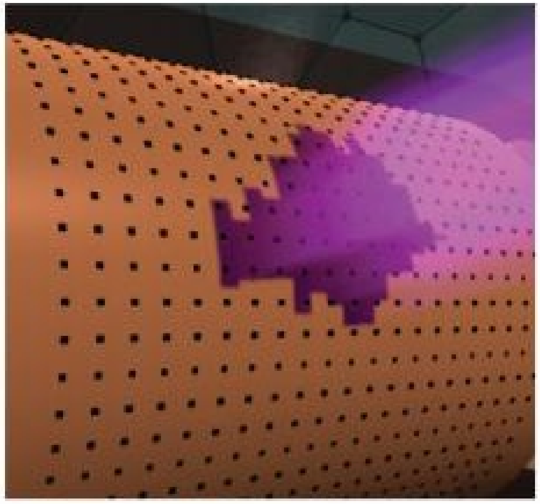

ArcCHECK Detector

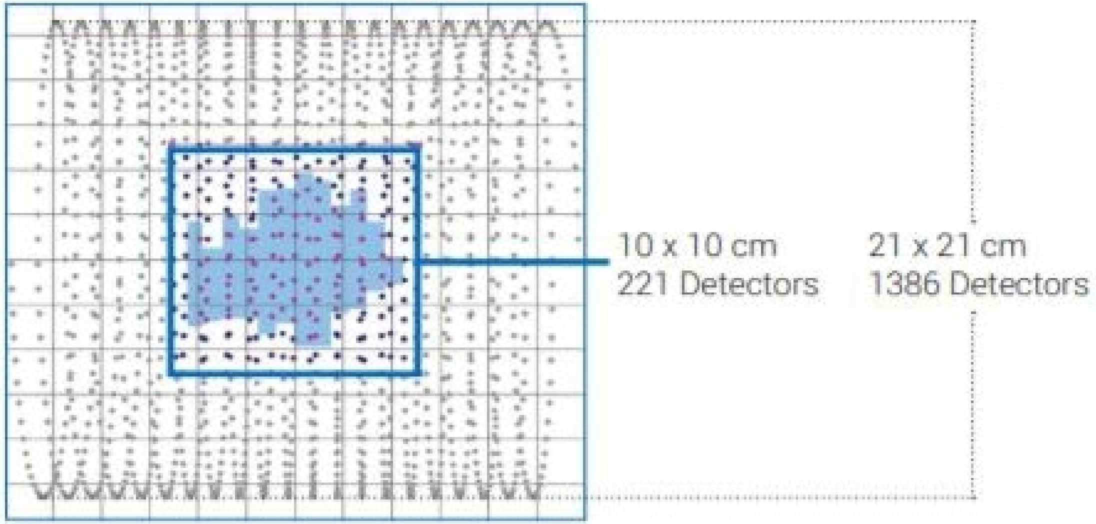

The Silicon Choice

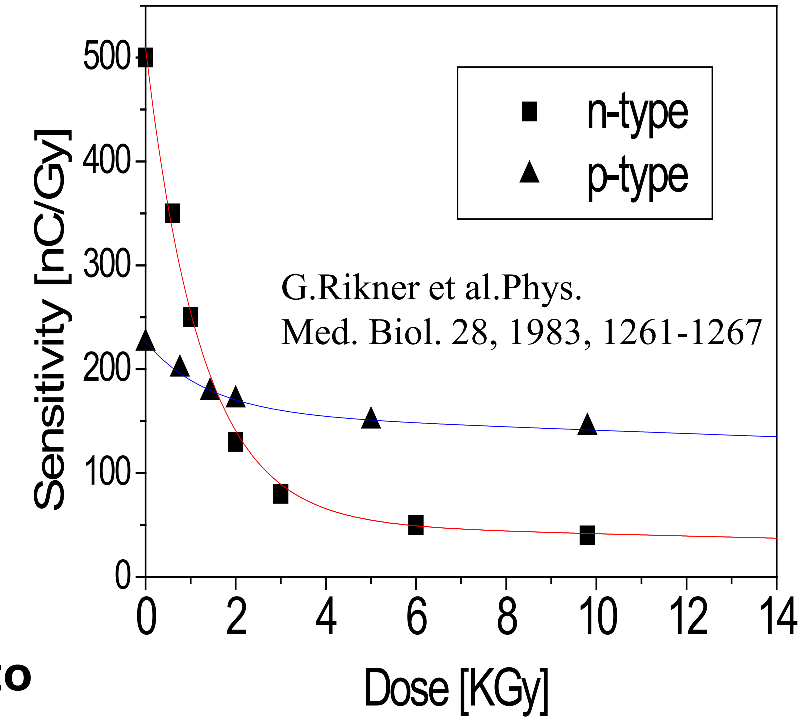

Advantages:
- High sensitivity (18000 times higher than IC).
- Well developed manufacture technology.
- high spatial resolution.
- work in null bias mode (in-vivo).

Drawbacks:
- Sensitivity decrease with accumulated dose due to increase of concentration of recombination centers (recalibrations needed).
- Dose rate dependency due to centers saturation at high dose rates.
- Energy dependence: Si not "water equivalent".

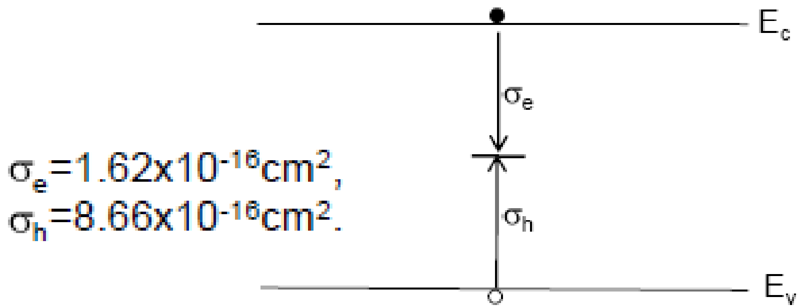

Radiation Resistant ?
p-type radiation harder material

hole capture more efficient -> Lifetime for minority carriers higher in case of electrons.

Radiation damage in standard Si dosimeters (thickness 300um)

Sensitivity as a function of trap concentration in a Si dosimeter

$$S = \frac{q\rho_{Si}}{E_i}\sqrt{\frac{D_e}{\sigma_e v_e N_t}} \propto N_t^{-1/2}.$$

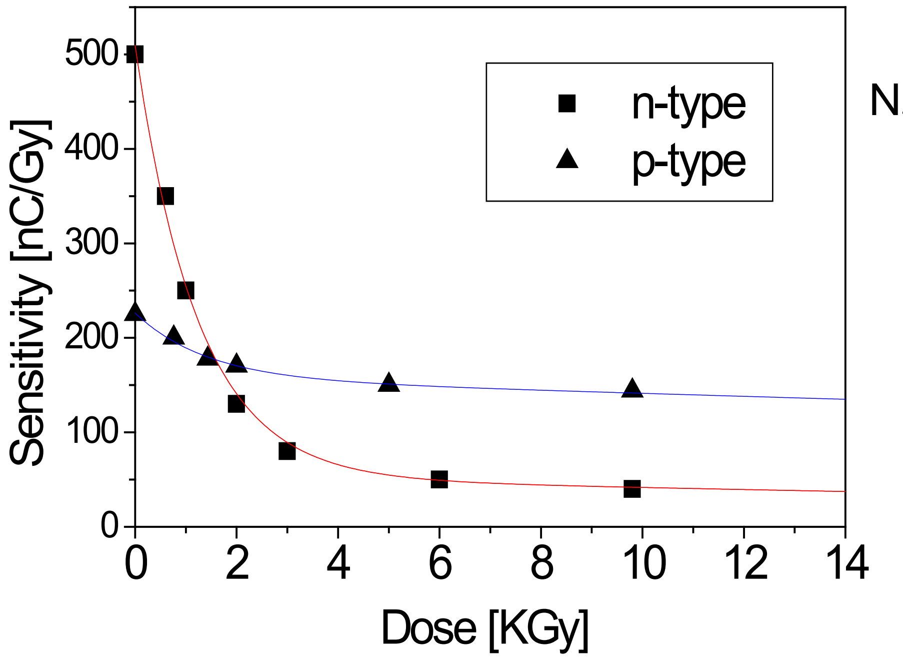

N_t linearly increasing with dose so:

$$S \propto \frac{1}{\sqrt{Dose}}$$

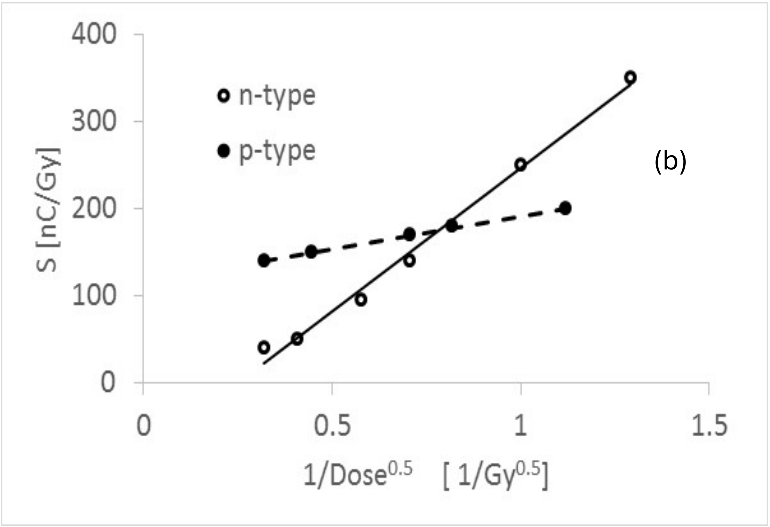

M. Bruzzi, NIMA 809, 2016 Novel Silicon Devices for Radiation Therapy Monitoring, 105-112

Pre-irradiation (≈10kGy) to reduce the dependence of the signal on the dose.

Epitaxial p-type Si on MCz substrates to limit active thickness

Epitaxial Layer used to limit active depth to less than diffusion length

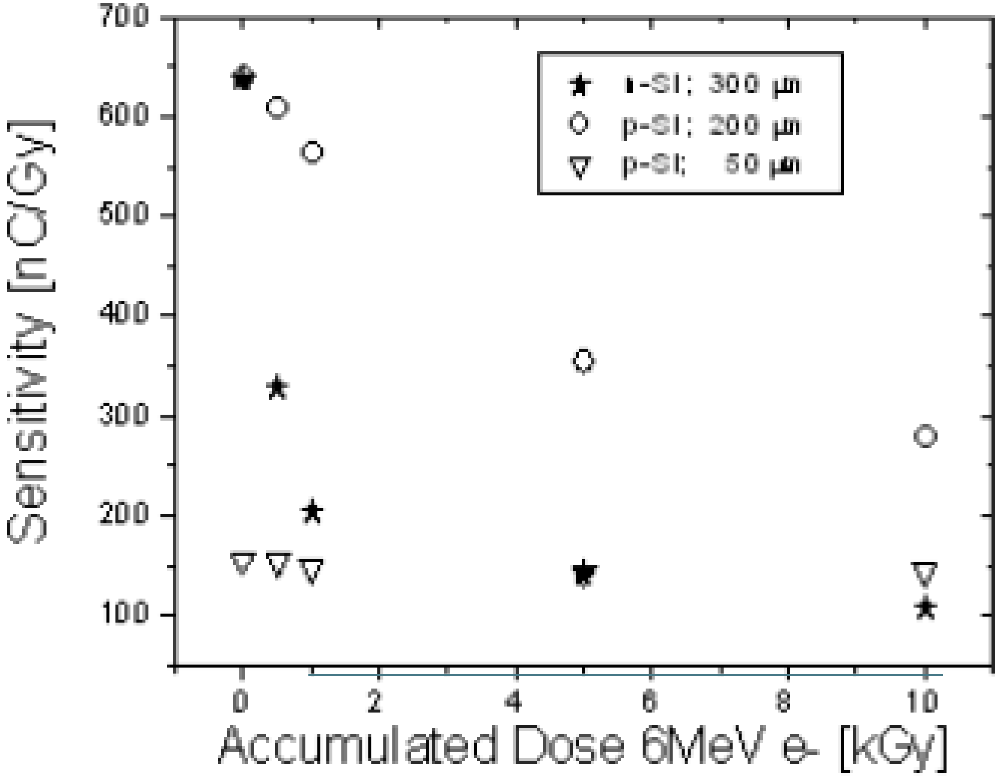

M. Bruzzi et al., "Epitaxial silicon devices for dosimetry applications," Appl. Phys. Lett., vol. 90 (2007) 172109 1-3.

Si bidimensional dosimeter

Matrix: 21x21pixels

Pixel: 2x2mm Pitch: 3mm
Detector size: 6.3x6.3cm^2

C.Talamonti, M.Bruzzi et al. 2011 Nucl. Instr. Meth A, vol. 658, p. 84-89.

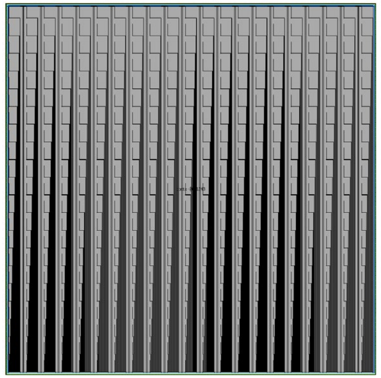

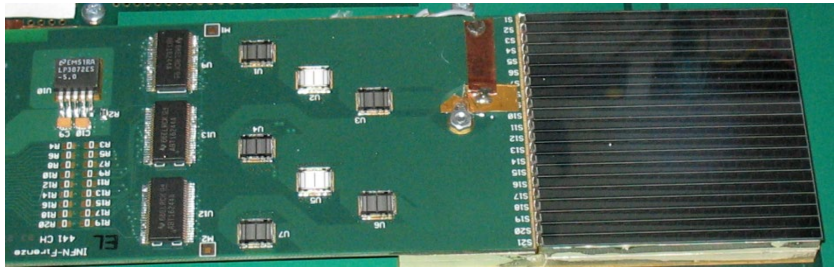

Covered area 20×20 cm^2
~4k channels

Measured time structure of dose segments

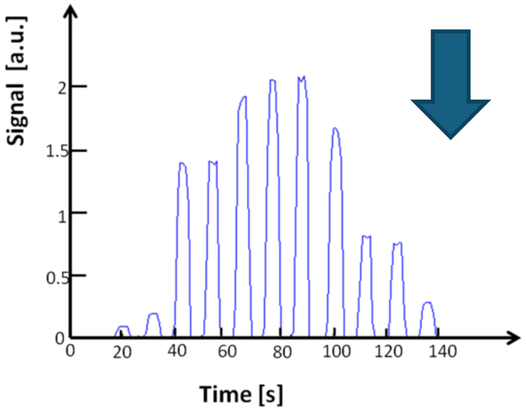

Large area IMRT covered by mosaic composition and/or shifting modules along x-y axes.

Dose map of an IMRT field for prostate cancer as measured by the Epi-Si 2D silicon dosimeter.

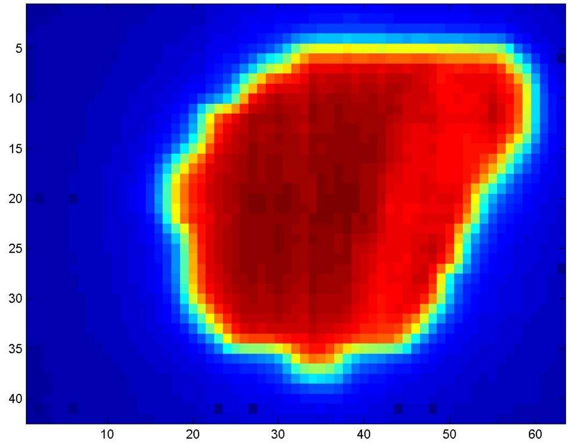

United States Patent
Bruzzi et al.

(10) Patent No.: US 8,563,936 B2
(45) Date of Patent: Oct. 22, 2013

The Diamond Choice

☺

- **water equivalent**
  it doesn't perturb the radiation field → small fields
  the energy is absorbed as in the water → no correction factors
- high radiation hardness → long term stability
- high density → high sensitivity → small dimensions
- non toxic
- it can be used as TL dosimeter (off-line) or for on-line applications

material	Z
Air	7.78
Water	7.51
Muscle	7.64
Fat	6.46
bone	12.31
C	6
Si	14
SiC	≈10

Overview | Specifications | Learn more

Nearly as good as water.

microDiamond

Key Features

- Nearly water equivalent for all beam energies
- Very small sensitive volume (0.004 mm³) - perfect choice for small field dosimetry
- Suitable for all field sizes up to 40 cm x 40 cm
- Precise, accurate measurements in photon, electron and proton fields
- Excellent radiation hardness, minimal energy, temperature and directional dependence
- No high voltage required. Suitable for all connecting systems (BNT, TNC, M)

microDiamond
Synthetic Diamond Detector

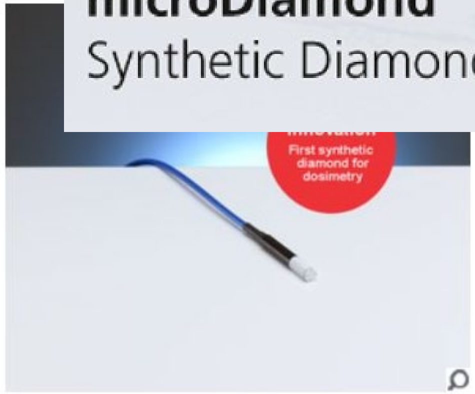

Type No.	60019
Design:	waterproof, disk-shaped, sensitive volume perpendicular to detector axis
Measuring quantity:	absorbed dose to water
Nominal sensitive volume:	0.004 mm³, radius 1.1 mm, thickness 1 µm
Reference point:	on detector axis, 1 mm from detector tip, marked by ring
Nominal response:	1 nC/Gy
Detector bias:	0 V
Radiation quality:	100 keV ... 25 MV photons (6 ... 25) MeV electrons (70 ... 230) MeV protons
Field size:	(1 x 1) cm² ... (40 x 40) cm²
Connectors:	BNT, TNC or M

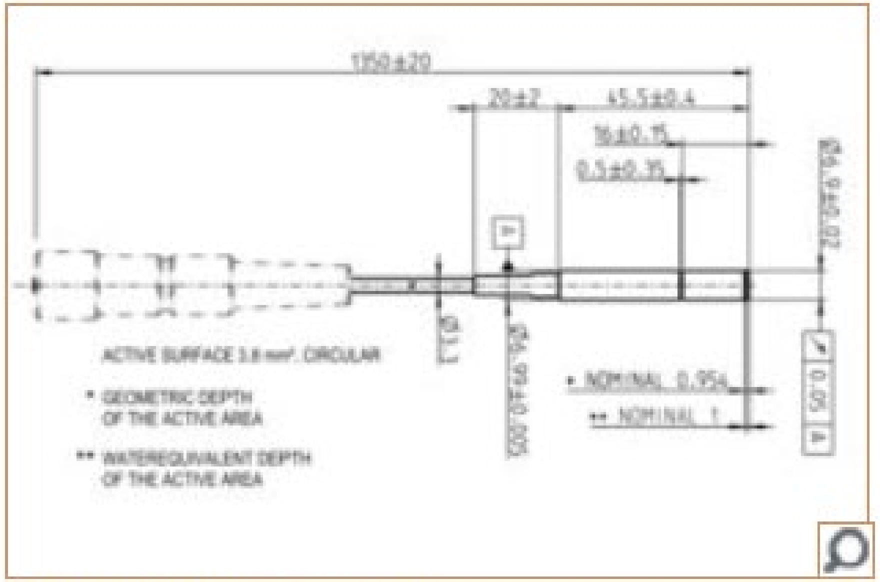

microDiamond Detector Design

Single Crystal Diamond Dosimeter

device manufactured by Università di Roma Tor Vergata

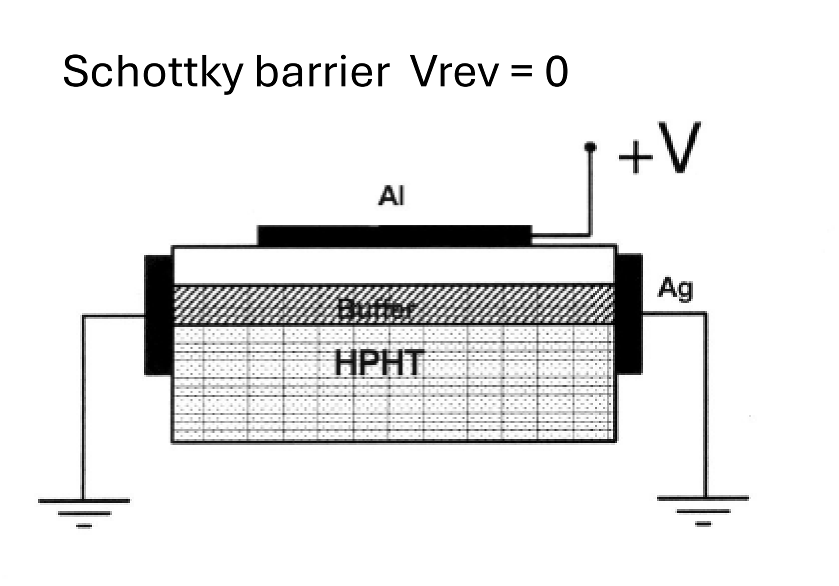

- HPHT p+ boron doped substrate - 300 μm thick
- 35 μm thick p+ buffer layer (CVD)
- Active epilayer 17 μm thick
- Al 100 nm ϕ 2mm upper electrode
- Buffer layer contacted at the perifery with Ag paste

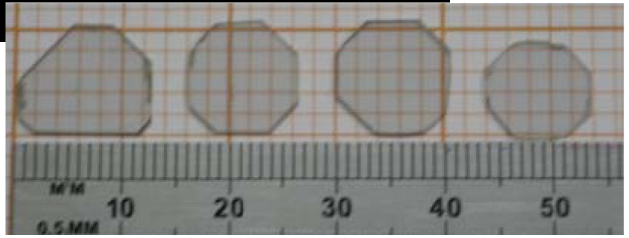

Problem : No large area array available

The Polycrystalline diamond Choice

- **it is almost water equivalent**
  - it doesn't perturb the radiation field → small fields
  - the energy is absorbed as in the water → no correction factors
- **high radiation hardness** → long term stability
- high density → high sensitivity → small dimensions
- non toxic

Natural diamond

- **very high production costs, difficult to select stones with proper dosimetric response**

Single crystal CVD (Chemically Vapour Deposited) diamond

- **grown on HPHT diamond, not available in large areas**

Polycrystalline CVD diamond

ability to produce large area wafers of 3-5"

- **persistent currents due to trapping → slow dynamics**

polycrystalline diamond segmented dosimeter prototype made in Florence

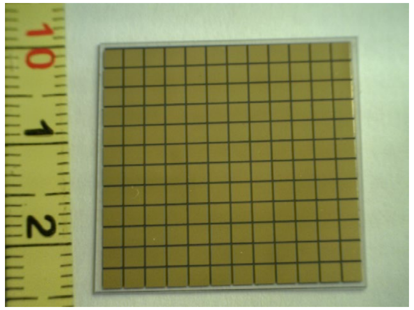

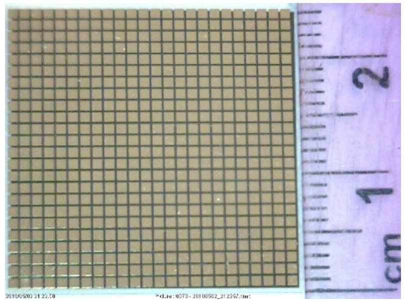

- Material

- Up to three polycrystalline diamond films $2.5x2.5cm^2$ active area each, 300μm thick;
- Premium Detector Grade Element Six, UK

- Contacts

• Schottky Barriers produced @ University of Florence
•12 x 12 matrix, pixel size: $1.8x1.8\ mm^2$ → 288 pixels in total

- Read Out Electronics

•four 64 channels 20 bit current-input analog to digital converter chips able of measuring currents from fAs to mAs; 160μs-1s integration time (50ms)
•custom printed circuit board;
•semi-rigid silver-polymer pin-contacts produced by us connecting each pixel of the 144 matrix connecting vias on PCB .

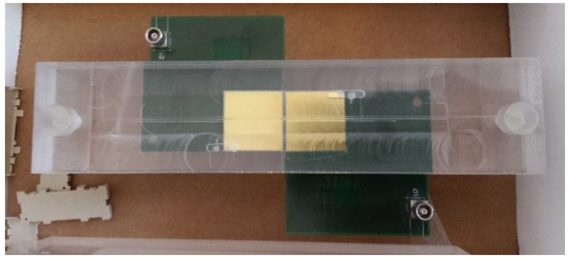

-Measurement

•Low voltage to get fast and reproducible signals;
•Device can be moved in x-y directions to cover a
•wider radiation field area.

Performance under conventional and IMRT radiotherapy beam

Current response of all pixels in a conventional X-ray beam (V_{app} = 1V) Dose-rate 50 Mu/min

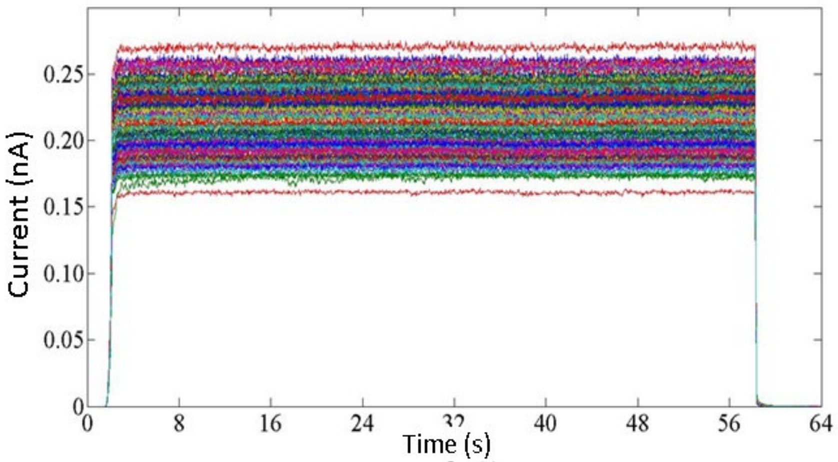

Bartoli et al. 2017 JINST 12 C03052

- ✓ negligible dark current → high S/N
- ✓ negligible polarization effects → stable response , fast dynamics

Current response of one pixel under an IMRT beam in step and shoot modality

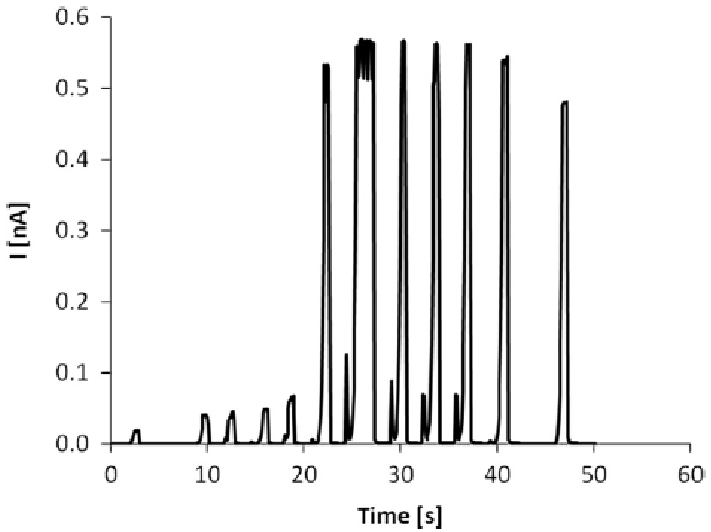

Fig. 5. Time structure of the IMRT segments as measured by one of the pCVD diamond pixels under an IMRT prostate cancer treatment.

M. Scaringella et al.

Nuclear Instruments and Methods in Physics Research A 796 (2015) 89–92

First IMRT map with Diamond Device

2.5x2.5cm^2 pCVD Diamond prototype
IMRT map 14x10cm^2
measured by shifting the diamond dosimeter

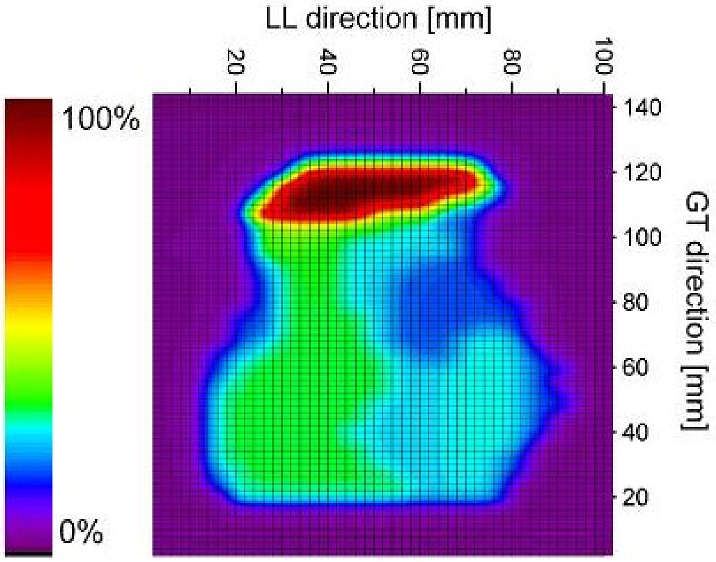

IMRT breast cancer map **as measured by the pCVD Diamond .**

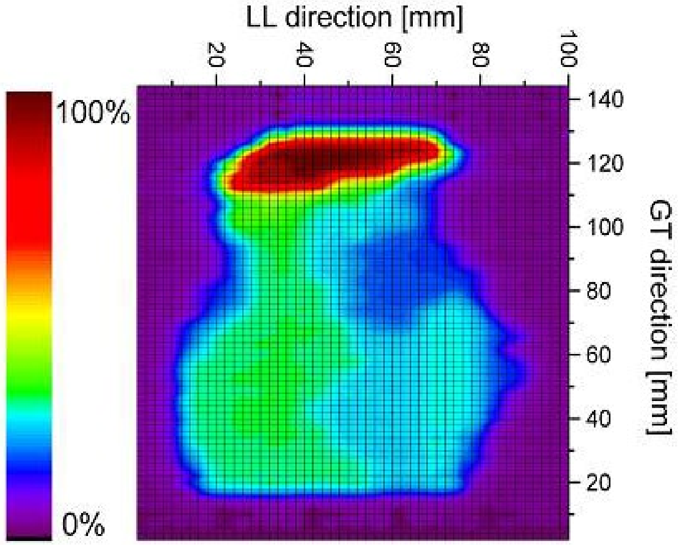

IMRT breast cancer map **as calculated by the TPS (treatment planning system)**

(GT = gantry target direction; LL = lateral-lateral direction) Grid spacing 3 mm.

M. Scaringella et al. / Nuclear Instruments and Methods in Physics Research A 796 (2015) 89–92

The SiC choice

☺ Low Leakage Current

Working without applying bias

Very low active volume

Fast Response

More tissue equivalent than Si

material	Z
Air	7.78
Water	7.51
Muscle	7.64
Fat	6.46
bone	12.31
C	6
Si	14
SiC	≈10

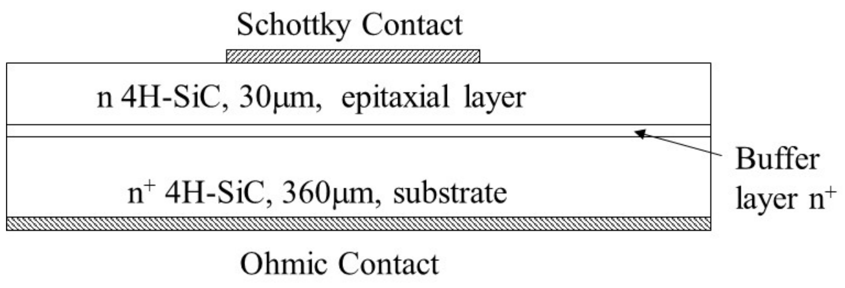

4H-SiC - Dosimetric Characterisation

Stable signal - high S/N ratio - no priming effects

22 MeV Electrons
dose-rate 4.2Gy/min

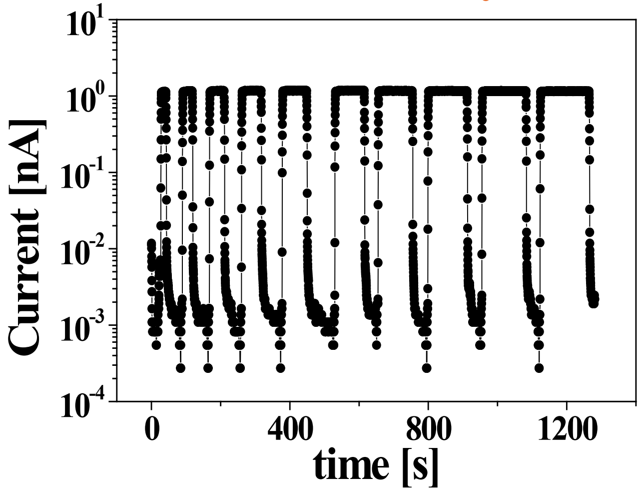

V_{rev} = 150 Volt I_{signal} ~ 1nA
I_{dark} ~0.1pA

Co^{60} γ
dose-rate 0.21Gy/min

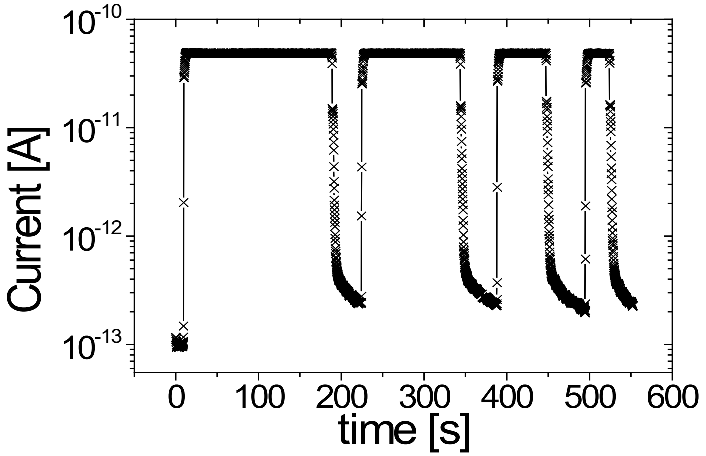

V_{rev} = 0 Volt I_{signal} ~ 50pA
I_{dark} ~ 0.1pA

M. Bruzzi, F. Nava, S. Pini, S. Russo, App. Surf. Sci, 184 (2001) 425-430

Comparison between Epitaxial SiC and standard dosimeters

Device	bias [V]	Vol. [mm^3]	S [nC/Gy]	S per unit volume [nC/(Gy·mm^3)]
Standard Farmer Ionisation chamber	300	600	**21.5**	**0.036**
Miniature Farmer Ionisation chamber	300	50	**1.38**	**0.028**
Scanditronix GR-p BS **Silicon**	0	0.295	**140**	**474**
Scanditronix SFD stereotactic **Silicon**	0	0.017	**6**	**353**
Epitaxial SiC diode	0	0.0415	**14.1**	**340**

$CsPbBr_3/CsPbCl_3$ thin films
Room temperature magnetron sputtering (MS)

- ❑ 300nm -1μm-thick
- ❑ Substrates flexible (PET ≈ 100μm) and glass interdigitated electrodes (IDE) Pd - Au/Ti
- ❑ intercontact distance 10-100 μm.

Perovskite films on glass IDEs

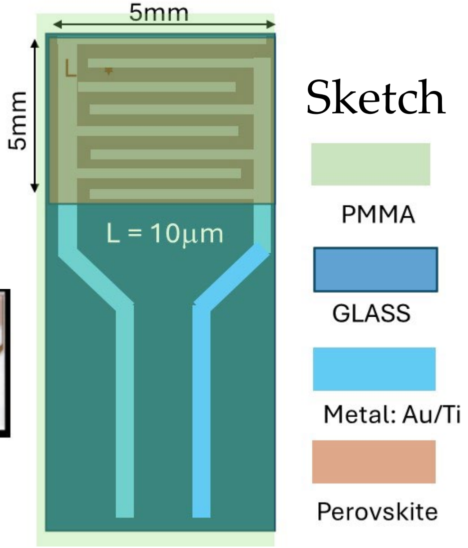

$CsPbBr_3$ encapsulated in PMMA

$$J = \frac{9\varepsilon_0 \varepsilon_r \mu_n}{8\, L^3} V^2$$

Resistivity/mobility derived from polynomial coefficients . - $\varepsilon_r = 7$

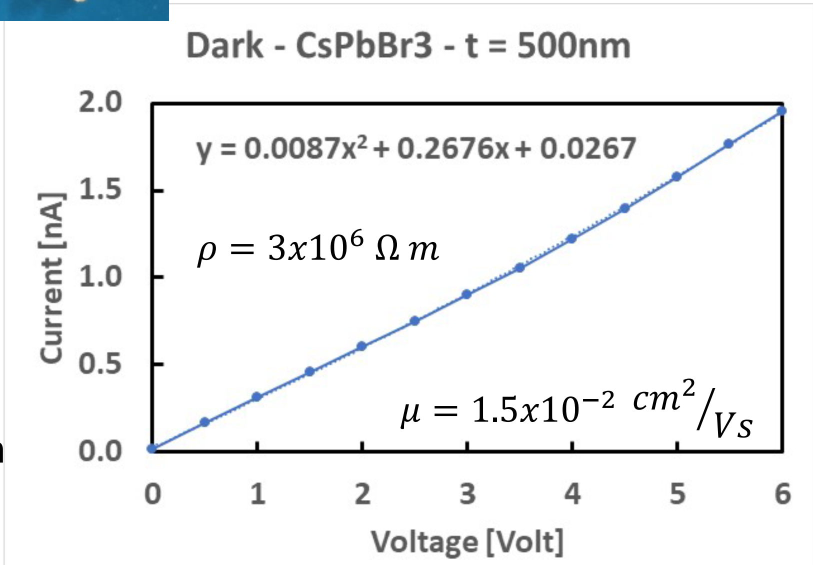

$CsPbCl_3$

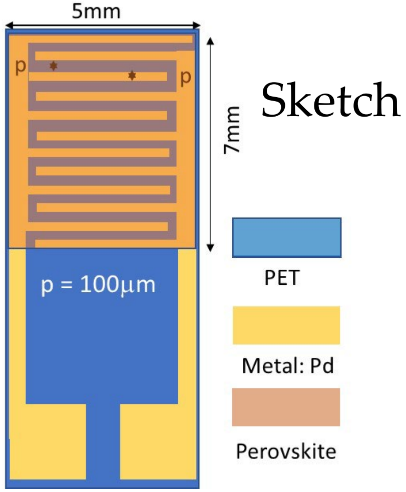

Perovskite films on Flex PET IDEs

Measurements under test beam at Trento Proton Therapy facility

Istituto Nazionale di Fisica Nucleare
SEZIONE DI FIRENZE

UNIVERSITÀ DEGLI STUDI FIRENZE

APSS-TIFPA INFN proton therapy center Italy

IBA PROTEUS 235 Cyclotron

Energy range:
100–228MeV;
Dose rates
0.02 – 0.14 Gy/s

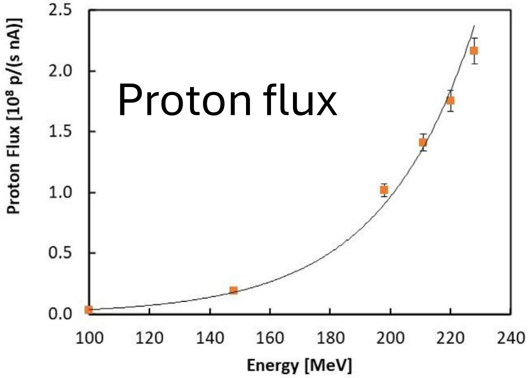

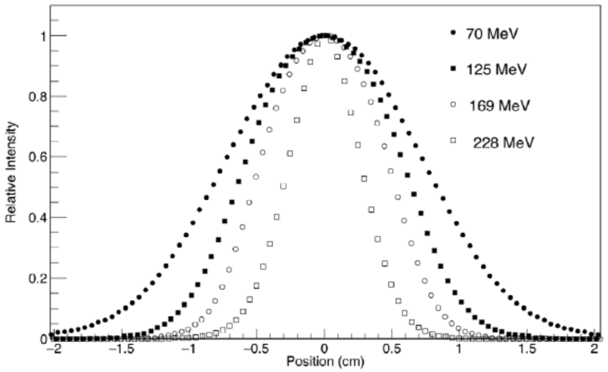

Beam spot profile at isocenter

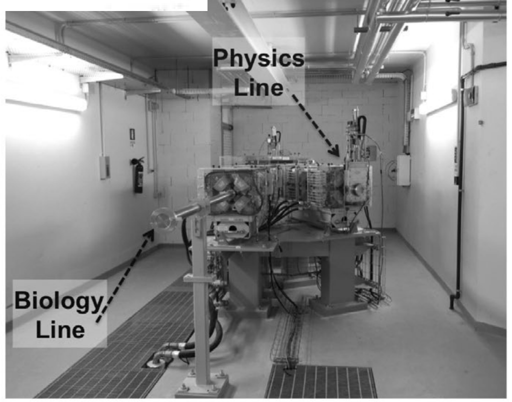

TIFPA experimental line

Ionization chamber

Proton flux monitor

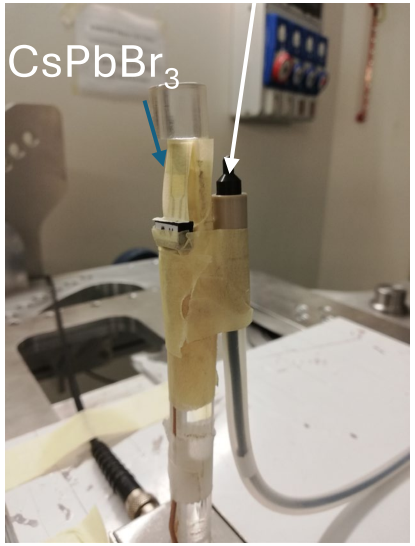

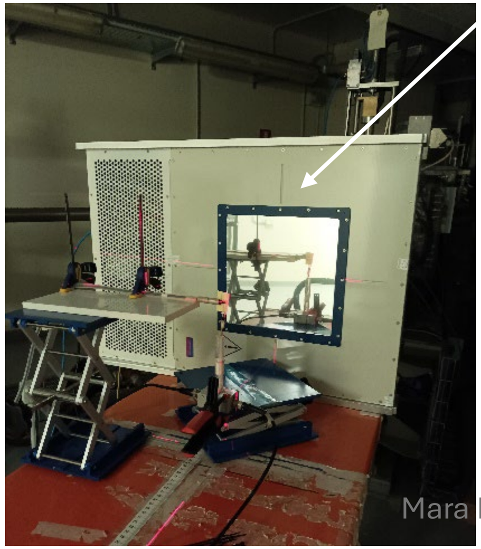

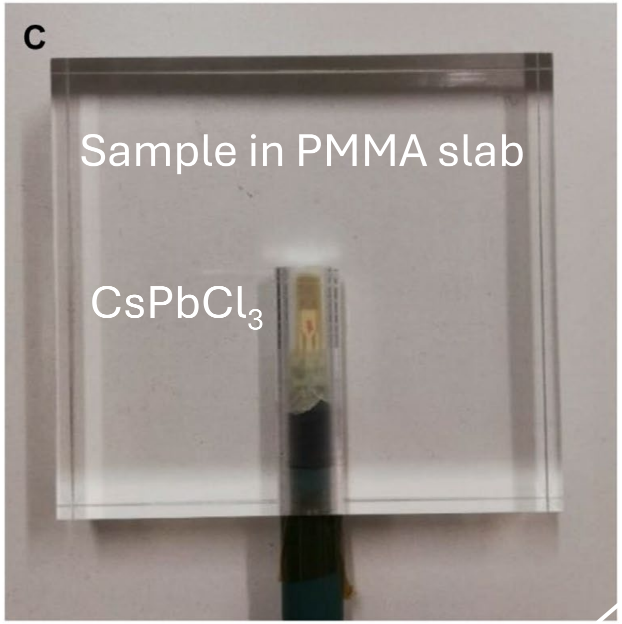

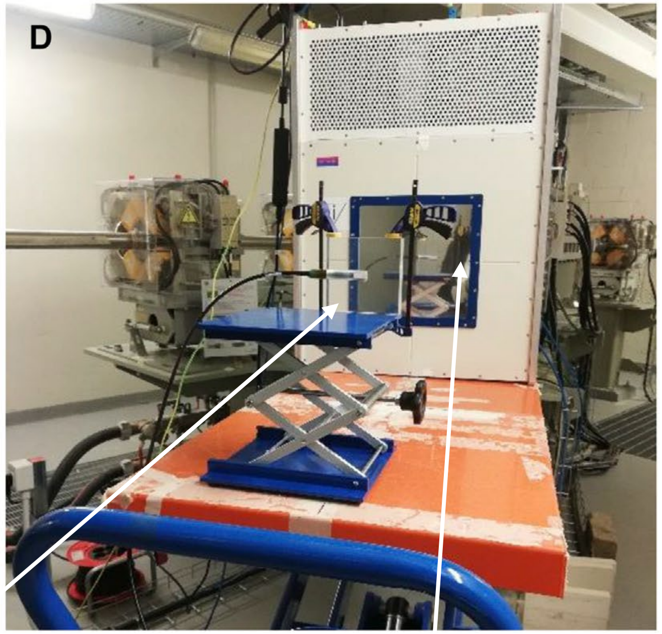

Sample under study

Proton flux monitor

Current vs Proton flux proton therapy facility Linearity plot $CsPbCl_3$

1μm-thick $CsPbCl_3$ on IDE/Pd substrate, L = 100μm as a function of time for different proton beam energies; Vbias = 2 V.

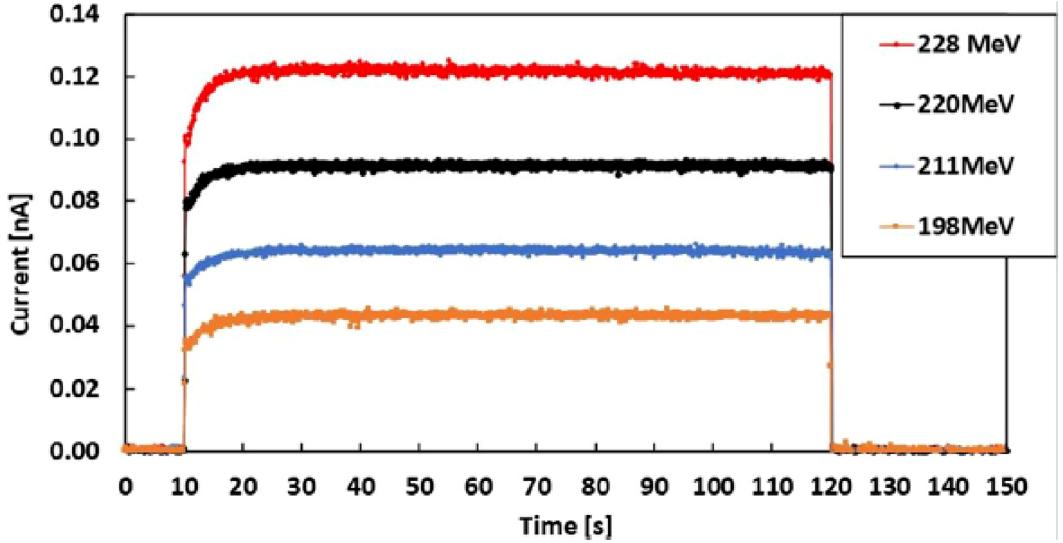

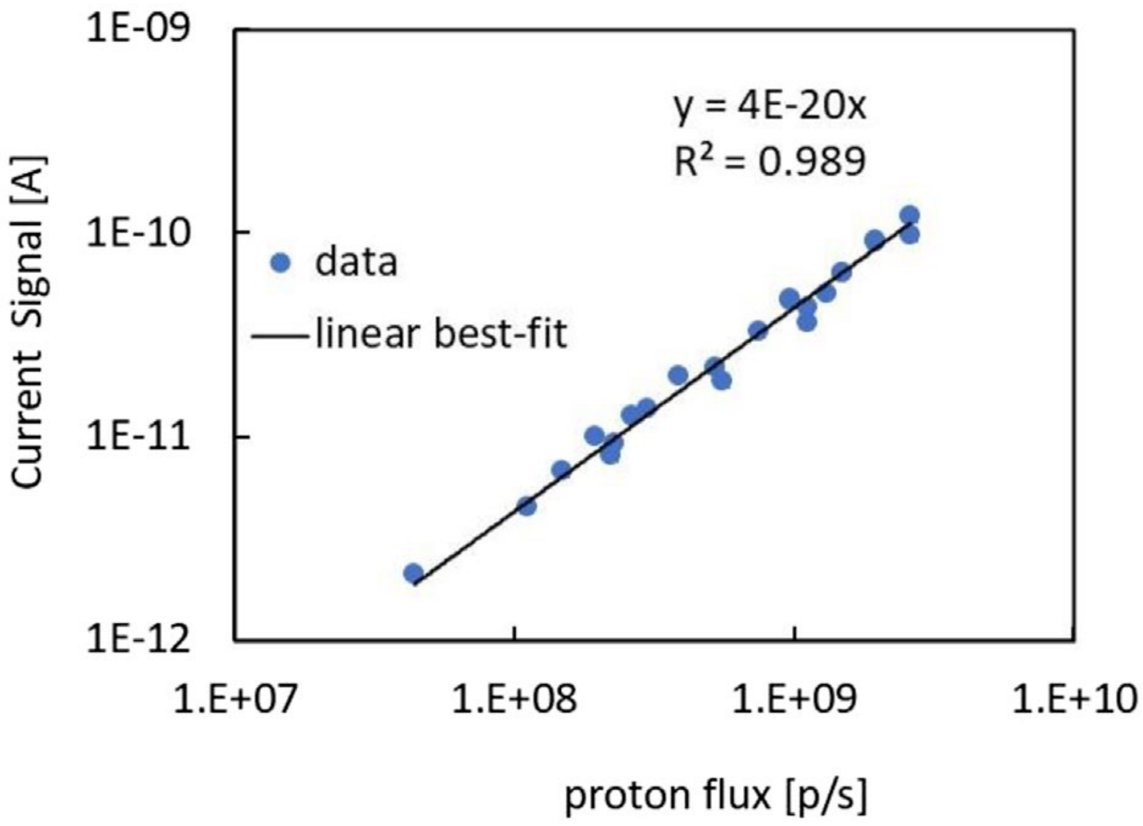

Average current measured by the 1 μm-thick CsPbCl3 IDE/Pd as a function of the proton flux impinging on the detector area, measured 100–228 MeV and 1–10 nA proton beam.
Best-fit to data shows a linear trend.

$CsPbCl_3$ thin film 1μm suitable as proton flux monitor in proton therapy application

M Bruzzi, N Calisi, N Enea, E Verroi, A Vinattieri
Flexible $CsPbCl_3$ inorganic perovskite thin-film detectors for real-time monitoring in protontherapy Frontiers in Physics 11, 1126753

FLASH Radiotherapy

ULTRA HIGH DOSE RATE BEAMS

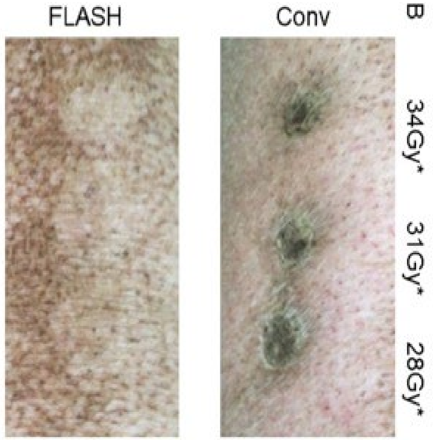

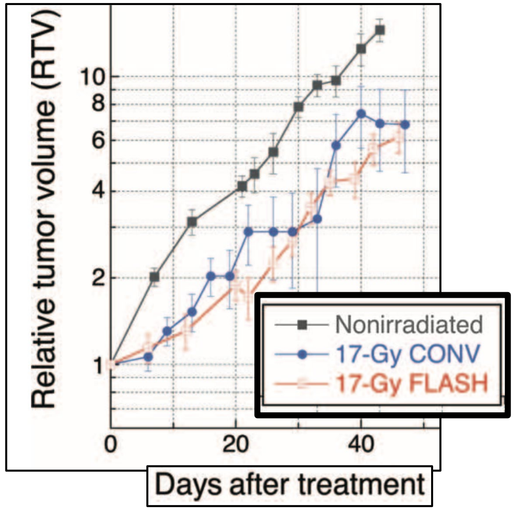

V. Favaudon et al. 2014, Sci. Transl.

	CONVENTIONAL	FLASH
Dose	2 Gy/fraction (x 30 fractions)	>10 Gy (x 1 fraction)
Dose rate	~1 Gy/min	>40 Gy/s
Irradiation Time	few minutes	<200 ms

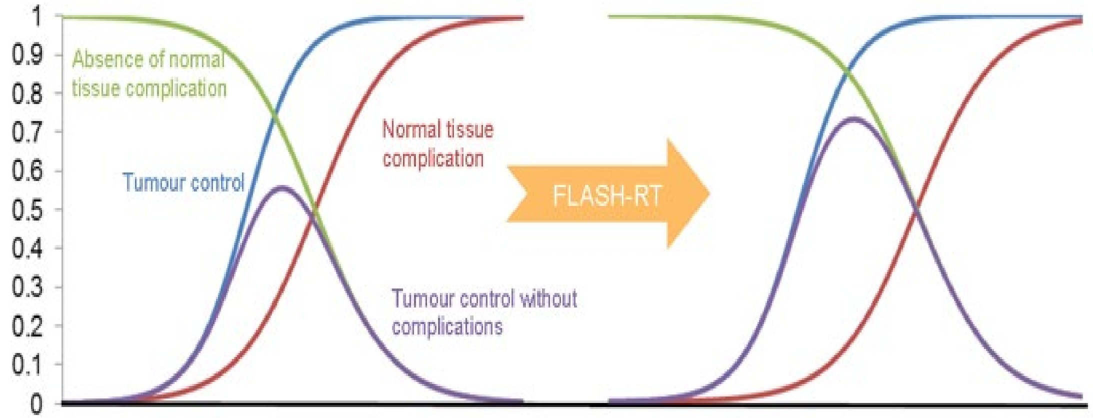

Ultra high dose rate beams pulse time structure

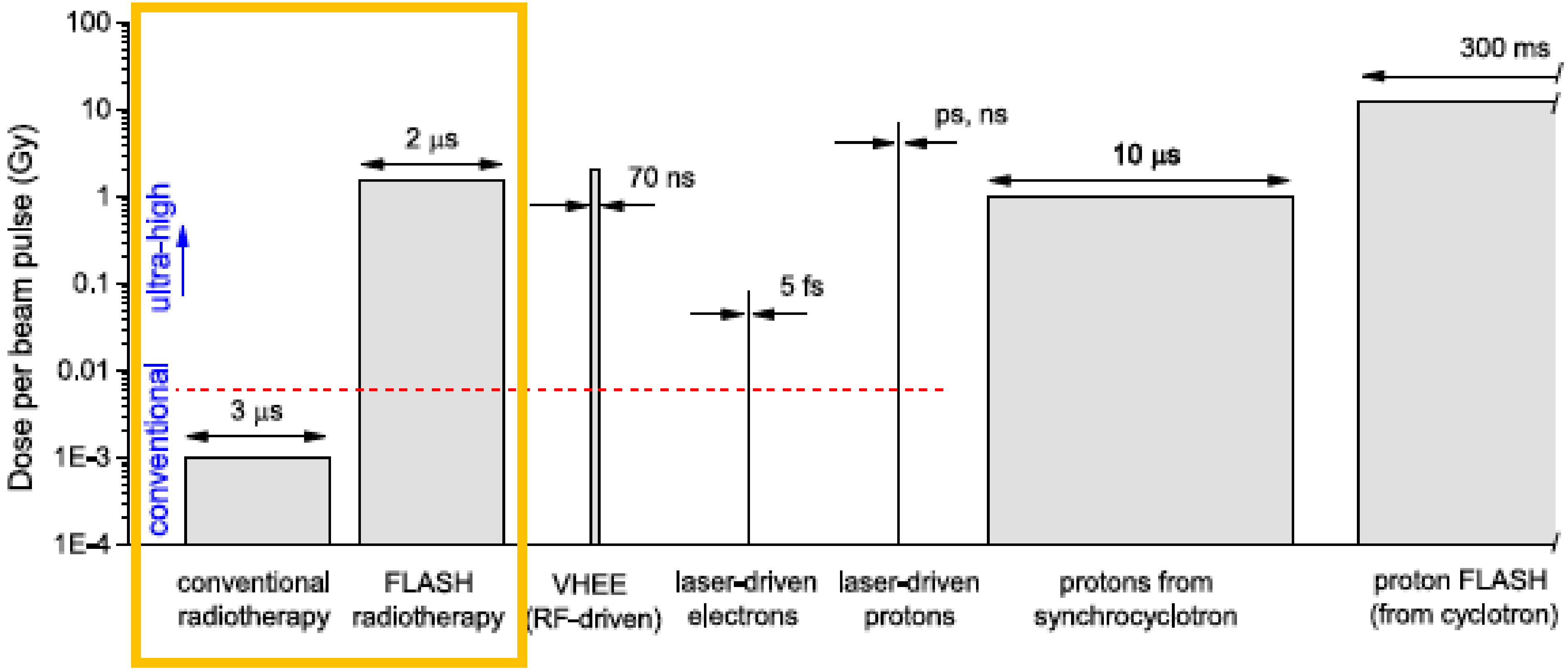

Physica Medica 80 (2020) 134–150

Multidisciplinary Center for the Development and Implementation of Flash Radiotherapy (CPFR)

Funding Grant

AOO "CLE" - Prot.: 0104712/2021 del 06/09/2021 - Convenzioni - 385/2021

FONDAZIONE PISA

SIT ELECTRONFLASH 4000

Dose rate 4000 Gy/s

Electrons 9 MeV

Triode gun

1 cm Ø smallest applicator

Ionization chamber crisis in ultra high dose rate

The measurement of commercial chambers in UHDR showed that **general or volume recombination effect was very large compromising the usability of these standards**

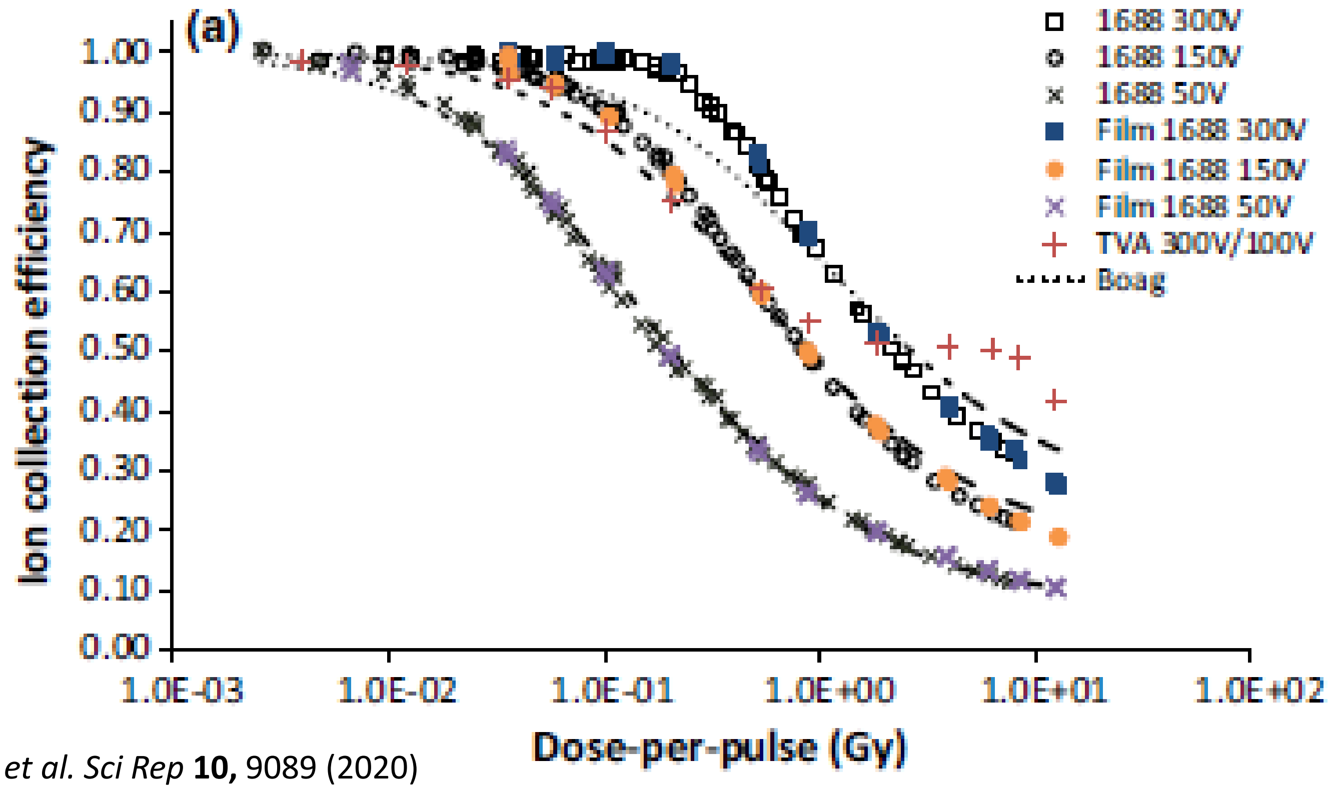

Advanced Markus parallel plate chamber (electrode distance 1 mm)

McManus, M., Romano, F., Lee, N.D. *et al. Sci Rep* **10,** 9089 (2020)
Rafael Kranzer et al. Med Phys; 48(2): 819-830 (2020)

Courtesy of F. Gomez, USC

FLASHDiamond

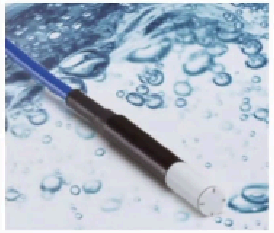

- Synthetic diamond Schottky diode
- Self biased (~1.5 V built-in potential)
- Sensitivity about 1nC/Gy

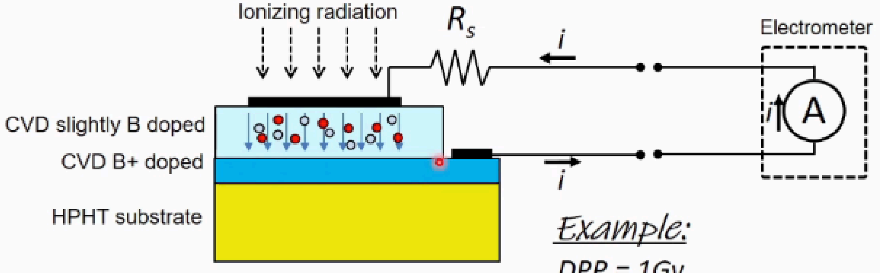

Università di Roma Tor Vergata

PTW

Courtesy of A. Marinelli and G. Verona Rinati, Roma “Tor Vergata” and PTW

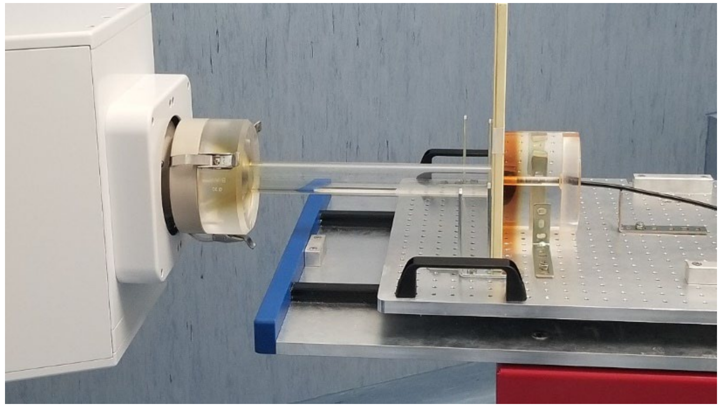

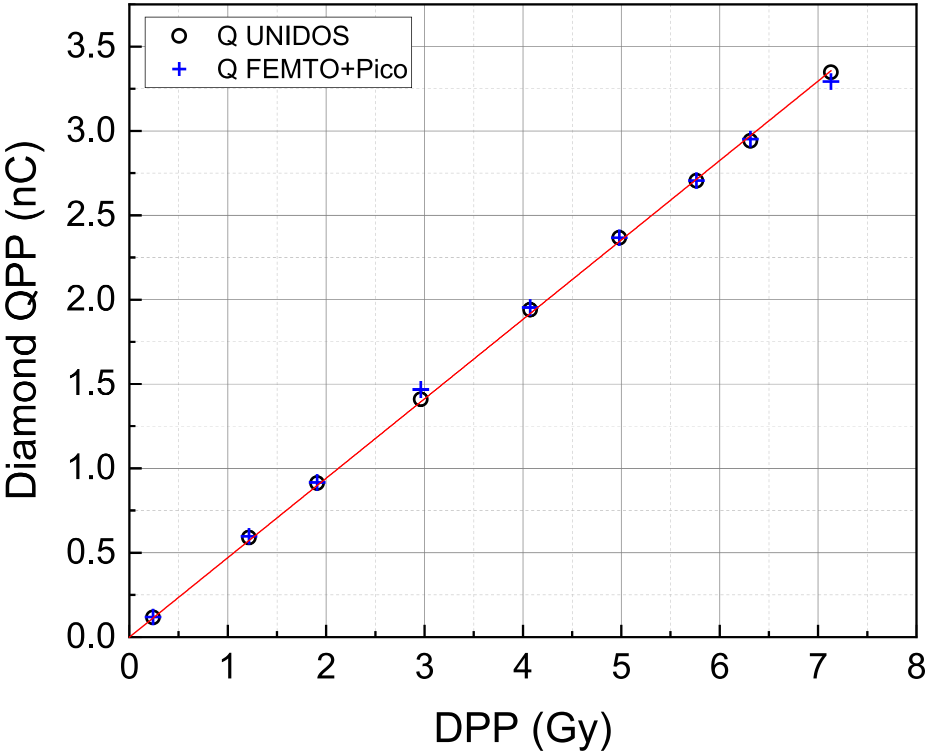

Marinelli et al 2023 Phys. Med. Biol. 68 175011

Facility	Sensitivity (nC/Gy)
PTW (^{60}Co)	0.465
CPFR (9 MeV electrons)	0.470

Instantaneous Dose Rate

ACCT (AC current transformer)

(no position sensitive)

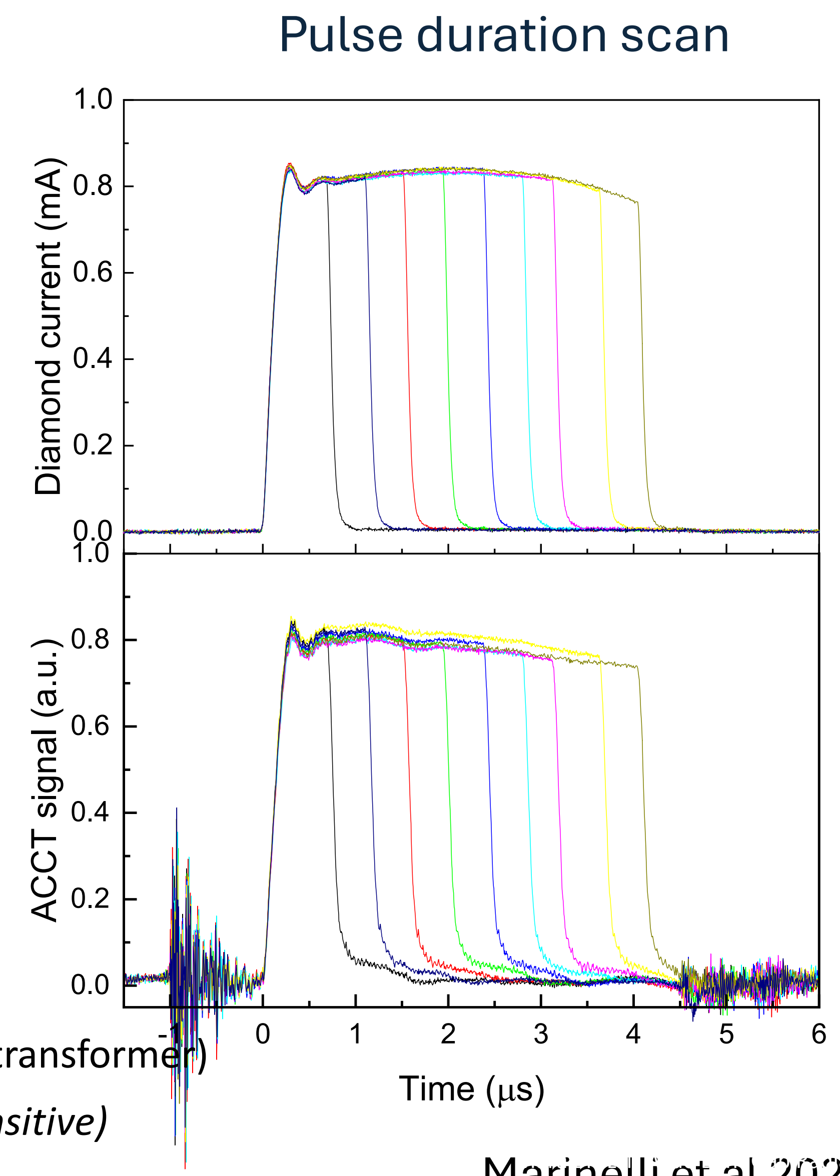

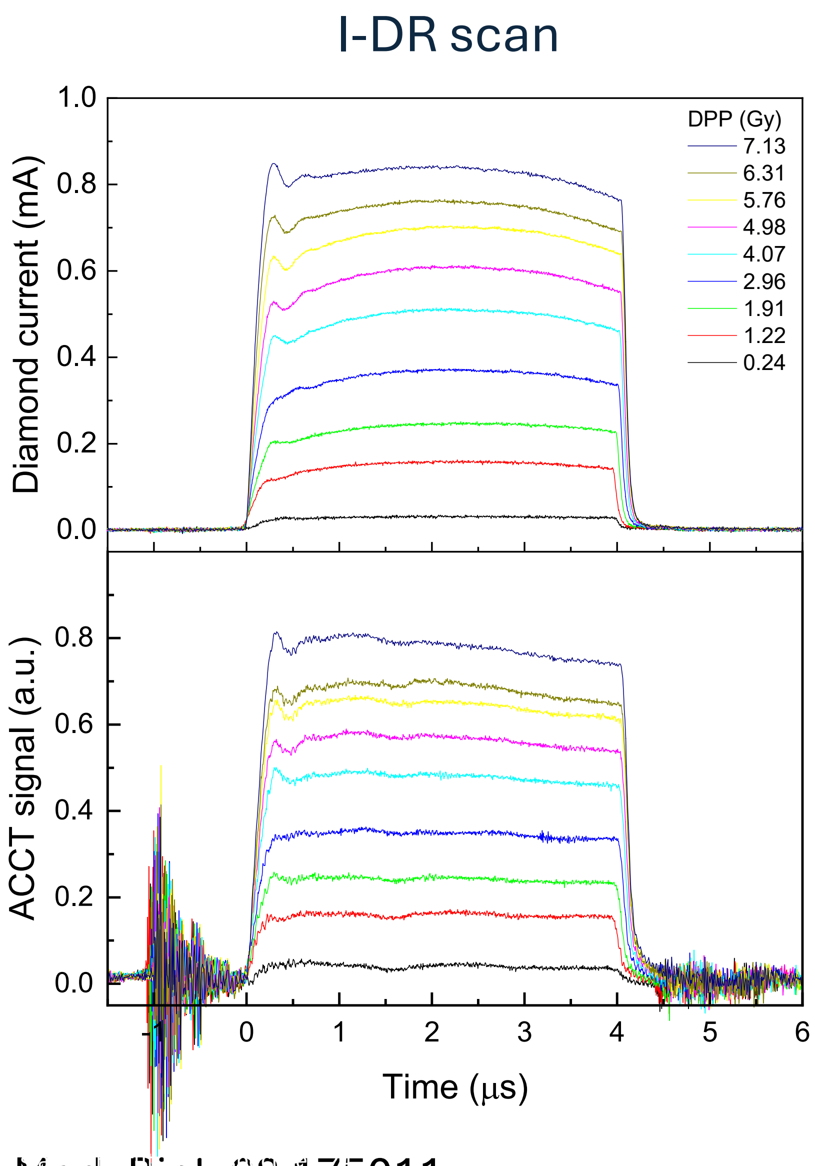

Marinelli et al 2023 Phys. Med. Biol. 68 175011

Silicon carbide detectors

Silicon

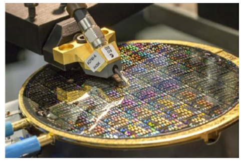

\+

Diamond

SiC

Radiation **hardness**
High signal to noise ratio
High **time resolution (ns)** and fast collection time
Large area devices

Free-standing membranes

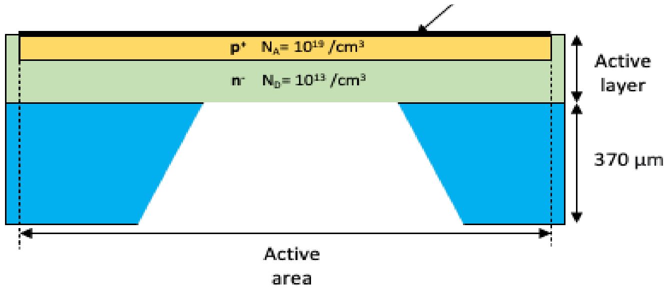

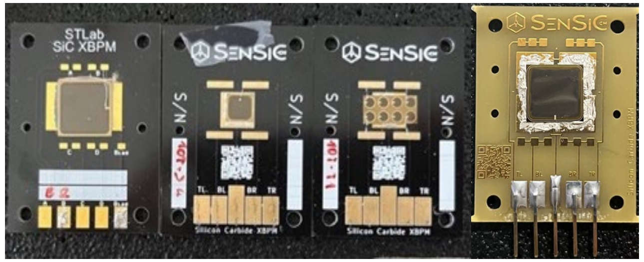

FULL DOSIMETRIC CHARACTERIZATION WITH UHDR ELECTRON BEAMS

F. Romano et al., Appl. Sci. 2023, 13, 2986.
G. Milluzzo et al., Medical Physics 2024
C. Okpuwe et al, 2024 JINST 19 C03064

COMPARISON WITH FLASH DIAMOND

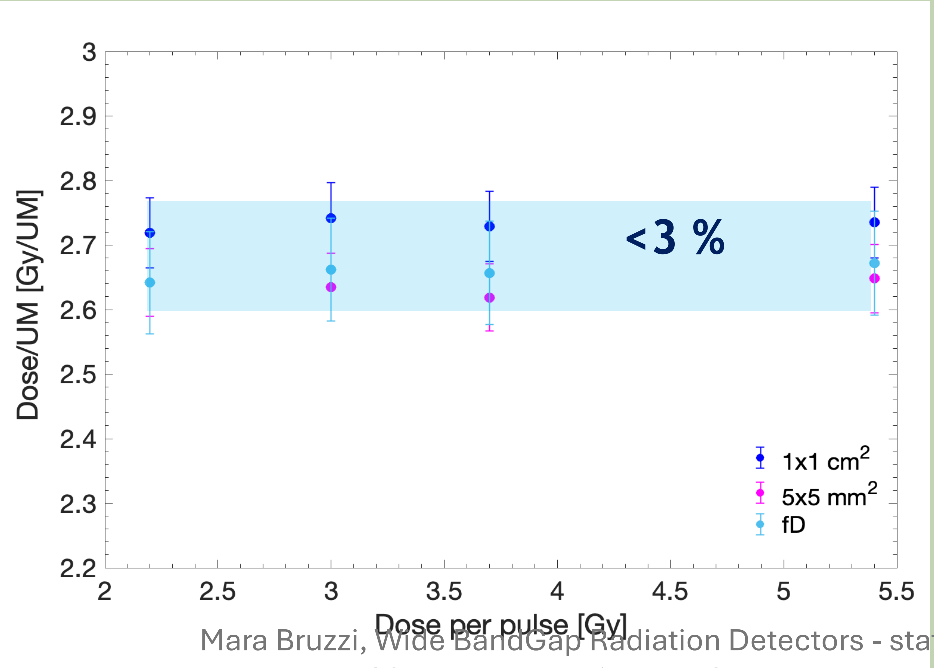

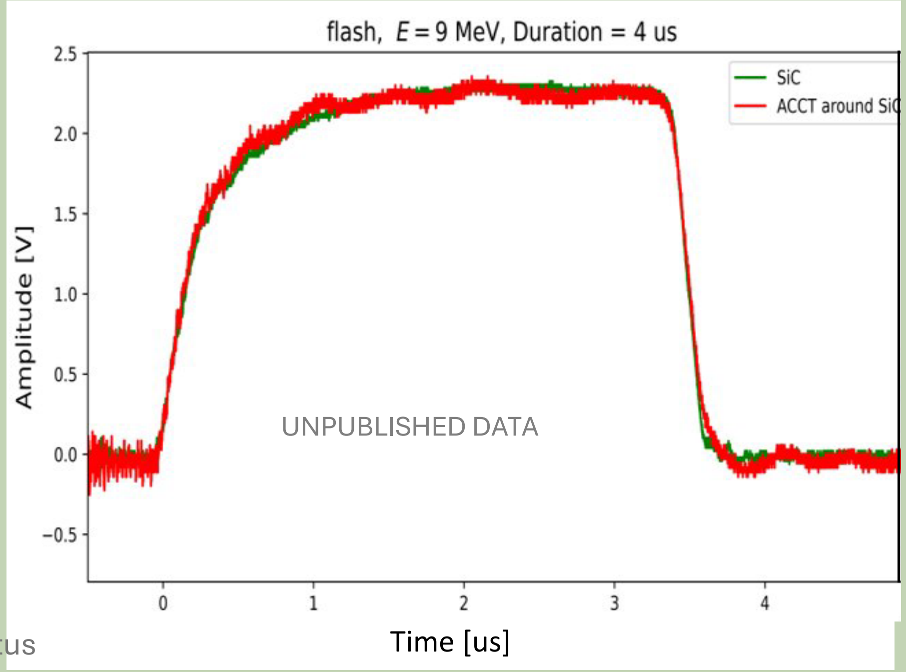

Courtesy of F. Romano and C. Okpuwe, INFN Catania

Perovskite detectors at electronFlash linac at CPFR (Pisa Italy)

- 9 MeV electron beams
- 4μs long pulses
- Single pulse and different pulse frequencies (1-200 Hz).
- Different Dose per pulse (DPP) 0.2 - 11.6 Gy
- Pulse during irradiation investigated by oscilloscope monitoring
- Real-time current monitoring during repeated pulses Keithley 6517B
- Sample Bias 1-4V

Perovskite detector under irradiation at LINAC 9MeV electron beam at Pisa CPFR

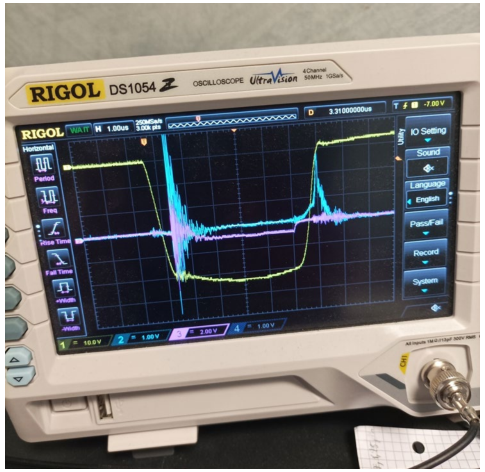

Trigger

Single pulse: 4μs - different DPP

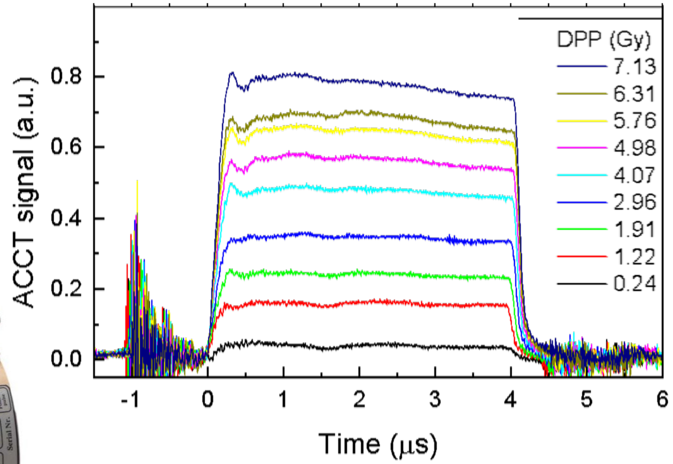

ACCT (AC current transformer)

(no position sensitive)

bergoz INSTRUMENTATION

Marinelli et al 2023
Phys. Med. Biol. 68 175011

Normal and transverse configurations:

SOLID WATER SLAB

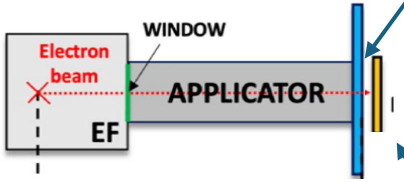

PSK detector

PSK detector

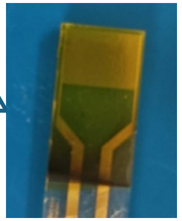

INFN Istituto Nazionale di Fisica Nucleare

Repeated Pulses

- **Normal**

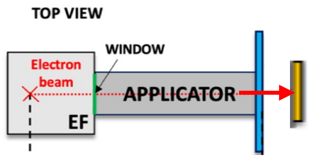

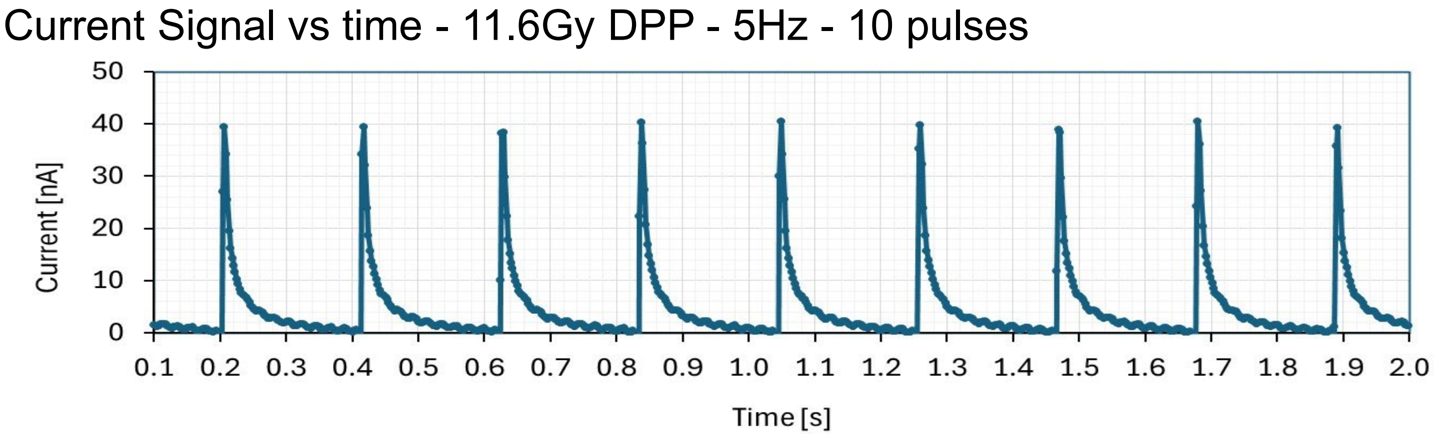

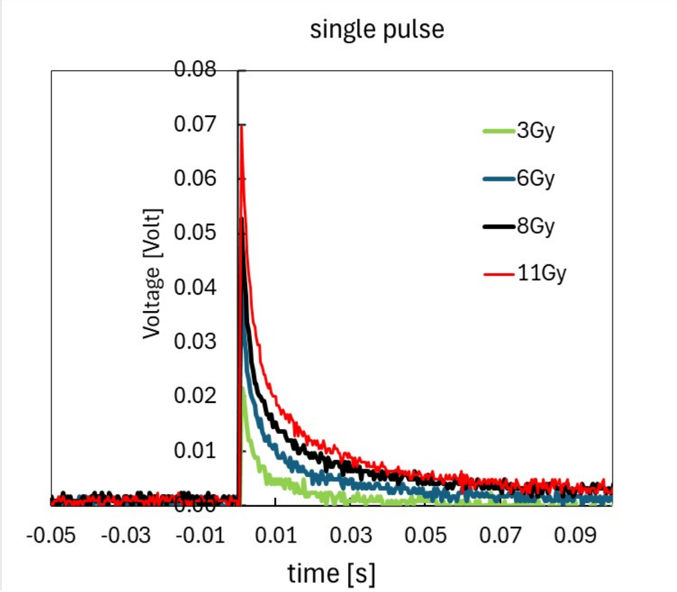

- **Transverse**

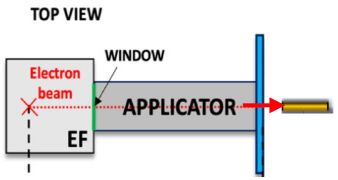

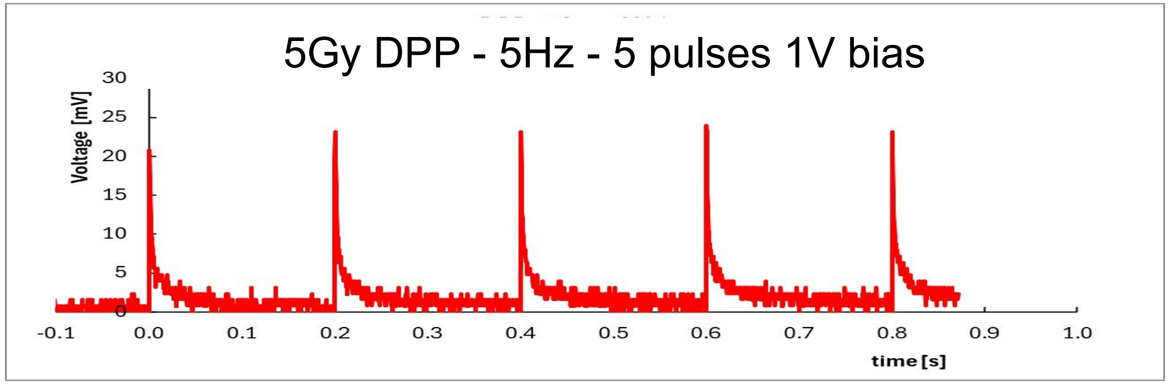

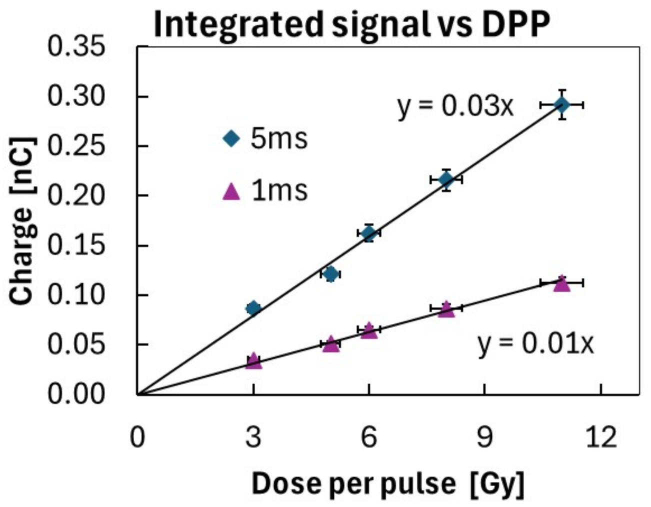

- Repeatable response under train-pulses of same DPP;
- Signal Response with S/N > 10 at any DPP;
- Integrated Charge linear with DPP in entire DPP range;
- Transverse configuration possible, increased spatial resolution

PROVIDE - PeROVskIte DEtectors for innovative strategies in radiation therapy and diagnostics

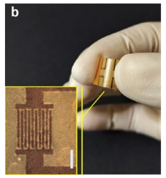

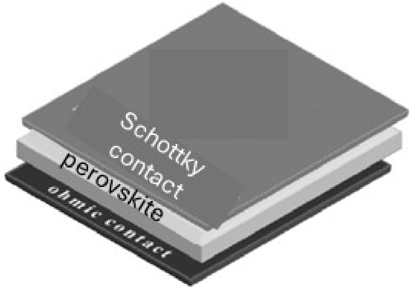

A project funded by INFN Istituto Nazionale di Fisica Nucleare CSN5 Technologic Research 2025-2027

INFN-Bologna, Firenze, Lecce, Pisa, TIFPA-Trento

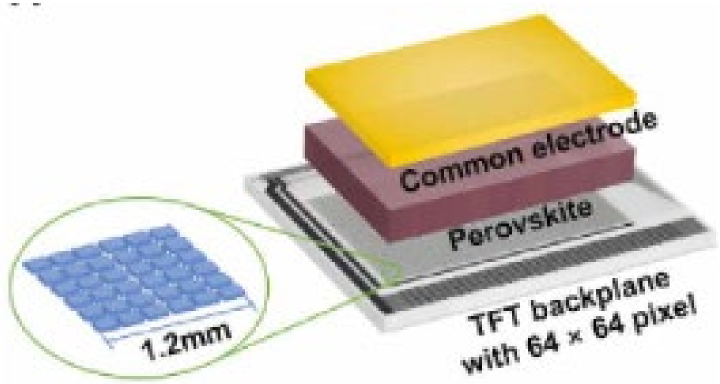

- **Best match of perovskite vs electrodes materials / geometry**
- **Schottky barrier detectors for fast / efficient charge collection**
- **Single-event perovskite thin film detectors**
- **pixelated detectors matrices for 2D/3D dose distributions on a few cm^2 scale**
- **HP based scintillator detectors on flexible substrates for bendable and fast X-ray imaging;**
- **HP based metascintillators for TOF-PET application.**
- **Fix radiation hardness requirements for RT&D;**
- **Radiation Damage Characterization.**

Figure-of merit	state-of-art	this project
Time resolution	10-40ms	0.1 us
Active size (single pixel)	5mm	500µm
Sensitivity	10 - 50 μC/Gy/cm2	100 - 500 μC/Gy/cm2
Active thickness	0.1-10 µm	0.1-10 µm
Field of view matrix	2 cm array	3x3 cm^2

CONCLUSIONS

- Wide bandgap materials are promising to address the challenges of future particle physics experiments.

- Common properties are superior displacement energy and charge carrier velocities, translating to radiation hardness and speed.

- Synergy with industry trends allows particle physics to profit from exciting new developments in this field.

- **A variety of deposition techniques tailoring specific requirements now available**

- **Already established results in the field of radiation detectors for radiotherapy (UHDR FLASH, protons)**